3-14-2014

Fully Automated Sunspot Detection and Classification Using SDO HMI Imagery in MATLAB

Gordon M. Spahr

FULLY AUTOMATED SUNSPOT DETECTION AND CLASSIFICATION USING SDO HMI IMAGERY IN MATLAB

THESIS

Gordon M. Spahr, Second Lieutenant, USAF

AFIT-ENP-14-M-34

DEPARTMENT OF THE AIR FORCE
AIR UNIVERSITY

AIR FORCE INSTITUTE OF TECHNOLOGY

Wright-Patterson Air Force Base, Ohio

AFIT-ENP-14-M-34

FULLY AUTOMATED SUNSPOT DETECTION AND CLASSIFICATION USING SDO HMI IMAGERY IN MATLAB

THESIS

Presented to the Faculty

Department of Engineering Physics

Graduate School of Engineering and Management

Air Force Institute of Technology

Air University

Air Education and Training Command

in Partial Fulfillment of the Requirements for the

Degree of Master of Science in Applied Physics

Gordon M. Spahr, BS

Second Lieutenant, USAF

March 2014

AFIT-ENP-14-M-34

FULLY AUTOMATED SUNSPOT DETECTION AND CLASSIFICATION USING SDO HMI IMAGERY IN MATLAB

Gordon M. Spahr, BS
Second Lieutenant, USAF

Approved:

//signed//	5 March 2014
Ariel O. Acebal, PhD (Chairman)	Date
//signed//	5 March 2014
Col Karl C. Walli, PhD (Member)	Date
//signed//	5 March 2014
William R. Bailey, PhD (Member)	Date

AFIT-ENP-14-M-34

Abstract

An automatic sunspot detection and classification method is developed combining HMII and HMIM imagery procured from the Solar Dynamics Observatory. Iterative global thresholding methods are employed for detecting sunspots. Groups are selected based on heliographic distance between sunspots via area-based grouping lengths. Classifications are applied through logical operators adhering to the standard McIntosh classification system. Calculated sunspot parameters and classifications are validated in three way comparisons between code output, Holloman AFB and the Space Weather Prediction Center. Accuracy is achieved within the margin of difference between Holloman and SWPC reports for sunspot area, number of groups, number of spots, and McIntosh classification using data spanning 6 July 2012 to 29 June 2013: SWPC/Holloman (33.38%,57.48%,87.67%), SWPC/SDO (20.22%,51.25%,83.80%), and SDO/Holloman (24.54%,50.91%,80.65%). The automatic classification system is used to evaluate bias inherent in Holloman classification methods. Parameters are altered to reach optimal match percentages with Holloman, indicating differences between computed parameter values and hand-calculated counterparts. Group length cutoffs are shown to differ by 2.5°, eccentricity is quantified at 0.8, and penumbra length cutoffs are shown to exceed differences of 1.4° from McIntosh values.

This one's for you, Owen

Acknowledgements

First and foremost, I would like to thank Dr. Ariel Acebal for the guidance he has given me over the 14 months I've had the privilege of working with him. Coupled with the knowledge and experience of Dr. William Bailey and Col. Karl Walli, I could not have asked for a better committee. For pushing me in the right direction when I needed it and letting my curiosity run free when I didn't, I am eternally grateful.

Thank you to my family and friends. For listening to me talk about physics when I'm sure you had 100 better things to do, I can never thank you enough.

Thanks to the team at Holloman Solar Observatory. Mr. Pietrzak, SMSgt Siebert, TSgt Bell, SSgt Mullins, SSgt Stewman, SSgt O'Connell, your patience with a new Lieutenant and his flood of questions was much appreciated. Thanks to Tim Henry at the NSO for un-sticking me when the math got tough.

My deepest thanks to each of you, named and unnamed, for what you do every day. Your passion makes it easy to give my best.

Gordon M. Spahr

Table of Contents

Page

Page

List of Figures

List of Tables

List of Abbreviations

FULLY AUTOMATED SUNSPOT DETECTION AND CLASSIFICATION USING SDO HMI IMAGERY IN MATLAB

I. Introduction

1.1 Space Weather Operations

United States Air Force (USAF) instructions currently dictate that weather personnel at three optical solar observatories around the world complete sunspot drawings by hand once a day and transmit the results to the Space Weather Prediction Center (SWPC). These sunspot drawings are performed by solar analysts at three geographically separated bases: Holloman Air Force Base (AFB) in New Mexico, Learmonth Solar Observatory in Australia, and San Vito Solar Observatory in Italy. Drawings are completed on a sheet of paper, copying a projected image of the sun from a solar telescope at optimal times throughout the day, generally when visibility is best. Because seeing conditions change throughout the day and atmospheric conditions can cause difficulties with observing quality, this method can fail to produce accurate results or produce biased results under a number of different circumstances. Each solar analyst may trace spots differently, and the technique by which sunspots are grouped is not uniform across analysts, especially for sunspots found in regions near the outer limb of the Sun. Geometric foreshortening effects may also lead to poor area approximations and misjudgment of the size or completeness of penumbra surrounding each umbra.

Once sunspot analysis at each base is complete, drawings are collected by SWPC and subsequently used to determine the location and classification of

sunspots and a flare probability for the next 24 hours. When the weather does not allow for a drawing to be performed, no report is submitted to SWPC. While this method can be effective, sunspot evolution can often times be more dynamic and change on time scales shorter than 24 hours.

Sunspot location and classification have been correlated with solar flares and Coronal Mass Ejections (CMEs)[*Bornmann and Shaw*, 1994]. This correlation can be used to forecast the probability of solar flares for any given day which can impact military and civilian operations. While forehand knowledge of a flare or CME does not eliminate the effects of the storm, it can provide useful information for finding the degree of influence each solar storm can have on earth. In any case, prior knowledge is valuable to the Air Force in order to create a better system for analyzing and predicting solar weather to a point that saves time and money, subsequently increasing Air Force effectiveness in global reach and power projection.

1.2 Objectives

Flare statistics are calculated by dividing the number of times a flare was seen from a group with a specific classification by the total number of times that classification has been seen. For example, if a flare results every time a classification is seen, that category of sunspot will be given a flare probability of 1. However, pairing the fact that sunspot evolution is dynamic with the fact that sunspot classifications may only be updated once a day, it can be seen that there exists a potential to wrongfully attribute flares to classes that have little connection to solar flares. In addition, because of human bias, incorrectly classified sunspot groups may wrongfully acquire flare counts. Therefore, a better understanding of the time evolution of sunspot groups and a consistent, unbiased classification method may help improve forecasting. Two ways to implement this improvement include

increasing the speed of detection and classification of sunspots as well as eliminating human bias through automation of the process. While past attempts at this task have yielded accurate results, summarized by Aschwanden's review of automated solar analysis tools [*Aschwanden*, 2010], implementation of the automation process using images from the Solar Dynamics Observatory (SDO) has only recently been adopted [*Watson*, 2012]. SDO images can significantly improve the process due to greater resolution images and the absence of terrestrial atmosphere between the source and observation point. Successful development of this process has the potential to provide an updated classification to AF weather personnel every minute and will give large amounts of new information on sunspot evolution that may improve flare prediction in the future. The purpose of this research is to provide a better algorithm for sunspot detection and classification based in Matrix Laboratory (MATLAB) that can be useful for AF implementation aiding solar analysts in their classification duties.

1.3 Previous Research

Because of the cost and practicality associated with physically measuring aspects of interplanetary space and the solar atmosphere, modeling based on solar observations is the primary method for researching the Sun. A robust formulation of sunspot classification was put to use for thousands of previous observations made over the course of nearly a decade from 1969-1976 [*McIntosh*, 1990]. This process greatly improved the previously used Zurich classification by modifying the general groups outlined by Kiepenheuer [*Kiepenheuer*, 1953], and supplementing with additional elements to differentiate between sunspot groups. Automation of the detection process has been in the works since the late 1990s [*Al-Omari et al.*, 2009; *Benkhalil et al.*, 2004, 2003; *Colak and Qahwaji*, 2008; *Curto et al.*, 2008; *De Wit*,

2006; *Delouille et al.*, 2012; *Nguyen et al.*, 2005, 2006; *Park*, 2011; *Qahwaji and Colak*, 2005, 2006, 2007; *Turmon et al.*, 1998, 2002; *Verbeeck et al.*, 2013; *Watson and Fletcher*, 2010; *Watson*, 2012; *Zharkov et al.*, 2005], but a widely successful algorithm for both detection and classification has yet to be developed. Accurate methods for active region detection exist, but systems for successfully assigning a classification in a wide variety of circumstances have generally dwindled around a 50-70% [*Benkhalil et al.*, 2004; *Colak and Qahwaji*, 2008; *Jewalikar and Singh*; *Nguyen et al.*, 2006; *Park*, 2011; *Watson*, 2012; *Turmon et al.*, 1998].

Many previous methods focus on a specific type of image processing, relying purely on a variation of mathematical morphology or simple logical operations [*Gonzalez and Eddins*, 2009]. In addition, some methods have attempted to incorporate magnetogram images [*Colak and Qahwaji*, 2008] into the classification section to better determine spot polarity. Previous iterations of this research have combined other resources to come up with automatic detection and classification, but only one group has looked at using SDO images for classification (most others use ground based telescopes or imagery from the Solar and Heliospheric Observatory (SOHO) satellite). The main benefit with SDO imagery will be a minimum of four times improvement on spatial resolution. Additionally, the SDO is located in an inclined geosynchronous orbit meaning images it produces do not require corrections from random atmospheric disturbances as terrestrial satellites would [*Pesnell et al.*, 2012]. The method pursued by [*Watson*, 2012] was different in that the goal for each processed image was to provide a time evolution step for a sunspot tracking algorithm. In addition to various other grouping methods, the use of neural networks has been pursued [*Colak and Qahwaji*, 2008; *De Wit*, 2006; *Socas-Navarro*, 2005] for implementation in the classification process. The use of an adaptive classification process based on previously made classifications is, by

definition, biased and therefore, the use of neural networks (beyond the simple forward-propagating network model of input to output) is neglected in this research.

1.4 Document Outline

The following chapters of this thesis are organized into background information, research methodology, results analysis, and conclusions. Background information presented in Chapter II includes a discussion of the Sun as a whole, and introduces specific terms and concepts used throughout the document. Chapter III outlines the development of the automated code and discusses some of the features associated with the specific route of image processing that was taken. An analysis of the data produced by the automated code is presented in Chapter IV. Finally, Chapter V summarizes the results of this research and presents additional topics for future work. Each of these sections incorporates information identified in previous chapters and assumes a small working knowledge of solar physics.

II. Background

A general outline of solar physics is presented for completeness. The Solar Cycle is discussed to illustrate how sunspot groups appear over large amounts of time. Additionally, differential rotation and limb darkening are developed to illustrate the purpose of these correction steps written into the following chapters. The classification system for sunspots is reiterated from the McIntosh paper and for reference. Finally, the automatic approach through the use of SDO imagery is addressed in conjunction with background on the imagery itself.

2.1 Solar Cycle

The dynamic evolution of solar properties lead to the discovery of a cyclical pattern of increasing and decreasing solar activity [*Foukal*, 2008]. Made evident by the increasingly common presence of sunspots on the solar disk, this oscillatory pattern is repeated with a fairly regular period. This Solar Cycle is marked by increasing solar activity over the corresponding 11 year time span. Beginning with the solar minimum when the sun exhibits the least amount of magnetic activity, the solar cycle starts by ramping up the intensity and occurrences of active regions. As the magnetic field of the sun becomes more twisted with time, the frequency of sunspot appearances on the surface of the sun increases, and the latitude of these sunspot groups begins to shift towards the solar equator. Culminating with the solar maximum at the end of the cycle, the magnetic field of the sun experiences a full reversal before the process begins again. Therefore, the magnetic field of the sun reverses polarity every 11 years. This reversal is thought to come about as a result of active regions shifting towards the solar equator as the cycle progresses, slowly flipping the polarity of the sun's magnetic field [*Foukal*, 2008].

2.2 Differential Rotation

The general orbit-like flow of plasma at varying speeds in the sun is known as differential rotation. Radially driven convective regions seem to be the cause of the different flow rates of plasma at different heights in the sun. This radial motion of plasma is a result of the buoyancy of hot plasma at the bottom of the convective region moving towards the photosphere. The rotational motion of plasma can be measured, seen as a slight blue and red shift near the edge of the sun, the degree of which changes with latitude. The rotation is referred to as differential because the speed of rotation varies with solar latitude and radial depth into the sun. The differential rotation rate varies up to 10 full days for a complete rotation depending on the specific part of the photosphere being observed. While this effect is considered in sunspot tracking methods, it has no effect on the limb darkening correction applied to the solar disk to flatten the intensity drop off.

2.3 Limb Darkening

The photosphere is considered to be the surface of the sun with a depth of approximately 500 km [*Foukal*, 2008]. This definition is awkward however, because there is no hard cut off where the density of gaseous plasma from the sun becomes negligible, as would be the case in a solid or liquid. Instead, the Beer-Lambert law is used to concretely define a surface using the optical depth definition for a region of the sun at a specific wavelength. In looking at the change in emission intensity from an origin point to a location at angle θ inside an absorbing medium, it can be shown that

$$I_\lambda(\theta, z + dz) - I_\lambda(\theta, z) = [\epsilon_\lambda(z) - \kappa_\lambda(z) I_\lambda(\theta, z)] sec\theta dz \tag{1}$$

where κ_λ and ϵ_λ are the absorption and emission coefficients respectively. If this change is approximated as a derivative with respect to z, the instantaneous change of intensity yields a relationship for the distance a wave can penetrate. If the optical depth is defined as $d\tau_\lambda = -\kappa_\lambda dz$ and emission is neglected, the ratio of final to initial intensity takes the form

$$\frac{dI'_\lambda}{I_\lambda} = e^{-\tau_\lambda} \tag{2}$$

From this equation, it can be seen that as τ increases, the intensity drops exponentially. This means that as depth increases and τ also increases, the amount of light that penetrates the plasma in the sun decreases rapidly. For $\tau = 1$, the intensity of the source has dropped to 37% of the original value. The surface of the sun (Photosphere) is defined to be the location where optical depth τ is equal to one at the hydrogen α wavelength at $6173.3\mathring{A}$. Because the optical depth of the sun depends on a specific wavelength, it is necessary to define a specific part of the electromagnetic spectrum. The optical depth is also a function of temperature. The large variation in temperature in the radial direction of the sun therefore causes the change in optical depth to vary radially. This variation ultimately implies that as an observer looks more towards the edge of the solar disk, the radial component of their observation line decreases and they look increasingly tangent to the surface of the sun. An observation towards the edge of the sun therefore means that one does not see as deep into the sun, but that the location where $\tau = 1$ is higher up and therefore cooler as seen in Figure 1. The location where $\tau = 1$ is not at an equal radius for all values of θ, meaning that the temperature of the plasma at the $\tau = 1$ surface is not uniform. This variation in temperature along the τ surface means that the maximum emitted wavelength of light for a particular region depends on the angle θ between the normal vector of that position and the observer's location.

The left sun shows concentric rings of isothermal regions with the optical depth surfaces of 1 and 10 in black as seen from a distant observer. The right sun shows concentric rings of the same optical depth surfaces with the corresponding temperature profiles varying along those curves. This sun represents the change in maximum emitted wavelength with distance from the center of the solar disk from the observer's perspective. It is important to note that neither sun is drawn to scale; the optical depth surfaces are idealized.

The Plank Distribution function that determines the spread of electromagnetic waves from a blackbody for a specific temperature illustrates that the peak wavelength for which intensity is maximum shifts to shorter wavelength for higher temperature is given by

$$I_\lambda = \frac{2\pi hc^2}{\lambda^5} \frac{1}{exp(\frac{hc}{k\lambda T}) - 1}. \tag{3}$$

If this distribution is integrated over all wavelengths λ, the result would be 1 when normalized properly, indicating that the total intensity of emitted light is distributed over all possible wavelengths. From Wein's displacement law, it can be shown that as the temperature increases, the wavelength at which the blackbody emission is maximized decreases [*Foukal*, 2008]. Conceptually, this makes sense because as wavelength decreases, frequency increases and so does the energy of each photon. As a consequence, when the sun gets cooler further out on the limbs, the maximum emitted wavelength seen at an optical depth of 1 in those regions becomes longer, making the limbs appear more red and darker than the center of the solar disk which will be more yellow.

This effect can also be visualized as the intensity drop off for large angles. When an observer receives the emitted radiation at an angle θ from the normal, there will be a decrease in the amount of photons he or she can receive. If the

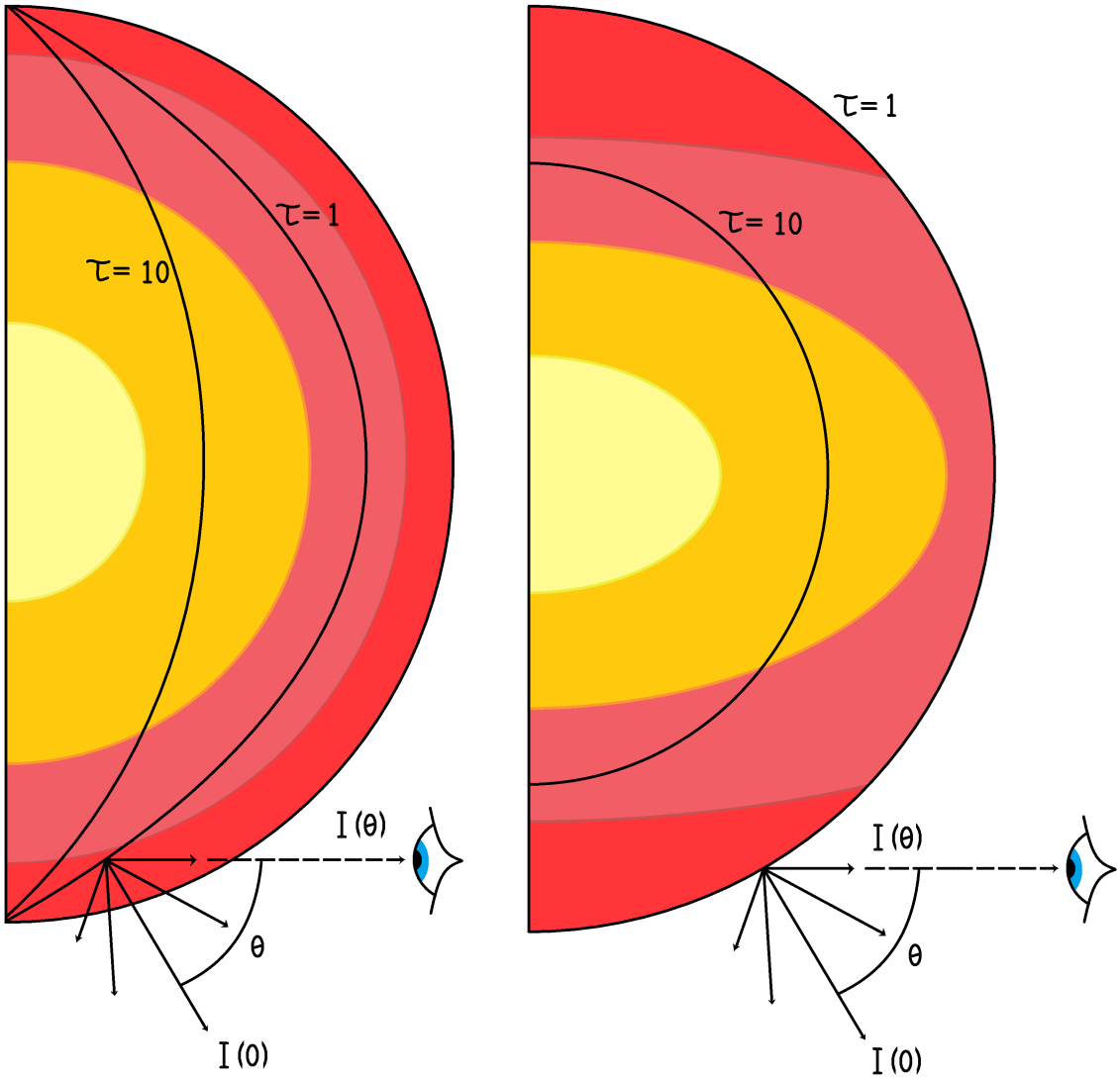

Figure 1. Optical depth dictates the intensity profile of the sun. Near the center of the disk, an observer can see farther into the sun where the temperature of the plasma is hotter. I is the intensity of light coming from any point on the sun and is a function of θ which represents the angle off from center towards an observer. τ is the optical depth surface where $\tau = 1$ is the surface of the photosphere.

radiator emits in the r direction, an observer only accepts the absolute value of the dot product between the propagation vector and the surface normal. Looking at the radiated power per solid angle,

$$dP_\lambda = I_\lambda(r, \theta) dA cos\theta d\omega d\lambda \tag{4}$$

where the $cos(\theta)$ term originates from this dot product, the radiated power falls off as a function of cosine near the edges of the sun. This additional way of viewing limb darkening is also summarized in Figure 1.

2.4 Sunspots

Sunspots are cooler regions on the photosphere that emit a lower intensity of light in all directions, therefore appearing darker than the rest of the sun. Sunspots are different from sunspot groups, the latter being a collection of the former. Because the magnetic field of the sun becomes twisted as a result of differential rotation, magnetic pressure can build up and force regions of higher magnetic field to compile within the sun. As the balance between magnetic and thermal pressure must remain constant, these regions with higher magnetic field become buoyant and rise to the surface, carrying the magnetic field along for the ride [*Foukal*, 2008]. The Magnetic Reynolds Number is a quantity that indicates whether or not flowing plasma will influence, or be influenced by, a magnetic field and is given by

$$R_m = \frac{\bigtriangledown \times (V \times B)}{\frac{1}{\mu_0 \sigma} \bigtriangledown^2 B} \approx \mu_0 \sigma L \tag{5}$$

where σ is the conductivity of the plasma and L is the characteristic length of the plasma [*Foukal*, 2008]. Because the Magnetic Reynolds Number shrinks outside of the region where convection dominates, the plasma entangled with the magnetic field in that region becomes trapped and eventually suspended against the gravity of the sun. Convection in these regions is mostly suppressed, eliminating the biggest source for heat on the photosphere . In this case, the magnetic field holds plasma in place, preventing sections from cycling back down to reheat. As the heat of these suspended regions is radiated away, the local opacity within the magnetic field begins to increase. When opacity increases, the region becomes optically thick to

light from the lower levels of the sun, giving the active region a darker appearance. Sunspots still emit radiation, but their lower temperature causes them to appear dark compared to the surrounding unobstructed photosphere. Sunspots can be different shapes and sizes but are likely proportional to the configuration of the magnetic field in their immediate region.

2.4.1 Evolution of Sunspots.

Although suspended by the magnetic field of the sun in the photosphere, sunspots are not static objects. As the magnetic field of the sun changes, sunspot groups can change shape, size and orientation on a short time scale. These groups can also develop additional spots, a characteristic that will contribute to the classification of the group, discussed in Section 2.5. Additionally, sunspot groups can drift on the solar surface, and the location of sunspot groups on the solar disk tend to decrease in latitude as the solar cycle progresses towards a maximum, known as Spörer's Law [*Foukal*, 2008]. It is therefore more likely to find spots near the solar equator when nearing a solar maximum.

2.4.2 Important Sunspot Features.

Because there are many different aspects that make up a sunspot group, it is necessary to identify key features that could be identified across different types of groups. Determined from observations and experience, important features include the number and proximity of spots, area of each sunspot in the group, as well as the presence or absence of a penumbra around the central umbra [*McIntosh*, 1990]. The proximity of spots refers to the angular separation between different spots that could make up a group. The area of each sunspot means the total area of the sunspot appearing on the surface of the sun at the bottom of the photosphere. The

umbra is defined to be the darker center region in the sunspot while the penumbra is the region surrounding the umbra that is still optically thick but is less dark than the umbra [*Foukal*, 2008]. Depending on the combination of these elements, a sunspot or sunspot group can be given one of 60 different classes through the McIntosh system [*McIntosh*, 1990] that are each associated with a flare probability based on previous spot-flare relations with that same classification.

2.5 McIntosh Classification

The features of a sunspot and other local sunspots considered part of a group are assigned a classification, defined by the solar astrophysics community using a three tier classification [*McIntosh*, 1990]. Based on a previous classification system developed by [*Kiepenheuer*, 1953], this method introduces two additional categories by which analysts can differentiate sunspot groups. This system takes into account size, area, orientation, fullness, and density of spots within a group and assigns a three letter code reported in the form 'Zpc'. In this notation, 'Z' represents the first letter, 'p' represents the second, and 'c' the third letter. Each letter series, shown in Figure 2, will be explained in the subsequent sections (Sections 2.5.1 - 2.5.3).

The term Zurich classification is sometimes used to describe the first letter in the code report ('Z'), but this refers to the modified Zurich classification used in the McIntosh scheme. Each part of the McIntosh code may also be referred to as "letters", sometimes interchangeably with the description of what each letter represents. For example, 'p' may be called the second letter, meaning that it is reported as the second part of the McIntosh code, even though it may be written as a single letter in this context. It may also be simple to think about the second letter as though it were written '-p-' where the 1st and 3rd classifications are omitted. Although the letters may be referred to as single items, they represent one part of

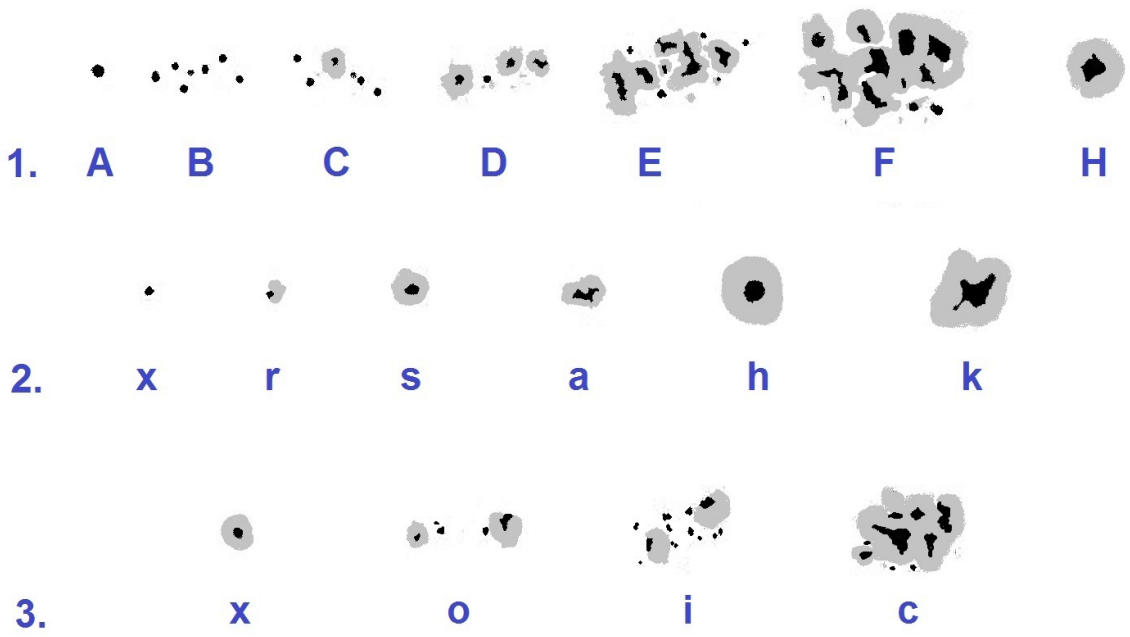

Figure 2. The different letters of th McIntosh classification scheme are shown; The full classification requires one letter from each series. Series 1 shows the modified Zurich classification letters. Series 2 shows the penumbra classification letters. Series 3 shows the compactness classification letters.

the three letter code. Every sunspot group must have a code for each letter, even though these letters could be addressed one at a time. The Zurich classification is always reported as a capital letter while the 2nd and 3rd letters are reported as lower case. The second two letters do not overlap by using any of the same designators (with the exception of 'x' which has the same meaning in both cases).

2.5.1 Modified Zurich Classification: 'Z'.

The first section of the McIntosh classification relates to the modified Zurich classification of a sunspot and is purely determined by the size or length of a sunspot group and presence of a penumbra within the spot group. This part of the classification is shown in series 1 in Figure 2. While there are plenty of elements to look at for this classification, certain subgroups will always yield a given

Table 1. Each letter of the modified Zurich classification is defined by a specific set of parameters including the presence or absence of penumbra within the sunspot group and the length of the sunspot group.

A	Unipolar sunspot group with no penumbra, either the formative or final stage of a group
B	Bipolar group with no penumbra
C	Bipolar group with penumbra on one end of the group
D	Bipolar group with penumbra on spots at both ends of the group with length $\leq 10^{\circ}$
E	Bipolar group with penumbra on spots at both ends of the group with length $10^{\circ} \leq 15^{\circ}$
F	Bipolar group with penumbra on spots at both ends of the group with length $> 15^{\circ}$
H	Unipolar group with penumbra

classification and some classifications are rare and do not occur on a regular basis. For example, if the spot is unipolar with no penumbra, the only classification capable of being assigned is 'A'. The criteria for determining the modified Zurich classification is shown in Table 1.

2.5.2 The Penumbra: 'p'.

The second classification depends on the presence or absence of a penumbra around the largest spot in the sunspot group. This is denoted by the number 2 in Figure 2. This step depends on the definition of a satisfactory threshold for determining both the penumbra and the umbra. Clearly, as not all leading spots have penumbra, there is a limit where certain groups will not even qualify for the second tier of classification. Therefore, logical determinations for this step are dependent on certain situations and will not always be necessary. The criteria for determining the Penumbra classification is shown in Table 2.

Table 2. Each letter of the penumbra classification is defined by parameters including the size and shape of penumbra on the largest sunspot within the sunspot group.

x	Undefined, no penumbra
r	Rudimentary, incomplete penumbra partially surrounding the largest spot and granular in nature.
s	Small, symmetric penumbra. Mature, dark penumbra surrounding the leading spot. The North-South diameter of the penumbra is $\leq 2.5°$
a	Small, asymmetric penumbra. Penumbra of the largest spot is irregular and multiple umbra within the penumbra exist. North-South diameter of the penumbra is $\leq 2.5°$
h	Large, symmetric penumbra. Same as class 's' but the North-South diameter of the penumbra is $> 2.5°$
k	Large, asymmetric penumbra. Same as class 'a' but the North-South diameter of the penumbra is $> 2.5°$

Table 3. Every letter of the compactness classification is defined by parameters including the number of sunspots in the group and the number of sunspots surrounded by penumbra in the group.

x	Undefined, group is unipolar.
o	Open group. Few, if any spots between leading and following spot. Interior spots are generally very small.
i	Intermediate group. Numerous spots between leading and following spots. No interior spots posses penumbra.
c	Compact group. Area between leading and trailing spots is heavily populated and at least one interior spot posses a mature penumbra.

2.5.3 Sunspot Distribution: 'c'.

The final classification relates to the presence or absence of additional spots between the leading and trailing spot in the sunspot group. The more spotted the group is, the more irregular the magnetic field in that region. Therefore, the three different types under this classification pay attention to the increase in magnetic complexity in the region of the sunspot group, in addition to the spread of the convection suppression. Examples of this third category are shown in Figure 2. The criteria for determining the sunspot distribution classification is shown in Table 3.

2.6 Solar Dynamics Observatory

The SDO is a NASA sponsored satellite that was launched in 2010 to observe the sun at various wavelengths of the electromagnetic spectrum. The SDO orbits the earth in a circular geosynchronous orbit at an inclination of 28° [*Pesnell et al.*, 2012]. An orbit of this type yields nearly continuous observation of the sun with the exception of a 1-2 month period during the year when the sun is blocked by the earth for a short period of time every day. The SDO takes a high resolution photo of the sun every minute at many different wavelengths in order to get a full picture of solar effects and their impact on the earth. This is done through a combination of instruments: the Atmospheric Imaging Assembly (AIA), Extreme Ultraviolet Variability Experiment (EVE), and the Helioseismic and Magnetic Imager (HMI) [*Pesnell et al.*, 2012]. There are two types of images focused on in this research. The first image used is a Helioseismic and Magnetic Imager Intensitygram (HMII) full disk continuum image centered at $6173.3 \pm 0.1\mathring{A}$ [*Schou et al.*, 2012], providing a high spatial resolution image of the photosphere that is synchronized with the second image, a full disk Helioseismic and Magnetic Imager Magnetogram (HMIM). The HMI instrument measures the Zeeman effect variation of the Fe I spectral line coming from different locations on the photosphere, yielding the Stokes parameters necessary to determine the magnetic polarity of those regions [*Pesnell et al.*, 2012]. The various pixel values in the HMIM image represent the intensity of the magnetic field in each region, white being opposite black and gray having no particular polarity. Pixel values in the HMII image represent the intensity of light, and images can be obtained in color or grayscale.

2.7 White Light to Fe I Line Comparison

Drawings performed on the Solar Optical Observing Network (SOON) telescope use white light projections spanning a wider range of wavelengths compared to SOHO MDI and SDO HMI images. Precedence has been set for using images centered on both the H-alpha line at $6563\mathring{A}$ and the Ca II K line at $3934\mathring{A}$ [*Zharkov et al.*, 2005] for automated detection and classification. In addition, groups have also used SOHO MDI imagery (upon which the SDO HMI instrument is based) centered on the Ni I $6768\mathring{A}$ line [*Aschwanden*, 2010; *Schou et al.*, 2012]. However, there are differences between filtered images and white light images, primarily having to do with the height at which the optical depth reaches unity, similar to the limb darkening effect discussed in Section 2.3. Therefore, depending on the wavelength being observed, the height of the observation surface will change and the features on that surface may be different than the features an observer would see in white light. Note that electing to use filtered imagery will change the height at which sunspots are observed. Wien's displacement law [*Foukal*, 2008] shows that

$$T = \frac{2.89776829 \times 10^6 [nmK]}{\lambda [nm]} \tag{6}$$

This law is used to show that the temperature at the surface of the H-alpha filtered image is approximately 4400K and the temperature at the surface of the Ca II K filtered image is approximately 7400K. Both of these temperatures are reached in the chromosphere, the layer above the photosphere. The SDO Fe I line at $6173\mathring{A}$ sits between both the Hα line and the Ca II K line, meaning that it's temperature will be between those line's temperatures as well. The maximum extent of the chromosphere above the photosphere is approximately 2000 km [*Foukal*, 2008], indicating that the change in height of the observation surface between any of the

absorption lines and the white light image (assumed to be at the base of the photosphere) will be less than $100(2000km/695500km) = 0.288\%$ the radius of the sun. While this height difference may have an effect on the shape and extent of the sunspots, there is precedence for neglecting this difference due to the fact that the features do not change much between the photosphere and the base of the chromosphere. The main difference is that filtering the sun to a specific wavelength reduces the contrast between sunspot and quiet sun, introducing some difficulty in detecting the darker regions.

Moreover, the SDO method uses both magnetic and optical information to perform a classification, an impossibility when using other types of images. No other image produces the required data for this process, so differences associated with comparing the Fe I line images to white light drawings are accepted. These errors are assumed to be negligible when comparing sunspot quantities and classifications.

2.8 Automation Approach

The first step in the completion of this research was to build a robust method for sunspot detection based on a set of objective rules outlined by McIntosh [*McIntosh*, 1990]. In using the largest size image available, produced every minute by the SDO, the resolution of the automated program is much higher than many previously implemented methods. This portion of low level image processing is completed carefully so as to minimize the error associated with quantized intensity values and the calculation of important elements that depend on approximations like the limb darkening. Once the initial task of detection is completed, a series of logical operators is arranged to establish groupings as well as a classification of each group based on the McIntosh Classification system covered in Section 2.5. While neural networks, similar to those used by [*Colak and Qahwaji*, 2008], can be advantageous

when training a computer's decision making with direct observational data, it can be argued that this process becomes compromised when applied to a system containing significant internal discrepancies. Discussed in Chapter IV, the inherent difference between a standard observatory and national standard published sunspot reports yield agreement percentages as low as 22.1%. While these observations are made at different times throughout the day and spot group evolution is expected, discrepancies between reporting groups are not small, often displaying differences of up to 4 levels in Zurich Classification (A to D or B to E, also addressed in Chapter IV). It is because of this difference that the implementation of a strictly objective classification and grouping process that is unbiased by any human input, past or present, is used. This emphasizes that comparisons made to observatories or reporting entities do not necessarily represent the proximity of the algorithm to ground truth. On the contrary, these comparisons simply represent the proximity of the algorithm to to the average classification published for that day based on the varying interpretation of McIntosh classification principles.

2.9 Hand Drawing Method

The Air Force has established methods for observing and classifying sunspots at three separate optical observatories around the world. Methodology for classifying and reporting of these sunspots is outlined in the Air Force Manual (AFMAN) 15-124 [*USAF*, 2013]. All analysts are trained through the same course taught at Holloman AFB, generally lasting a little over one month to cover not only the steps for performing the drawing and classification of each spot group observed, but also some of the underlying physics behind the process. It should be noted that spot drawings are only part of the work required of a solar analyst, so this instructional period also covers the additional duties that one would encounter while

on shift at a solar observatory, to include the time critical reporting of solar flares that may be seen on the solar limb. A full description of the hand drawing method used at AF Solar Observatories is addressed in Appendix 1.

2.10 Resolution Comparison

Resolution differences between a white light drawing board and a full size SDO image should be addressed. The CCD in the HMI instrument on the SDO satellite bins photons collected through the aperture and converts those signals into a digital count value corresponding to the intensity of the region. This binning causes a quantification error in that storing information in a pixel reduces a continuous span of intensity or magnetic polarity data from a span of the sun into discrete values that a computer can interpret. This quantization error can sometimes be significant, but it is important to realize that in the case of the full 4096 X 4096 SDO Intensitygram image, the spatial span of a single pixel is very small. To compare the resolution of the SDO image to the corresponding resolution on the AFWA Form 21, note that on average, the solar diameter in pixel space throughout the year on a full resolution SDO image is approximately 3800 pixels. Dividing the solar diameter of 18 cm on the Form 21, the ratio of pixels to meters is obtained, and the resolution that one pixel corresponds to in real space:

$$(1pixel)\frac{0.18m}{3800pixels} = 9.474 \times 10^{-5}m \tag{7}$$

Converting this value into a recognizable unit, it can be seen that in order to draw to the same spatial resolution as an SDO image, an analyst would need pencil accuracy of about 95 microns, a difficult feat to achieve. It can therefore be said with high confidence that the spatial resolution of SDO HMI images is better than the spatial resolution of the SOON telescope.

III. Methodology

This chapter details the development of the sunspot detection and classification algorithm using SDO imagery. To do this, a series of 5 distinct stages are accomplished in order to produce the final result: the sunspot classification. The first stage involves the acquisition of SDO imagery at a basic level of processing. In the second stage, elementary image processing techniques are used to condition the data. The third stage involves the detection of sunspots on the conditioned solar images. In the fourth stage, polarity and sunspot location information is incorporated to obtain sunspot groupings. Finally, the classification stage produces the end result in the form of a McIntosh classification for each detected sunspot group. This process is summarized in Figure 3.

A simple analysis of each image processing tool used in the SDO program justifies every step, but these tools are well established and therefore not addressed in high detail. Following the development of the automated program, methodology for analysis of the output is discussed by first establishing the accuracy of the method compared to the output from two trusted sunspot reporting sources. This accuracy analysis will be performed in Chapter IV with respect to elements such as sunspot area, group length, and McIntosh classification.

3.1 Image Acquisition

Images were downloaded in the highest available resolution from the NASA SDO archives for processing in MATLAB. In order to procure a current image of the sun, or any archived images at 15 minute time steps [*Pesnell et al.*, 2012], the SDO main website was used (*http://sdo.gsfc.nasa.gov/*). During the testing process, a years worth of data spanning from 1 July 2012 to 30 June 2013 was

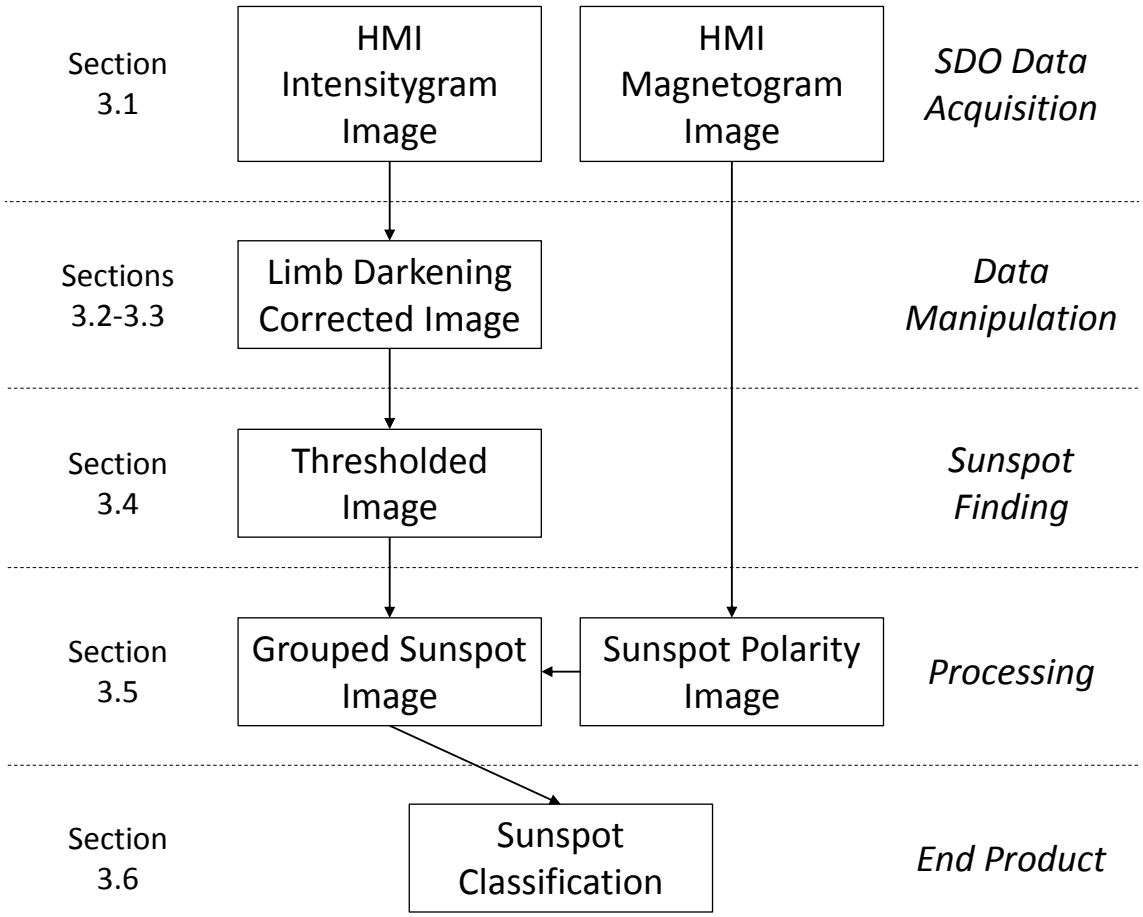

Figure 3. The five basic phases of the SDO code are summarized in a flow chart. The corresponding Sections of this document are listed adjacent to each step.

downloaded from the SDO website with the aid of NASA Goddard's input of image queries. The HMIM image is downloaded in gray scale to limit the size of the image as color is not necessary for classification.

3.2 Solar Ephemeris

In order to obtain the rotation parameters of the sun and the approximate position of the SDO with respect to the sun at the time any image is taken, the solar ephemeris is needed [*Seidelmann and Urban*, 2010]. Conveniently, there are several other useful parameters that can be extracted from the solar ephemeris that

become necessary in subsequent sections of the program, so the computation of the position of the SDO satellite is essential to the automation process. Numerical methods for calculating the solar ephemeris were duplicated from the Improved Solar Observing Optical Network (ISOON) code [*Meeus*, 1982; *Wilson*, 1980].

First, the time of observation is taken from the image header and processed into a Julian Date, a simple single digit representation of time. The elapsed time is determined from January 1st, 1900 and reported in terms of Julian Days. This number is used to calculate the longitude of perigee, mean anomaly, equation of center, eccentricity, and the right ascension of the ascending node, all described in [*Meeus*, 1982]. These parameters, displayed in Figure 4, are not used directly in the code but are important to mention for completeness.

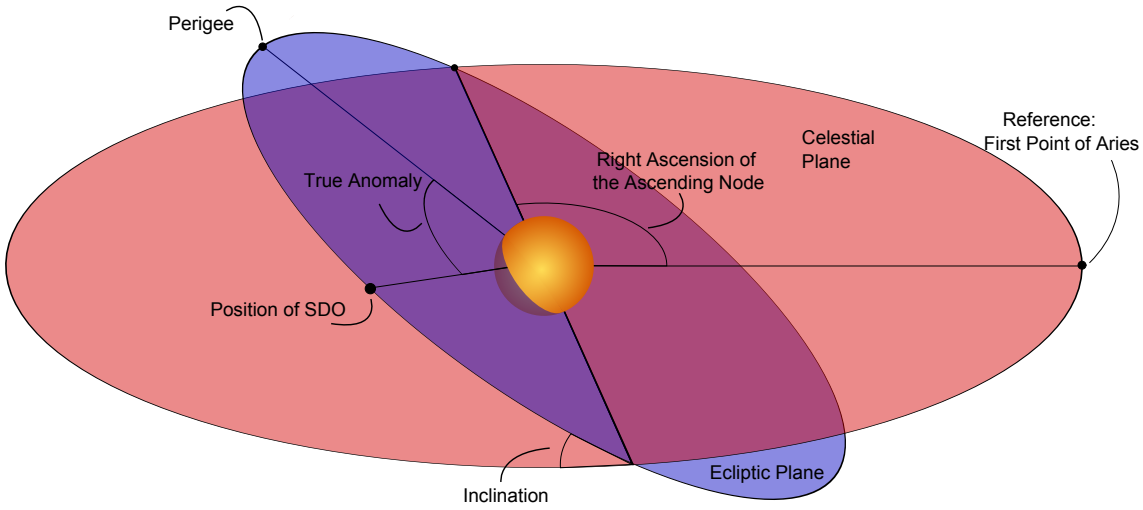

Figure 4. A simplification of the SDO orbit around the Sun is illustrated by the blue ellipse while the celestial plane is shown in red. Orbital parameters are calculated with reference to the location of the first point of Aries.

A main item that is useful in the calculation of the solar ephemeris is the approximate radius of the sun as seen from the SDO. Because the position of the earth with respect to the sun is also determined from the ephemeris, an approximation for the sun earth distance can be used to get an approximate solar

radius in pixels. To put the radius into the appropriate units, as it is calculated in meters, it must be multiplied by a constant of proportionality determined through a calibration step. To do this, the radius of images spanning an entire year was combined with the various orbital positions determined through the date. By averaging that ratio for radius and position values for each image sampled, the average constant of proportionality was experimentally determined to be 2.8476×10^{14}. Figure 5 shows the calculated radius values for a specified period of time. Sigma is the size of the smoothing filter used to calculate the radius of the sun in each individual image via the Laplacian of a Gaussian comparison, explained in Section 3.3.1. The approximate radius of the sun in pixels was then extracted from the ephemeris for the edge detection algorithm to ease the computational intensity of center and radius determination, discussed in Section 3.3.2.

An additional item extracted from the ephemeris was the B angle, defined to be the angle tilt of the solar north pole towards or away from the observer and orthogonal to the solar ecliptic [*Seidelmann and Urban*, 2010]. This angle is continuously changing as it is a function of time as the Earth orbits around the sun. When determining the coordinate system to use on the sun, the B angle was important to establish the location of both zero longitude and latitude [*Thompson*, 2006]. If the B angle is zero, then both longitude and latitude are equal to zero at the very center of the sun. However, non-zero B angles cause the latitude to shift either up or down on the disk. The Carrington Longitude is neglected when reporting the position of each spot group [*Thompson*, 2006], but the longitude is still affected by the tilt in the sun. The approximate solar diameter in radians is also extracted from the ephemeris because it helps speed the calculation of the radius in later steps.

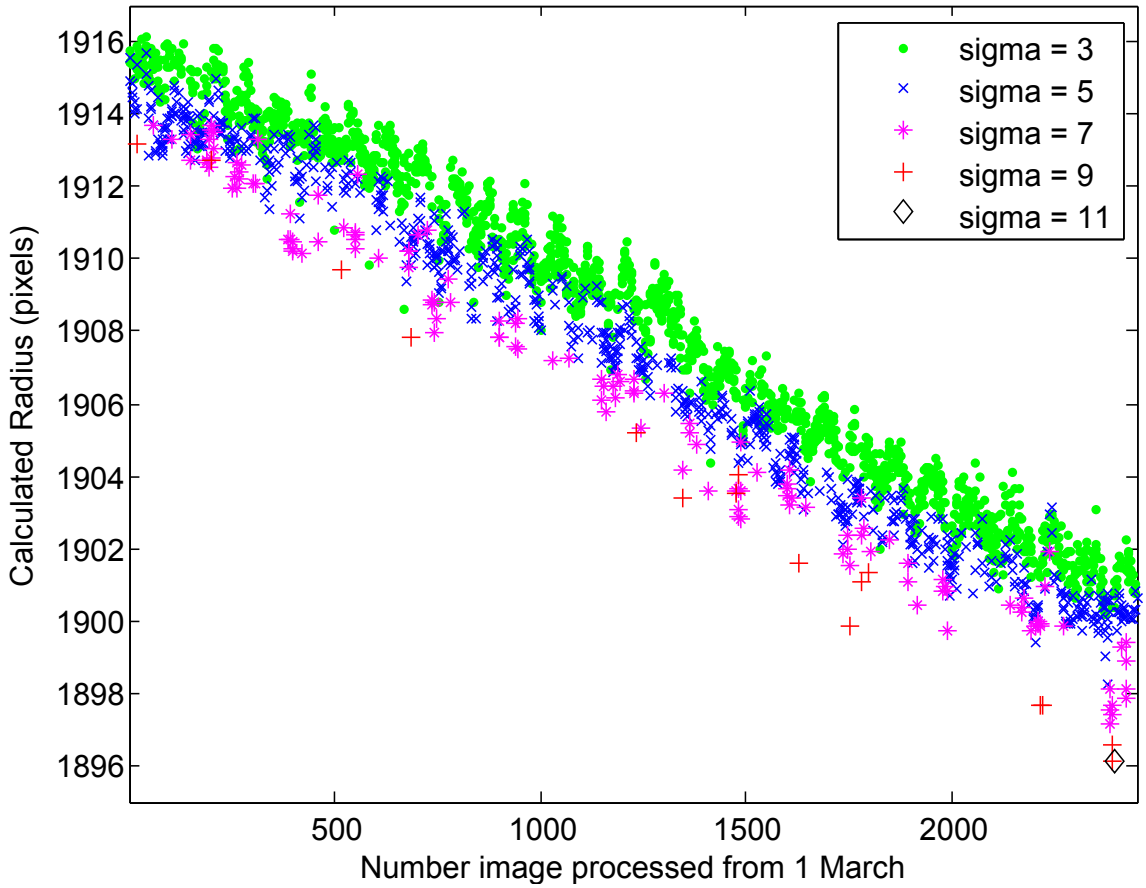

Figure 5. The radius of the sun in pixels is shown to linearly change over the month of March, 2013.

The P angle is defined as the angle of rotation between the solar North Pole and the celestial North Pole as seen from the observer's position. In SDO imagery, level 1 image processing corrects for the P angle beforehand , described by [*Lemen*, 2012], so the SDO algorithm does not incorporate a correction for this angle. If a P angle correction is needed, perhaps in follow on research to apply the code to a wider variety of images, it can be accounted for when determining the longitude and latitude of a point on the disk. The value of the P angle for any given time is determined from the ephemeris and was calculated in the program. The method for this calculation is specified in [*Meeus*, 1982], but is not essential for this research.

3.3 Image Preparation

After an image has been selected, it is imported with its counterpart magnetic map in the form of the HMIM image. Both HMII and HMIM images match each other in terms of time, a luxury not available to previous renditions of this endeavor using SOHO images [*Aschwanden*, 2010]. Additionally, they will also have the same spatial resolution, useful in future steps for overlaying the two images as points will not need to be mapped to a different coordinate system for processing. Each color band of the HMII image is not necessary for any steps in the code development, but is useful in visualization of calculated features. The Red, Green, and Blue (RGB) image is converted to gray scale for processing, shown as number 1 to number 2 in figure 6 by averaging the elements in adjacent color bands. This choice was made because each color band does not yield the same size sun, so it is difficult to use them in conjunction. In the future, starting with grayscale images may be more practical.

With some previously implemented methods [*Watson and Fletcher*, 2010; *Watson*, 2012], sunspot tracking was the primary focus. Other previously explored automatic recognition and classification methods require a computation of longitude and latitude using a single image for sunspot recognition and tracking purposes outlined in the [*Aschwanden*, 2010] review of feature recognition techniques. In this method, it is necessary to know the pixel location of the center of the disk as well as the radius of the sun in pixel space if spot positions are to be mapped to heliographic coordinates (or any other coordinate system). Because the SDO algorithm must function on a single image and is not focused on any type of tracking, the route of edge detection first was pursued.

A combination of tracking with position detection is possible assuming image reconstruction is used after edge detection for recognition of sunspots. This method

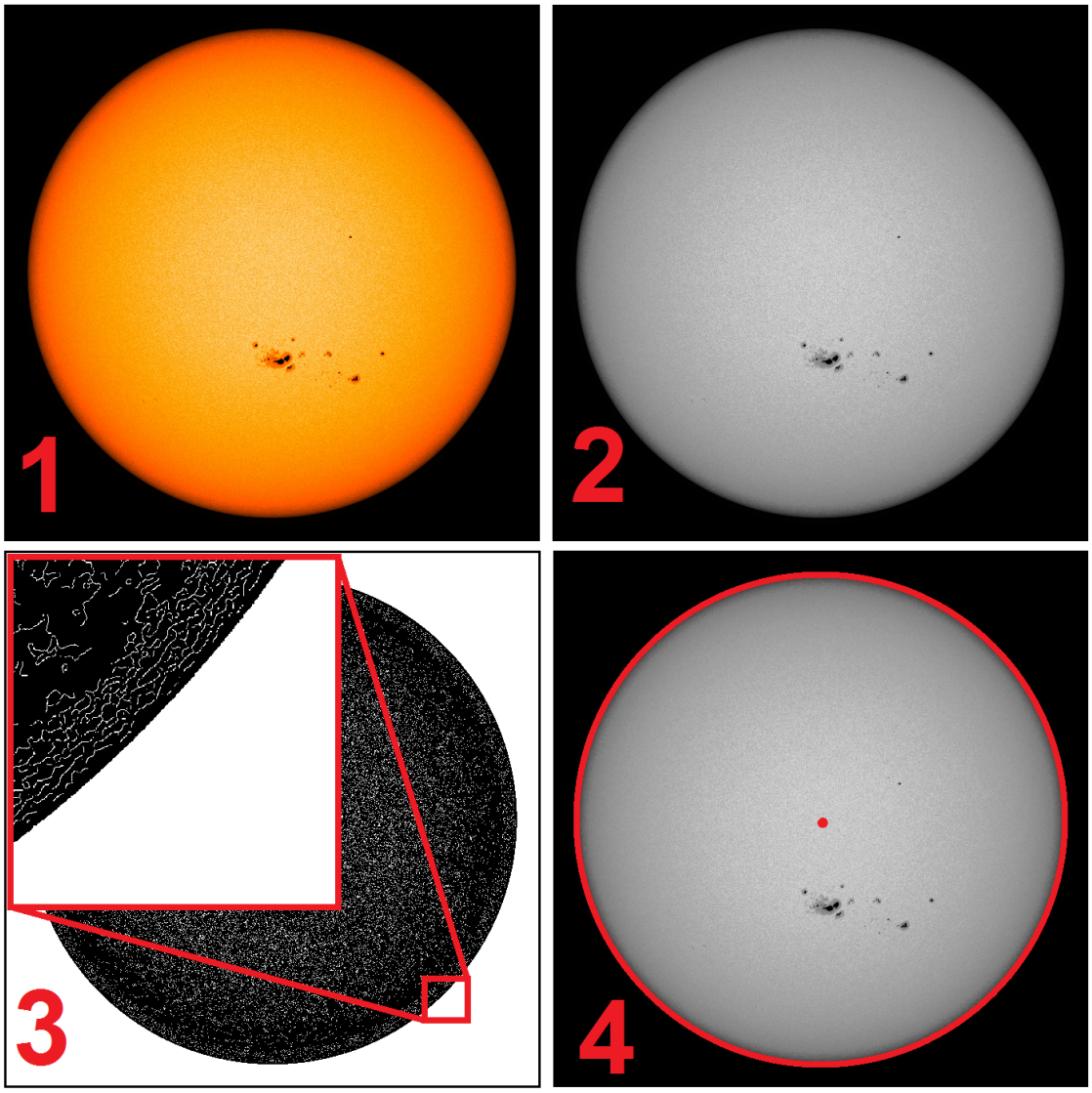

Figure 6. The color Intensitygram image is read into MATLAB and displayed in section one. Section two displays the grayscale image created by averaging the red, green, and blue planes of the color image and normalizing to the uint8 scale. Section three represents a filled black and white image post canny edge detection, demonstrating the extent of the sun to be used in the calculation of the radius and center of the sun, as displayed in the fourth section.

of morphological reconstruction has been previously preferred for its speed, but morphological methods like reconstruction are non-linear processes that alter the data in an unrecoverable way [*Gonzalez and Eddins*, 2009]. In order to avoid this loss of data, the SDO method minimizes morphological processing and instead uses

an iterative thresholding technique to grow spots in a similar manner without using reconstruction. This idea is explored in Section 3.4.

3.3.1 Edge Detection Process.

The next step in algorithm development is edge finding. The ultimate goal of defining the edges on the sun is to find both the center of the sun in pixel space as well as the radius in pixels of the sun. Representing the sun as a circle is the first step to accomplishing this goal. The edge detector selected to perform this task uses the Canny technique for edge definition [*Canny*, 1986] shown in Figure 6 as Image 3. Because of the large size of the images used (approximately 4-5 MBs), the kernal size convolved with the image during the Gaussian smoothing step to define edges is minimized in order to limit the number of calculation steps. In addition to limiting the calculation steps, reducing the size of the convolution kernal (the same sigma described by Figure 5) decreases the position error of the edge because a larger smoothing filter tends to introduce ambiguity in the line being detected [*Gonzalez and Eddins*, 2009]. When determining the size of the radius as well as the center of the sun, the edge must be roughly circular in order to determine a best fit circle. This means that there is a trade off between position error and minimizing kernal size for speed and maximizing kernal size for ease in the determination of the radius. A default value of 3 is used for the width and height of the Laplacian of a Gaussian filter, defined to be the weighted kernal type applied to an image during a convolution step. The default value is increased in steps of two if a radius and center is not found for a particular iteration of circle detection in order to keep symmetry in the kernal.

Edges are calculated through the evaluation of a the local gradient inside the convolution kernal. When pixel values associated with each element inside the

kernal change rapidly, the gradient for that kernal is large. Above a defined threshold, pixels that satisfy the gradient become white, while other pixels are set to be black resulting in a binary image. This image is then filled and processed by the center and radius calculations described in the next section. Iteration for edge detection is generally unnecessary as both the radius and center values are usually found on the first try because of the acurate approximation of the size of the sun in pixels from the ephemeris. If additional iterations are needed, the processing time needed to complete the image increases, and the accuracy of the radius decreases by one to two pixels, shrinking the value of the calculated radius. Upon testing this method for over a months' worth of images (approximately 2500 images from March of 2013 seen in Figure 5), images that required a sigma value of 5 or more yielded a radius value of about 2 pixels less than the average. This is corrected by adding a factor of $\sqrt{\frac{\sigma}{3}}$ to the radius for values that needed a sigma value over 3. This need for this correction factor can be seen in Figure 5 in that higher sigma values give lower radii values.

3.3.2 Center and Radius Determination.

The second part of this iterative loop is the determination of the center and radius of the sun in each image. This is done using a circular hough transform, encompassed in MATLAB's imfindcircles function [*Gonzalez and Eddins*, 2009]. The circular hough transform takes a binary image and maps all points with a value of one in real space into parameter space. Points that lie on perfect circles in real space will be mapped to a single point in parameter space with coordinates representing the descriptive parameters defining that circle in real space [*Gonzalez and Eddins*, 2009]. However, the discrete nature of binning in the CCD camera as well as the slight oblations of the sun causes an imperfect circle representation in an

image. In practice therefore, points are mapped to parameter space where axis define the radius and center of all possible circles. Points are given a weight based on their proximity to every other point in parameter space. Regions/local areas with enough points to satisfy a threshold value, selected by the user through specification of criteria, are fitted to yield a single point that best represents all the points in that group. The selected point is mapped back to real space, giving both the approximate radius and center that best describes the combination of points constructing the circle. This method yields sub-pixel accuracy, even on full 4096 $\times$ 4096 images [*Gonzalez and Eddins*, 2009]. In using the circular hough transform in MATLAB, a user can specify certain values that pertain to both the threshold level desired as well as the radius range in which points should be tested [*Gonzalez and Eddins*, 2009]. The threshold level is set through the alteration of a sensitivity parameter that was set to 0.99 in order to limit the number of circles found. For reference, a value of 1 corresponds to a perfect circle, likely an impossibility in a digital image. The radius range, on the other hand, can be hard coded, but it is simpler to pull out an approximate value and decide the range based on this initial guess of a radius. Because the SDO is in orbit around the Earth and therefore does not follow a perfectly circular orbit around the sun, the radius of the sun as viewed from the SDO position changes throughout the year. This change can be predicted using the ephemeris of the sun, as shown in Section 3.2. The eccentricity of the Earth's orbit allows the calculation of radial position:

$$r = \frac{1 - e^2}{1 + e\cos(\nu)} \tag{8}$$

where ν is the true anomaly (shown in Figure 4) of the SDO with respect to the sun and e is the eccentricity of the orbit [*Meeus*, 1982]. Although ν is numerically approximated and the value of r will not be exact, this value can still be used to get

a good guess for the radius of the sun. This radius will be in SI units, so the constant of proportionality mentioned in Section 3.2 will be needed to obtain the approximate radius in pixel space. From here, our program uses this number to put an upper and lower bound on the radius range through which MATLAB will search for circles. A range of 1% variation above and below the radius guess is sufficient to find the center and radius of the Sun in all images. This approach also significantly reduces the computation time required to find the radius as the range required to test is minimal.

If a faster result is required in order to get a quick classification, there is an option to compress the image before determining the center and radius. This compression combines pixels in a non-linear fashion and therefore introduces small errors in center position and radius depending on the amount of compression used. Additional compression, decreases the processing time required to determine the edge of the sun, but there is a trade off with accuracy. It should be noted that the compressed image is not used in subsequent calculations, this compression is solely used to calculate the radius and center of the sun. In practice, no compression is applied to processed images to ensure the most accuracy possible. In addition, this step is not necessarily the most computationally intensive step and in reality, does not add too much time to the total computation time for each image.

3.3.3 Limb Darkening Correction.

The next step in this process is to correct for the Limb Darkening effect outlined in Section 2.3 . The simplest way to complete this correction is to create an inverse image of solely quiet sun with the same radius. In this case, both the inverse quiet sun image could be added to the image being processed, simply canceling out any curvature in the intensity and leaving a flattened sun.

In order to create the inverse solar image to add to the SDO image being processed, an initial matrix is created and given the value of one at every position. Next, a linear range spanning the size of the solar image is mapped to the ones matrix to create a type of coordinate system in matrix form. The limb darkening approximation known as the Eddington approximation [*Foukal*, 2008] is then mapped to this coordinate matrix using the matrix as a position, resulting in an image containing intensity values corresponding to the Eddington approximation curve. This calculation is performed using the relation

$$I = 1 - \frac{1 + \sqrt{3}\rho}{1 + \sqrt{3}} \tag{9}$$

where I represents the intensity lost on the limb and ρ is the angle between the center of the Sun and the location being corrected [*Foukal*, 2008]. Both the center pixel obtained in the edge finding routine and the radius of the sun in the corresponding calculation are included in this approximation. The background of the image, meaning the part of the image that lies outside the radial distance from the center of the sun, was given an intensity value equal to the quiet sun to simplify the sunspot detection phase. This image can subsequently be added to the SDO image from which it was constructed in order to obtain a flattened image of the sun to a first order approximation, as shown in Figure 7.

3.4 Thresholding

Previous methodology for determining the location of sunspots in a given image generally involved region growing techniques through the use of morphological reconstruction outlined by [*Aschwanden*, 2010]. This process uses a matrix of starting guesses for the location of each sunspot in the image known as the marker image as well as the original image for a mask. The purpose of the mask is to allow

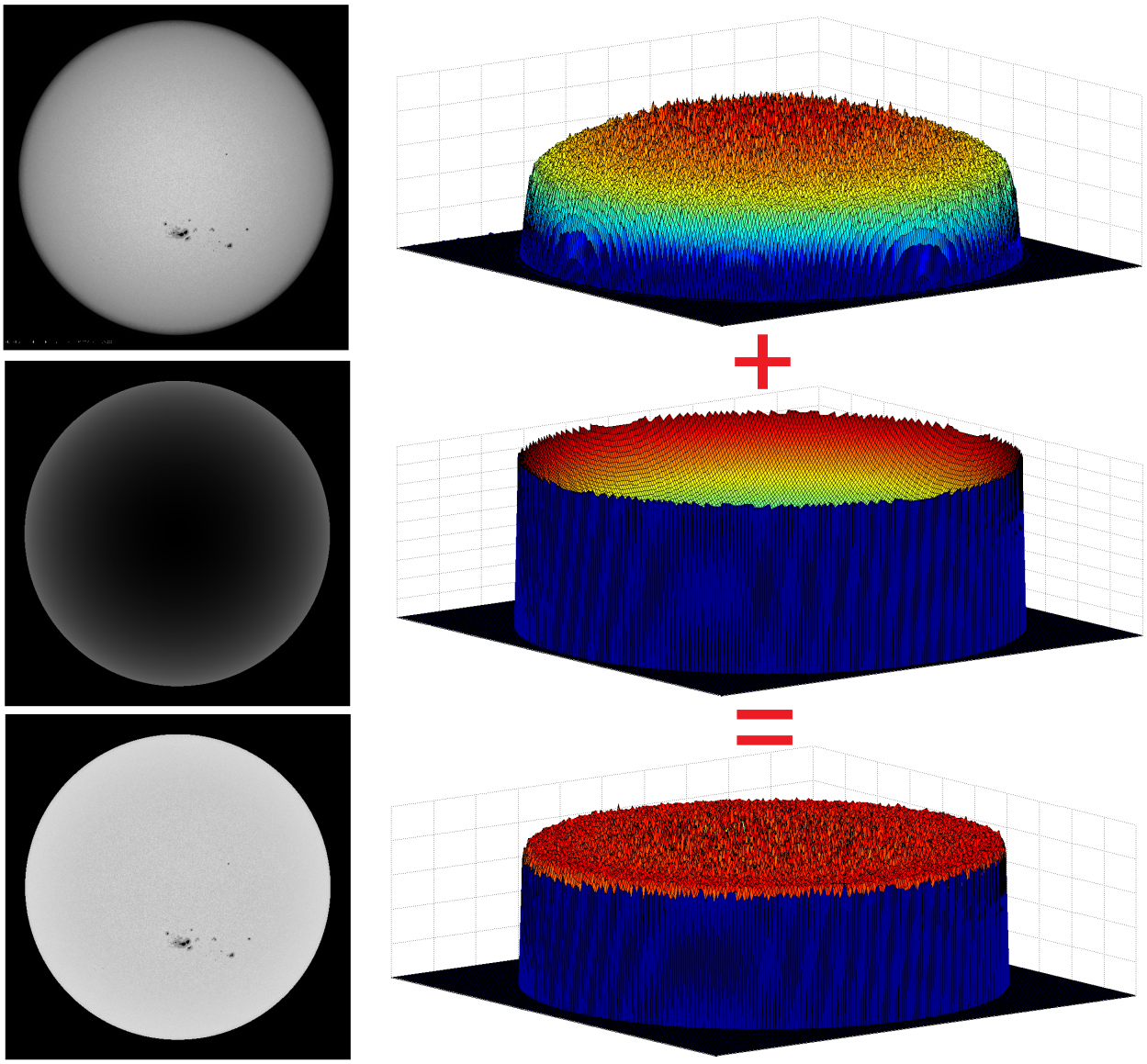

Figure 7. The original image in grayscale is plotted both as an image and using a three dimensional surface representation. In the center, the correction image determined by the Eddington Approximation is shown as an image and in three dimensional form. The two images are added together to reproduce the corrected "flat" sun shown at the bottom of the figure. This final image can inverted and thresholded in the next step to determine the location and size of each sunspot on the image.

regions to grow outward through morphological openings to the maximum extent of the spot seen on the original image [*Gonzalez and Eddins*, 2009]. The marker image is grown through gradual opening of single pixel regions until the edge of the object

being grown is reached in the mask image. From this point, reconstruction continues until the resulting image doesn't change with subsequent iterations. This final image should be a binary image with a full representation of each sunspot grown on the solar disk in a black and white format. Reconstruction of this type depends heavily on the starting positions in the marker image being accurate. Only regions that are marked will be grown to the correct extent in the final image. If a spot is not marked, it will be missed and appear dark on the final image. Many previous implementations of this process have had difficulty finding small spots/pores with their marker images [*Colak and Qahwaji*, 2008; *Zharkov et al.*, 2005]

In order to prevent this potential loss of spots and to avoid any morphological non-linear processes that may also be necessary to reconstruct the sunspots in our image, the SDO code uses a simple thresholding method to obtain the necessary black and white product similar to [*Curto et al.*, 2008]. This method is more susceptible to noise on the image as well as any granulation visible on the surface near the center of the disk due to the fact that pixels meeting the threshold requirement are accepted, although this can be minimized by limiting the rate of change of accepted sunspots discussed in the following section. Thresholding, instead of opening by reconstruction, is a simple way to select the regions to be labeled as sunspots. By systematically approaching the optimal threshold value at which the spot regions will be defined, this method avoids missing any starting point on a mask required in the morphological reconstruction of the image. In this way, the number of spots is solely dependent on the intensity value of the pixels used to describe each region.

The method takes advantage of the noise inherent to the system by capping not the number of sunspots detected, but the amount of change in the number of sunspots detected between different threshold levels. This detected number of

sunspots is found through the use of a connected components routine [*Gonzalez and Eddins*, 2009], a function that allows for clever representation of a black and white image. When the black and white image is acquired, a small 1×1 kernal is used to scan the image. When a white pixel is found, it is labeled one (or whichever region is being marked at that time). Next, the adjacent pixels are checked for color; if any are white, they are also labeled one. This process is continued until all pixels adjacent to the region are black and there are no other white pixels connected to the region [*Gonzalez and Eddins*, 2009]. After the region is defined, the function continues scanning for the next white pixel that hasn't been labeled (labeling the pixel with 2, 3 and so on), completing the same process until the entire image has been treated. This black and white labeling technique can be seen in a simplified example shown in Figure 8. The product of the labeling function is a matrix with each region, or in this case spot, labeled with a different number in the same location that region appears on the original image.

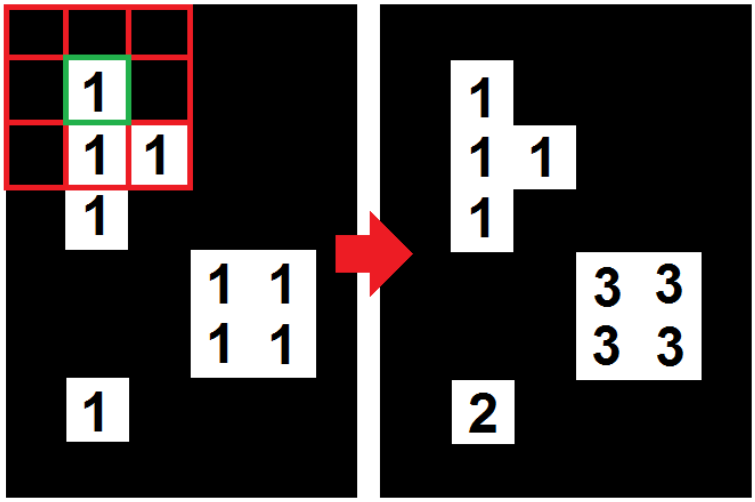

Figure 8. Images are convolved with the 1×1 kernal shown as green square. The pixels adjacent to the kernal (shown in red) are checked for matching pixel values. White pixels start out with a value of 1 while black pixels are 0. After the labeling technique, black pixels still have a value of zero while all white pixels are are given a pixel value equal to their region number.

The threshold at which the grayscale image is treated starts at a value of 0.8 in which few pixels are determined to be dark enough to satisfy the threshold requirement. Next, beginning with larger increments at first, the threshold is dropped in a sequential order. Every time the threshold value is dropped, the function runs a connected components routine that only returns the number of spots detected. This number is subsequently compared to the initially calculated number of spots to get a rate, and if the growth is below a set expansion rate, the threshold is permitted to drop once again. The threshold will continue to drop in this manner until the growth jumps up significantly, indicating that the method is beginning to pick up a large amount of noise. When this happens, the threshold increment previously subtracted is added back to the point where no noise was detected, and the increment by which the threshold level is dropped is reduced by a factor of ten. In addition to the increment by which the threshold level is changed, the amount by which the number of spots can change is reduced. Monitoring the change between a sequence of threshold levels is important for determining when the noise threshold has been reached, but if the value of change to which each iteration is compared is fixed, the method really only accepts up to a particular number of spots in the image. Therefore, it is necessary to alter the value of the change threshold so that the number of spots is permitted to grow to any number as long as the spots are dark enough to be distinguished from the noise in the image. The number of accepted change in spot counts starts large (50) and decreases to a small number (1) with multiple iterations. The process of iterative reduction is repeated until the step size by which the threshold is reduced reaches a magnitude of 10^{-4} accuracy at which point the resulting threshold level is applied to the corrected gray image for the resulting black and white image that is subsequently labeled using the same connected components routine [*Gonzalez and Eddins*, 2009].

This method performs exceptionally well when working to define the extent of the penumbra from the darkest areas in each spot groups. As the threshold level is dropped, the darkest portions of the image become accepted first. From these points, lower threshold values, in practice, will incorporate points surrounding these dark spots, effectively growing the size of each spot region. This growth is permitted to the point where a lower threshold value begins to incorporate noise, at which point, the method has defined the penumbra completely within the image. Typical threshold values determined to be acceptable by visual inspection generally end up at approximately 0.35 (also interpreted as 35% the intensity of the brightest pixel). Combining these results with knowledge of studies showing umbra intensity values typically prove to have 15% the intensity of the brightest part of the sun [*Foukal*, 2008], the umbral regions can be defined as the pixels that are 20% darker than the penumbral regions. To do this, the corrected gray image is converted to black and white again, but at a threshold level that is 0.2 higher than the threshold level used to define the penumbra. This level does a good job capturing all the pixels an observer would consider umbra on the image. The finalized black and white umbra image is also returned to the function for comparison to the penumbra image.

3.5 Group Definition

With the labeled matrix containing each of the penumbra regions defined by our thresholding routine, the next step involves separating each of these regions into their respective groups. Group definition involves an iterative loop that tests each region against a set of criteria to determine if that region belongs in the group currently being evaluated based on the McIntosh paper [*McIntosh*, 1990]. This process is computationally expensive due to the multiple criteria that go into

determining which spots belong in what group. This section of code therefore takes up the largest amount of time.

It is first important to establish the criteria for determining whether a spot belongs in a group. Because the SDO method will be compared with the product of solar analysts at Holloman AFB, it is important to use the same criteria in order to establish a baseline to compare the same groups for the same images [*USAF*, 2013]. Results will be meaningless if comparisons are made between two different products. All analysts follow the AFWAI, but subjectivity in the classification process can sometimes cause analysts to disagree on groupings. Groups are defined using a combination of length between spots in heliographic degrees and the different magnetic polarities of each spot being considered. For a spot pair that has the same polarity and small angular separation, the pair will be considered to be the same group if the distance between the two spots is less than or equal to 3 heliographic degrees. All the spots within 3 degrees of the centroid of a group therefore will be considered part of that same group. If there is separation outside of 3 degrees, spots of the same magnetic polarity will not be considered part of the same group. However, if the polarity of the two spots being considered for grouping is opposite, larger length values are considered appropriate. As long as there are spots along the path between the first spot in the group and the spot being evaluated that have alternate polarities, the evaluated spot will be considered part of the group beyond 15 degrees separation between the centroid of the group and the new spot [*USAF*, 2013].

In order to implement this process in MATLAB, the label matrix provided from the connected components routine is required [*Gonzalez and Eddins*, 2009]. Additionally, points taken from the image need to be transformed into heliographic coordinates in order to evaluate the true distance between each spot. Therefore,

before proceeding, it is important to establish the mapping system used to place positions in pixel space into real heliographic coordinates.

3.5.1 Distance Determinations.

Distance between spots is one of the two important factors used for determining spot groupings (the other being spot polarity). The mapping function

$$\cos(B)\cos(L - L_0) = [\cos(B_0)\cos(\rho) \pm \sin(B_0)\sin(\rho)\cos(\theta - P_0)] \tag{10}$$

can be used to determine longitude and latitude positions for each pixel determined to be part of a sunspot (See Appendix 2 for the complete derivation). After determining the location in pixel space of a particular spot, the center and radius values for the sun are used in conjunction with B angle values taken from the solar ephemeris to calculate spot positions in terms of heliographic coordinates. The spot position is subsequently compared to candidate groupings. Spot groups generally span from right to left as seen on the disk because the leading spot is generally closer to the equator [*Foukal*, 2008], but if a circular radius from the center of the spot group is used to determine which other spots belong in the group, spots may be admitted that don't necessarily line up with the East-West paradigm. With this in mind, a variable distance function is constructed weight the North-South direction more heavily so that groups will tend to form in a left to right fashion. This is done using the following latitude/longitude comparison:

$$d = \sqrt{(L_{spot1} - L_{spot2})^2 + 4(B_{spot1} - B_{spot2})^2} \tag{11}$$

where L is the longitude and B is the latitude. In addition to defining the distance in terms of heliographic coordinates, it is also important to establish an effective way for determining the magnetic polarity of each detected spot to compare with every other spot [*Foukal*, 2008]. To do this, a function is run that creates a logical matrix containing ones at the position of the spot group being analyzed, and this matrix is multiplied into the HMIM image to zero out all pixels that are not part of the current region on the HMIM image. Next, the pixels are summed and the total is divided by the number of pixels in the region to get an average pixel value of the group. If the average is below 127.5, meaning half of the maximum pixel value, the region is labeled as having polarity 1. Otherwise, the region is given a polarity label of 2. It should be mentioned that there is a possible scenario where a spot group has a δ configuration on the Mt Wilson scale (two separate polarities within the same penumbra). This would mean that part of the spot group would have a pixel value of less than the 127.5 cutoff while the other section would be above the cutoff. In this case, the function would simply label the spot with the predominant polarity in the region. This may make it difficult to expand the grouping method if a Mt Wilson classification scheme is desired later on, but for this research, it is unnecessary . In the case where a spot waiting to be grouped has magnetic polarity above the cutoff and the trailing spots in the group is also above the cutoff, there may be an issue with accepting the second spot if no other spots in the region have a low dominant pixel value indicating the opposite polarity, but this situation may rarely be the case and has never been observed. With this new tool set, each spot can now be compared effectively in a manner that appropriately groups the proper spots on the sun.

Grouping of detected sunspots is a problem that has been addressed multiple different ways and is the subject of ongoing research, summarized by [*Aschwanden*,

2010] and [*Verbeeck et al.*, 2013]. In order to prevent subjectivity form affecting the SDO system, this algorithm for grouping is defined in a manner that is precise and specific with regard to the physical characteristics of each spot. In other words, the algorithm is set up accepting some difference between reported spot groupings in favor of a method that is strictly defined in a way that can always be reproduced given the same variables. With this thought in mind, it should be noted that the algorithm does not attempt to diverge from the standard grouping technique, but is constructed in favor of a consistently biased result. The results here are supposed to be similar to those produced at all solar observatories as the grouping rules are still based on the McIntosh grouping techniques [*McIntosh*, 1990]. In many ways, this new grouping technique attempts to mimic the process of thinking that goes through an analyst's mind before choosing the grouping for a spread of sunspots [*USAF*, 2013]. The difference comes in that specific levels are laid out in a way that prevents overlap and when differences are found in grouping, the code user should be able to see why those differences arose.

3.5.2 Grouping Length.

Grouping length is different from a sunspot group length, the former being the parameter used by the SDO grouping technique to test candidate spots for acceptance into a specific group. After attempting to optimize the grouping length, the conclusion was reached that certain types of groups are grouped properly for a corresponding grouping length. This means that one group may benefit by having a grouping length of 10 while another group may be correctly grouped for a grouping length of 15. For groups that were large and had extensive and complex structures with many umbra in the group, a larger grouping length performed better. However, using this same grouping length for smaller sunspots tended to lump spots together

that did not belong in the same group. Conversely, small spot groups would favor a shorter grouping length, but their large group length counterparts would be over-partitioned by the grouping algorithm, leaving spots outside the group that actually belonged inside. In this way, it is impossible to optimize the grouping length for all group sizes. It was realized then that rather than choose a single grouping length and accept error for certain group types, the grouping length could be altered during the segmentation process. The process of grouping, therefore, is based on the area of each spot group to in order to give a range of grouping lengths for different group types. An analyst's eyes are drawn to the areas of the solar disk that have the greatest population of spots or that are the darkest, consuming large sections of the solar hemisphere. Interpreting this observation tendency into a coding scheme, the SDO code alters the grouping length depending on the area of the spots currently assigned to that group. For spots that have a large area, a larger grouping length is assigned, while conversely, small area groups have a smaller grouping length. This effect takes the best of both worlds and nicely compromises the two extremes. To obtain the grouping length function, three approaches were experimentally determined. Collecting data over the past year from San Vito, Learmonth and Holloman as well as 10 years of SWPC data, a set of points is obtained matching group lengths to the total area of that spot group. Trial 1 took the maximum group length for a particular area to create our data set, to which an exponential curve is fit resulting in an equation relating area to group length.

$$Length = 8.276\frac{Area}{10}^{0.2276} - 2.875 \tag{12}$$

Trial 2 takes the average value of group length for a particular area to create a set of data points to which an exponential curve is also fit. The result is another equation that relates area to group length

$$Length = -24.74\frac{Area}{10}^{-0.08423} + 32.96 \tag{13}$$

The final trial is simply a linear interpolation of points selected between the two curves, resulting in the most accurate results after testing. Each point is approximately equal to the average of both previous curves. These curves are summarized in Figure 9.

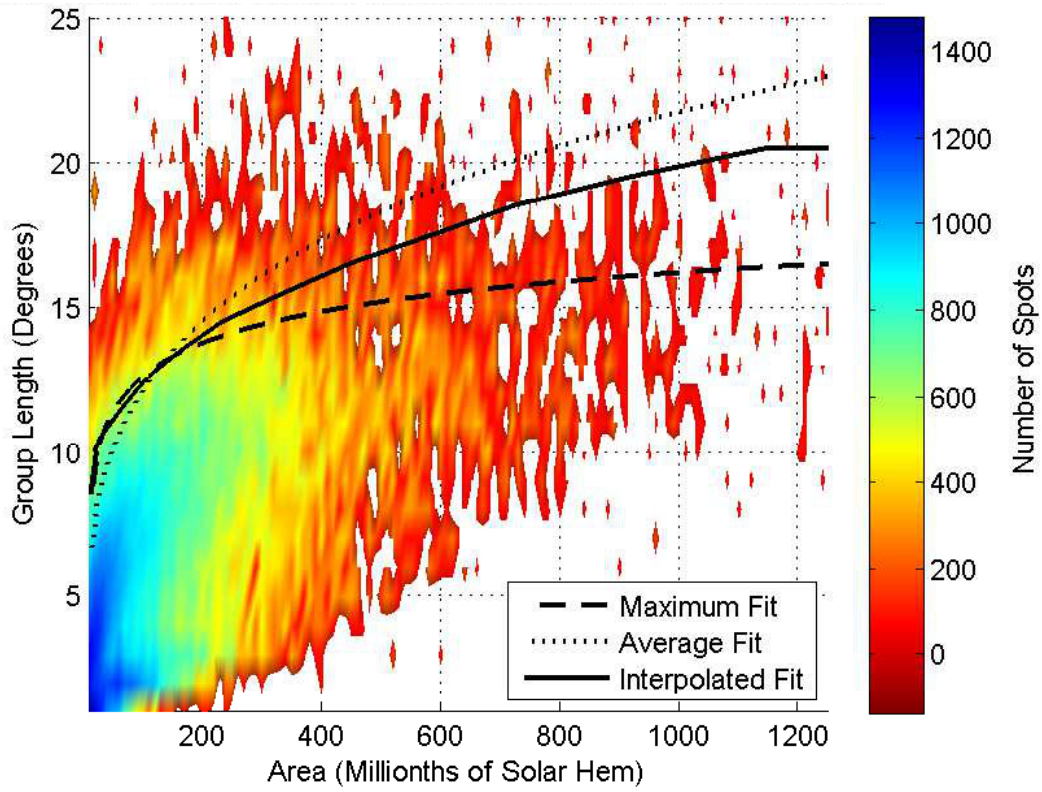

Figure 9. All sunspot groups reported by SWPC, Holloman, Learmonth and San Vito are shown in terms of color density, plotted with the area of the spot group on the x axis and the total length of the spot group on the y axis. The three AF Solar Observatories make up a years worth of data each, while SWPC contributes 10 years of spot data. The first exponential curve is the result of fitting the maximum group length for each area. The second exponential curve is the result of fitting the average group length for each particular area. The final curve is approximately the average value between the first two curves, cut off at a group length of 20.

To calculate the area of a spot, the code applies the same general steps used by Holloman AFB. Because the locations of each sunspot are known in pixel space and each sunspot is represented in a black and white image, we sum up all of the pixels that are representing each sunspot. This yields an area in pixel space that is then converted to a percentage of the total area of the sun. By dividing A, the area in pixels

$$Area = \frac{A}{2\pi r^2} \tag{14}$$

by the area of a solar hemisphere in pixel space where r is the solar radius in pixels. The resulting number is then multiplied by the geometric foreshortening correction factor that is found by determining the angle ρ off from center that describes the sunspot's position which can be found by taking the inverse cosine of equation 22. The foreshortening correction factor is found by

$$f_c = \frac{1 \times 10^6}{\rho} \tag{15}$$

where it is then multiplied by 1×10^6 to put the area in units of millionths of a solar hemisphere [$USAF$, 2013].

3.5.3 Grouping Process.

In order to perform the grouping, the variable grouping length method is used based on the total area of sunspots already assigned to a group. Starting with the biggest spot visible on the disk, new spot candidates are tested and accepted into the group based on the grouping length defined in Section 3.5.2. To do this, a case statement must be set up inside a loop. The purpose of this initial loop is to iterate through every numbered spot contained in the label matrix from the thresholding

routine in Section 3.4. The case statement is needed to check the existence of the second spot being compared to the first spot. In the case where the spot being compared has already been assigned to another group, this statement skips to the next spot to compare. In the case where the spot does exist and has not been given a group number yet, a second loop is started. The purpose of this second loop is to establish whether or not there are spots within the grouping distance defined by the area of the current spot group. These other spots must have the opposite polarity of the current spot being compared. In addition, if a spot being tested lies within 5 heliographic degrees, it is labeled as part of the current group. If a spot with opposite polarity does exist within 5 heliographic degrees, the polarity criteria is met, and a third loop is triggered. This third loop also moves through each spot not yet labeled, but instead of the 5 degree separation as the criteria for group labeling, there is an extended limit based on the area of the spot group using the average of equations 12 and 13. If the bipolar criteria is triggered, the current group is marked as a bipolar group at the end of this loop. The final product of this grouping algorithm is a label matrix that contains the number of groups in the image according to the Holloman AFB grouping criteria [*USAF*, 2013].

3.6 Feature Extraction

The final stage of processing before the classification scheme involves extracting information out of the image using a data representation function [*Gonzalez and Eddins*, 2009]. The end goal for this section of code is to come up with a way to represent the McIntosh classification in terms of extractable features from the label matrix that has already been created. In MATLAB, key features are removed via the function regionprops [*Gonzalez and Eddins*, 2009] which takes a label matrix along with any number of specified parameter values to calculate

certain items that are useful for classifications. These key features include the length of the sunspot group, length of largest sunspot penumbra, eccentricity of the largest sunspot, area of the sunspot group, polarity of each sunspot, the completeness of the penumbra, and the spread of sunspots within the group. When the McIntosh system explicitly defined the classification parameters, those values were used. When wording was unspecific, the words were interpreted in the most logical way. These interpretations are stated explicitly throughout Sections 3.6.1-3.6.3.

It is difficult to compare the intensity values between different sunspots on a white light board without significant experience. Additionally, it is difficult for an analyst to discern the relative darkness of the penumbra compared to the umbra of the spot. All of this information is not necessary when drawing on a piece of paper, but is essential when determining the extent of the penumbra and umbra on a digital image. When small spots are detected on a white light board, there may not be enough spatial resolution to either determine the darkness of each spot, or the potential presence of penumbra. In a digital image created by a CCD, however, the computer needs to interpret each pixel as a digital count value [*Gonzalez and Eddins*, 2009]. The formation of sunspots described by the Babcock model is driven by suppression of plasma flow in the photosphere [*Foukal*, 2008]. Because suppressed plasma can no longer circle back down to the radiative zone to re-heat, the intensity of light in the visible spectrum decreases and the regions of higher magnetic field appear darker than those regions of the sun that are quiet with little magnetic activity. Below a certain intensity value on each image, these regions of suppressed convection will be counted as sunspots in the code, as discussed in Section 3.4. In practice, when small sunspots are detected on the digital image, they will pass the penumbra threshold but may rarely pass the umbra threshold. These small spots must still be considered umbra, though, even if they do not appear on

the umbra image. Therefore, a routine is developed to establish whether a sunspot on the penumbra image has a co-located umbra spot. If this is not the case, that spot on the penumbra image is considered part of the umbra image, even though its intensity level was higher.

3.6.1 Zurich Classification.

With this spot definition in mind, the task in classification becomes representing each detected spot group in the McIntosh fashion. Under the Zurich Classification, or first letter designation, the length of the sunspot group and completeness of penumbra surrounding the leading and trailing spots are primary factors. These items are shown in Figure 2. To start, a new spot is defined as one that possesses umbra with little to no penumbra. These types of spots are given the designation 'A' as they represent the first stage in a sunspot's life at the lowest detectable intensity level. If a spot group is unipolar and has a defined penumbra, it will be given an 'H' designation. In practice, there are usually pixels around the central dark spot that satisfy the penumbra threshold level, but if the spot is small, these are neglected because their intensity may have to do with the binning used in the CCD. Because of this, area restrictions are applied in order to prevent small spots with very small areas from receiving 'H' classifications. Because 'H' classifications are supposed to be for higher levels of a sunspot's life, it is not logical to allow this classification for groups that could be comprised of 3-5 pixels. Therefore, the definition of the 'A' designation is altered to include unipolar groups with umbra that have an area of less than 5 millionths of a solar hemisphere in addition to the other criteria.

As the spot group grows, it will likely develop a trailing spot with penumbra intensity levels, traditionally considered a spot group with the Zurich designator 'B'.

For cases with darker spots, the presence of penumbra is the indicator for full development of a spot [*Foukal*, 2008; *McIntosh*, 1990]. The validity of any penumbra/umbra combination seen on the image is checked by multiplying the binary image of the penumbra with the binary image of the umbra. Given that both regions will overlap, the resulting image will either have a sum of zero for spots that no corresponding mark on the umbra image, or non-zero for spot groups that do have the corresponding mark. In order to define which spot groups have a mature penumbra, it was interpreted that the overlap could not be greater than 85% of the total area of the penumbra as this would imply that the majority of the spot group is dark umbra. If this experimentally determined threshold is passed, this penumbra group is labeled as a mature spot. Subsequently, spot groups with mature spots on one end of the group but not the other end will be considered of the 'C' designation, while spot groups with mature spots on both ends are 'D'. This determination is done by calculating the maximum extent of the spot group in all directions to find the length of the spot group. Then, iterating through all the mature spots in the group, the distance in heliographic degrees between each mature spot is determined. If any of the determined distances are greater than 70% of the total spot group length, this is interpreted as satisfying the condition that mature spots be on both ends of the group. This cutoff was determined during the development process to function appropriately in classification of each sunspot group. For the higher classes of 'E' or 'F', the length of the group is looked at in addition to the criteria that is necessary to designate a group as 'D'. The necessary values for each classification are defined in Section 2.5.1.

The possibility of detecting a spot group that is comprised of a few spots in close proximity (meaning a few pixels) to one another is considered, where one large spot is centered among a few small spots. This group would be considered one

group on a drawing board, but because of the additional spatial resolution, parts of the spot may be separated. In the case where all spots detected have the same polarity, there is no issue and the group will be labeled 'H' in line with what an observer would say. However, in the case that there is fringing and part of the penumbra has an opposite polarity to the rest of the spot, the group will be labeled bipolar therefore given a 'C' designation. To correct for this possibility, a case statement is included where spot groups of this type are still given the designation 'H' but will still be considered bipolar. Specifically, if the length of the largest spot in the group makes up greater than 85% of the total length of the group, in both East to West and North to South directions, this switch is made.

3.6.2 Penumbra Classification.

The penumbra classification, illustrated by series 2 in Figure 2, begins by checking the Zurich Classification applied to the spot group by the previous section of code. If the first letter is given as either 'A' or 'B', there can be no penumbra visible in that particular spot group by definition. In this case, these groups are assigned a penumbra class of 'x' for non-existent penumbra, following the rules in Table 2.

The next possible outcome is one where the penumbra of the group is fairly limited in extent. Each classification beyond the non-existent penumbra notation looks at the penumbra surrounding the largest spot in the group. Because of this, a connected components routine [*Gonzalez and Eddins*, 2009], illustrated in Figure 8, is run on the individual spot group to get the total number of spots and to separate those spots into their respective sizes. The area correction is applied to each spot in the group before re-ordering the spots from largest to smallest. After this point, the largest spot is addressed and the umbra contained within that spot's penumbra is

summed and divided by the area of the surrounding penumbra. If the ratio of these two numbers exceeds 0.5, this penumbra is considered to be rudimentary and the label 'r' is given. This indicates that the umbra of the spot group makes up more than half of the total area of the spot. The penumbra of this spot group therefore does not comprise a significant portion of the area and is likely underdeveloped.

The next case to consider is for fully developed penumbra. Four separate classes can be assigned depending on the combination of eccentricity and length: the spot is asymmetric and has a penumbra length less than 2.5 degrees (labeled 'a'), the spot is symmetric and has a penumbra length less than 2.5 degrees (labeled 's'), the spot is asymmetric and has a penumbra length of greater than 2.5 degrees (labeled 'k'), or the spot is symmetric with a penumbra length of greater than 2.5 degrees (labeled 'h'). The length of the group is determined using the same technique of measuring the extreme points of the largest spot and calculating their position in heliographic degrees before comparing the extent to find the span. To find the eccentricity, the function regionprops [*Gonzalez and Eddins*, 2009] is called with the eccentricity option. This function determines the ratio of the semi-major axis to the semi-minor axis, yielding a value between 0 and 1. If the object is as wide as it is tall, the function will return an eccentricity of zero, indicating a circle. A line segment will receive an eccentricity of 1. The value corresponding to the largest spot in the group determines the eccentricity criteria. An eccentricity of less than 0.5 is interpreted to be symmetric while an eccentricity of greater than 0.5 is interpreted as asymmetric. Each of these pieces of information are compiled to fill in the rest of the possible scenarios.

3.6.3 Compactness Classification.

The compactness classification is given based on the concentration and number of additional spots seen in the group being analyzed, illustrated by the third series in Figure 2. For the case where the group is unipolar and the first letter of the classification is either 'A' or 'H', there can be no spread of spots between leader and trailer spot by definition. In this case, the compactness classification for these unipolar groups is given as 'x' or non-existent.

For the cases where the group is bipolar, three separate classifications can be assigned based on the observer's interpretation of three similar words: few, several, and many [*McIntosh*, 1990; *USAF*, 2013]. This wording ambiguity is shown in Table 3. In this research, many is defined as greater than 5 while 3 is several. For the SDO code, the compact and intermediate classifications are addressed first and any spot groups that don't qualify are assigned an open designation 'o', defined in Section 2.5.3. In order to receive a compact classification, the spot group's trailing spot must have mature penumbra in addition to mature penumbra present on at least one spot in between leader and trailer. This means that no classification below 'D' can be compact by definition combined with the requirement that the group must has greater than 5 umbras. In practice, the position of each umbra in each spot group is calculated with respect to the leading spot. If umbra is present on the trailing spot in addition to somewhere in between the leader and trailer, the group passes the first condition. The counted number of umbra defines the second condition. As an additional requirement due to the fact that small narrow groups are not given 'c' classifications, an area to length requirement is set. The group's area divided by the group length must also be over a set value of 30 to ensure that no groups with small area can be included in this compact category as a small, narrow group would otherwise be considered satisfactory.

It was selected that groups with greater than 3 individual spots with one spot within the group possessing mature penumbra should be given the intermediate classification 'i'. In the case where a group of the Zurich Classification 'C' meets all the requirements for a compactness class of 'c', a case statement re-labels that group to an 'i' due to that group not meeting the requirement of developed penumbra on both ends of the group. For spot groups that do not meet any of the requirements for the compact or intermediate classifications, the open classification 'o' is given as a catch all statement.

3.7 Evaluation of Code Product

This research can be viewed in two parts. The first part involves the creation of an automatic code capable of analyzing sunspots visible in the photosphere at a very high rate. The second part involves an analysis of the accuracy of sunspot detection and classification data produced by the first part. The method of research can then be said to require two sets of analysis, the first being in response to the code itself while the second should address the product of the code. In this thesis, only the latter is discussed. This is because the former focuses heavily on image processing techniques that have been well established. There are different ways to go about producing the results obtained by the SDO code, but these are less important than the actual resulting classifications produced.

To fully analyze the product of the SDO code, data is produced for two time series. The first is a testing period where a variety of images were used to construct the code in the manner outlined in this chapter. The second period was used to evaluate the performance of the finalized code developed using the data from the first period. Each of the data series used spans approximately 6 months of time. The testing period data was from 6 July, 2012 through 31 December, 2012. The

evaluation data spanned from 1 January, 2013 to 29 July, 2013. Analysis of the first time series is accomplished in Chapter IV while the second time series evaluation is shown in Appendix 3.

IV. Analysis and Results

To obtain a full picture of the accuracy of the SDO product, a comparison is done with respect to two sources in three directions (SWPC to Holloman, SDO to SWPC, and SDO to Holloman). The first comparison between a set of standard observers defines the acceptable difference range, while the second two comparisons demonstrate that results are within that established range. These comparisons are accomplished using the first 6 month testing period data while the same comparison is performed for the second 6 months in Appendix 3. After first showing that numbers for sunspot area, number of groups and number of sunspots detected by the SDO code are not anomalous, a metric for sunspot classification success is described. A final comparison subsequently shows bias in the hand drawn spot recording and classification system by altering specific parameters in the sunspot classification code.

4.1 Code Output

This SDO image analysis code outputs data to include the date and time, longitude and latitude, the area of the spot group, the number of umbras in each group, and the assigned McIntosh Classification for that spot group. Comparisons for the purpose of this research are performed with both Holloman AFB and SWPC. Holloman AFB was chosen to be the compared standard observatory because its report times are closest to SWPC, the national center for space weather. In this way, any differences in reports should be mostly due to a difference in interpretation of the classification rules as timing differences are minimized.

4.2 Area, Group, and Spot Accuracy

The first step in showing the accuracy of the SDO method of automated sunspot detection and classification is to verify quantities produced by the code in comparison to each of the other entities. These quantities include the total area of sunspot groups detected, the number of groups, and the number of spots detected on any given day. Each of these quantities will have a certain amount of bias included because of a multitude of different factors, so each item will be addressed in detail to show satisfactory values are achieved before progressing to demonstrate the accuracy of the classification method. The end goal, however, was to show that the SDO product provides results comparable to those produced by both SWPC and Holloman.

4.2.1 Area Comparison.

The first item compared is the total area of sunspots detected. This is done on a day by day basis where the total area is calculated by summing the area of each sunspot group reported on a given day from each reporting entity. Several caveats should be mentioned regarding the calculation of this number. First, the range of detection of the SDO code inhibits the detection of sunspot groups beyond roughly $\pm 75^{\circ}$ longitude, varying with the change of the B angle, uniformly applying to all other compared quantities. Higher B angles prevent the detection of sunspots at smaller values of longitude in the southern hemisphere of the sun while the opposite is true for lower B angles. This issue is compromised by cutting out all sunspots recorded by SWPC and Holloman from the data set that sit outside the $\pm 75^{\circ}$ cutoff. As a result, these sunspot groups don't contribute to any of the area totals for SWPC or Holloman. However, there is a possibility that the SDO code will catch portions of a sunspot group that exists on the edge of the cutoff region and

therefore count part of the sunspot group under the SDO area while the same spot group may have been cut out completely from SWPC or Holloman reports. Conversely, part of the area of the spot may be cut off by the $\pm 75^{\circ}$ cutoff meaning that the total area detected by the SDO will be less than the area seen by SWPC or Holloman. In addition to these discrepancies, the position of each sunspot group reported is determined using the latitude and longitude layover (discussed in Appendix 1) and the accuracy of this method is questionable near the edge of the solar disk due to the effect of geometric foreshortening and the interpolation analysts need to perform to obtain the region's position. In a similar display of error, the longitude for SWPC spot reports needs to be projected backwards approximately 8 hours in order to match the position of both Holloman and the SDO images. Projection of sunspot longitude from SWPC reports is executed uniformly by subtracting 4 degrees from the reported longitude, even though the actual correction may need to be slightly higher or lower. If a spot's position is miss-reported, that spot may not be cut out of the data set when it would be appropriate to do so. Fourthly, the SDO code calculates the area in a similar but more spatially precise manner than Holloman or SWPC as described in Section 2.10 and Section 3.5. Similar to decreasing the bin size on a Reimann sum to calculate the error under the curve, summing pixels in a sunspot group yields a more accurate area than the fitted ellipse. In addition, the foreshortening correction is calculated to a more precise degree. While the Holloman method of area calculation may still be considered accurate in order of magnitude, the precision of the method is reduced to increments of 10 millionths of a solar hemisphere while the SDO code calculates these values to a much smaller decimal. There is something to be said for the quantization of the area value into individual pixels, but as was stated in Section 2.10, the spatial resolution of these pixels is still significantly better than

that of a pencil tip compared to quantization effects. Finally, the factor determining which pixels qualify as sunspots has been iteratively determined. The pixels assigned to be considered part of each sunspot satisfy the requirement of being darker than their surrounding pixels by a determinable amount. With these caveats in mind, the analysis proceeds with the relationship between the SDO code total area product and the reports collected from both Holloman AFB and SWPC.

Figure 10 summarizes the differences between the calculations of total area from each of the reporting entities from 6 July 2012. The first thing to notice is that there exists no significant trend of difference between any of the three plotted relationships. There are single days scattered throughout the 6 month period where the difference in area spikes up to a larger value, but these incidents are few and correspond to days with large sunspots visible on the solar disk where the extent of the penumbra in each case may be interpreted differently by separate observers. Additionally, area layover accuracy for spots with an area over 500 millionths of a solar hemisphere is questionable (due to the size of the fitted ellipse), and is therefore a likely source of error. Overall, the difference plots illustrate that the areas produced by the SDO code fall concurrent with area measurements from the Holloman Observatory as well as SWPC reports. After the difference plot, each day's area total is plotted against the area total from another reporting entity in Figures 11-13. Under a perfect match, each point would lie along a line with a slope of one through the origin. Paying close attention to Figure 11 where the areas of Holloman and SWPC are compared, in general, the spread of points increases with increasing area. The R squared value for the linear regression line through each point is 0.778. In both of the subsequent plots, the regression displays similar results to the baseline, returning an R squared value of 0.780 for the SDO to SWPC comparison and 0.749 for the Holloman to SDO comparison, seen in Figures 12 and

13 respectively. Looking next at the equations describing the trend line, some general conclusions can be drawn about the nature of area calculations in each of the three reporting entities with respect to the others. First, Holloman tends to overestimate the total area of sunspots on any given day for larger spot groups due to the fact that in both Figure 11 and Figure 13, the slope of the regression line is less than one (slopes of 0.86 and 0.95). Second, the SDO result is more similar to the SWPC result than Holloman, although using the same slope analysis, the SDO reported areas are generally greater than SWPC reported total area, seen from the 0.94 slope. This comparison shows that the SDO code produces area results that are in line with those of both SWPC and Holloman.

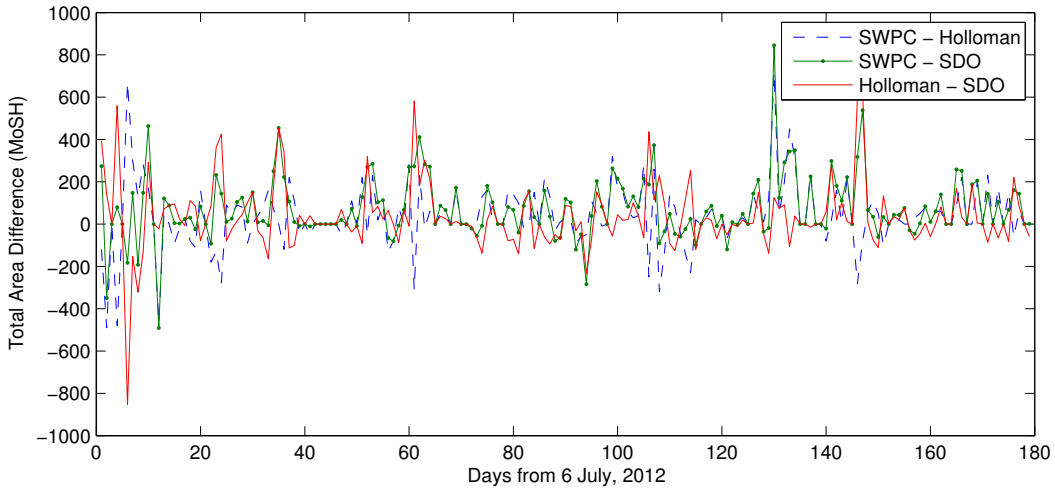

Figure 10. The difference between the daily total area calculated by each of the three reporting entities is plotted from 6 Jul - 31 Dec 2012.

4.2.2 Group Number Comparison.

The second comparison in this analysis is the number of groups reported by each entity. Again, this comparison is conducted on a day by day basis, summing the number of groups from each entity over the 179 day test period. When comparing groups between each entity, it is shown that while the grouping

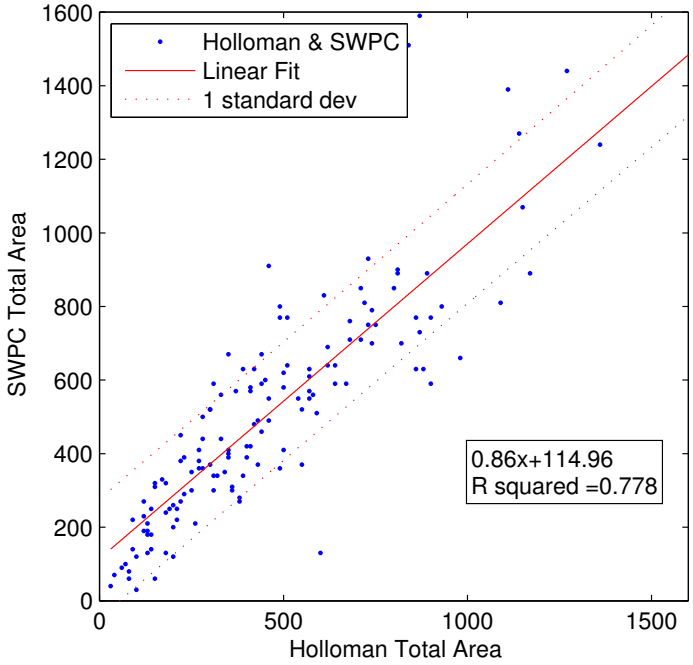

Figure 11. Regression of SWPC and Holloman total area from 6 Jul - 31 Dec 2012.

algorithm employed in the SDO code is different from past methods (Section 3.5.3), it stays close to the groupings provided by Holloman and SWPC. It is important to remember that while all reporting entities attempt to group sunspots in the same way, there may be differences between day to day reports. These grouping differences end up being very important when each group is classified into a certain McIntosh category. The majority of misclassified groups suffer from an incorrect grouping in the SDO code, so it is important to minimize error.

There are three elements of this algorithm that will contribute to differences in the sunspot group comparison. First,due to the additional spatial resolution of SDO images, the SDO code has the capability to detect smaller groups that may go unnoticed by an observer at an optical observatory. This additional detection capability will tend to increase the number of sunspot groups seen by the SDO code

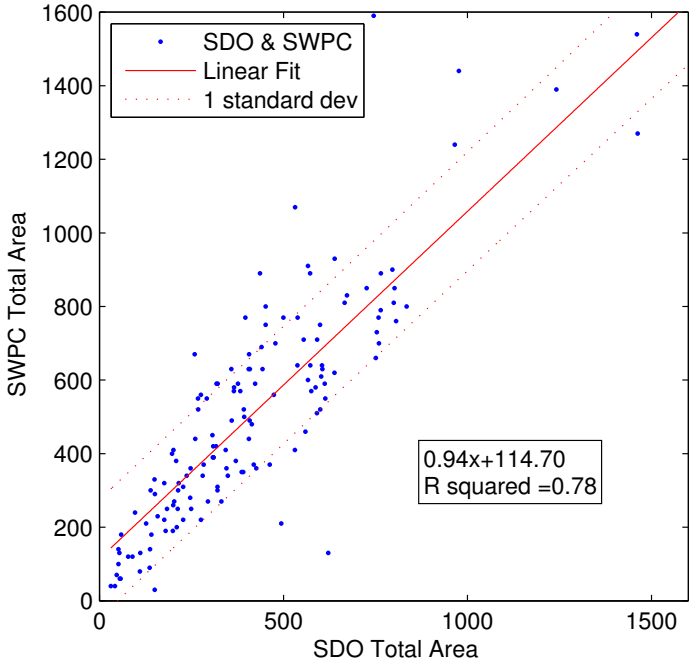

Figure 12. Regression of SWPC and SDO total area from 6 Jul - 31 Dec 2012.

compared to both Holloman and SWPC. The second item to consider is the fact that SWPC reports only include sunspot groups that were given region numbers prior to the publishing of the daily report. It is therefore possible for Holloman to see a group before any other observatory, or to see a group and have that group go unconfirmed by another observatory. This would result in the omission of that particular group in the SWPC report. Moreover, both Holloman and SDO may detect and report this spot group, but it may be missed by SWPC. The third possibility is that there is a difference in the way spots were grouped between any of the three observatories. While Holloman bases its groupings, to a certain extent, on the active region assignments from SWPC, there are still examples where the groupings differ between the two. Generally, this will be after an active region separation call is made by SWPC, leading to a different grouping in their report.

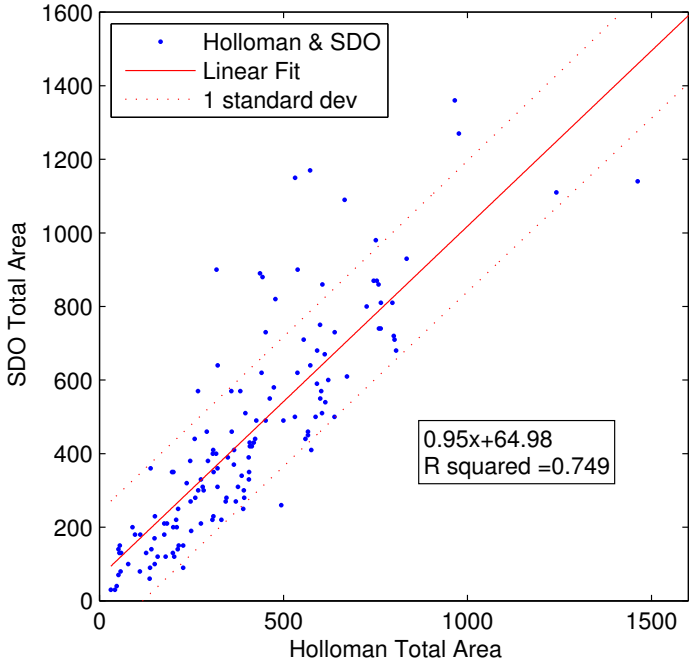

Figure 13. Regression of SDO and Holloman total area from 6 Jul - 31 Dec 2012.

However, the opposite process can also occur where SWPC does not follow the grouping made by Holloman. This determination of grouping will occur external to any adjustments in the SDO code (as it is uninfluenced by outside sources), resulting in a miss-grouping.

Comparing the different number of groups in Figure 14, we see that the differences are minimal, and all three lines oscillate around the zero difference line. When there are peaks that jump up to a larger difference, the SDO code tends to have more than either of the other two reporting entities. This fact is also made evident in the subsequent scatter plots that illustrate the trend of one particular reporting entity to another in Figures 15-17. Each axis shows the number of groups reported on a particular day corresponding to the report issued by that reporting entity. Again, perfect agreement results in a point lying along a line with a slope of

one through the origin. Scatter above that line illustrates an over-determination of the number of spot groups for that particular day with respect to the other entity while the opposite is true for scatter under the line. In this case, the Figure 15 regression shows that the number of groups reported by the SDO code roughly matches the number of groups from Holloman with a regression slope of 1.02 accompanied by an R value of 0.705, indicating that any significant variation in the difference between Holloman and SDO is anomalous. In contrast, Figure 16 demonstrates the differences between SWPC and Holloman, showing that there exists a trend suggesting Holloman tends to report more groups than SWPC with a regression slope of 0.81 tilted towards the Holloman axis with an R value of 0.703. Extending this to the third plot in Figure 17, SDO tends to have more groups reported than SWPC also, with a smaller regression slope of 1.07 tilted towards the SDO axis and the highest R squared value of all three plots, 0.722. This is important to mention because it helps show the interconnected nature of each comparison and illustrates the multiple factors that can go into determining a match. While there are clearly differences in the number of groups between each reporting entities, the comparison method can proceed under the knowledge that there is fairly good agreement across all observers. Some of these groups may be constructed with different sunspots causing a difference in classification, but it has been shown that the number of groups and the total area of sunspots reported by the SDO code is not anomalous.

Longitude and longitude matching error is closely linked with the difference in the number of reported sunspot groups. When comparing Holloman to SWPC, differences indicate either that Holloman missed a spot group on the drawing board or that a group Holloman reported has not been confirmed by another solar observatory. Generally speaking, the same spots are detected by all entities, but

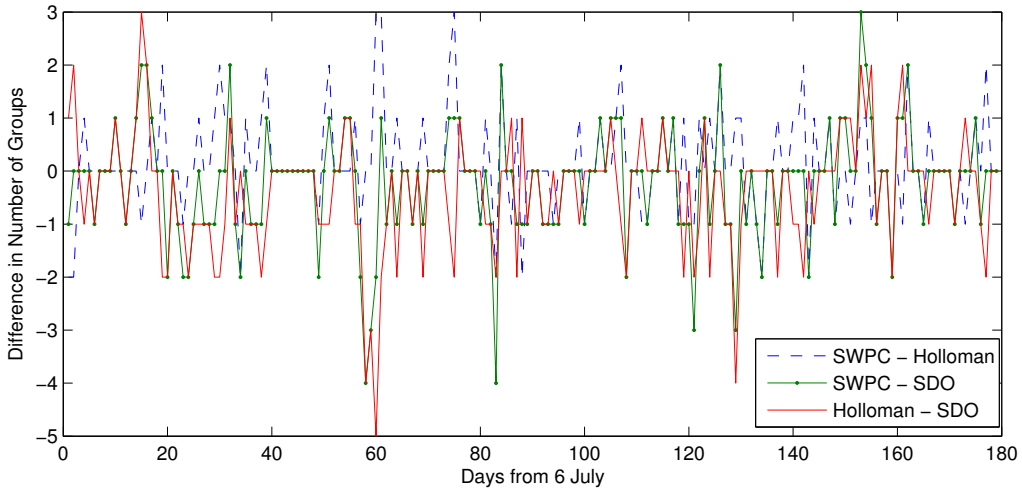

Figure 14. The difference between the daily total number of groups determined by each of the three reporting entities is plotted from 6 Jul - 31 Dec 2012.

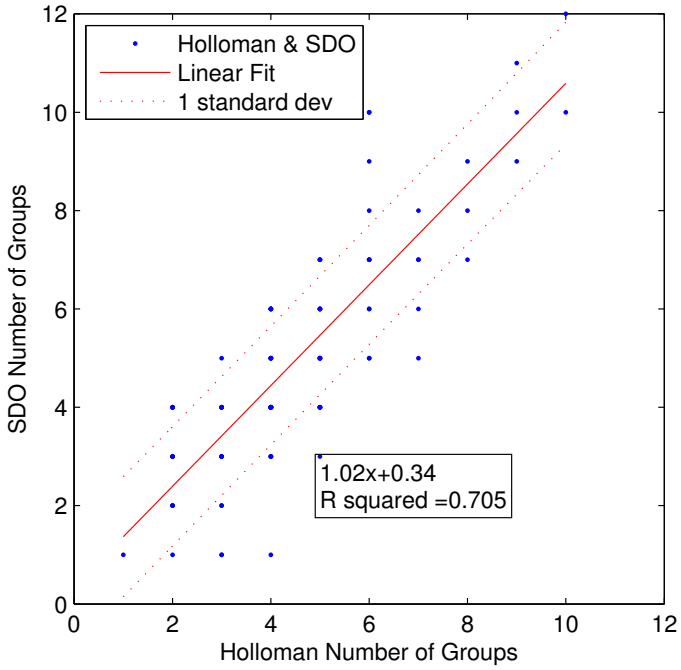

Figure 15. Regression of SDO and Holloman total number of groups from 6 Jul - 31 Dec 2012.

separated into groups in different manners related to the observatory, the particular solar analyst, or some additional analysis performed on the particular region.

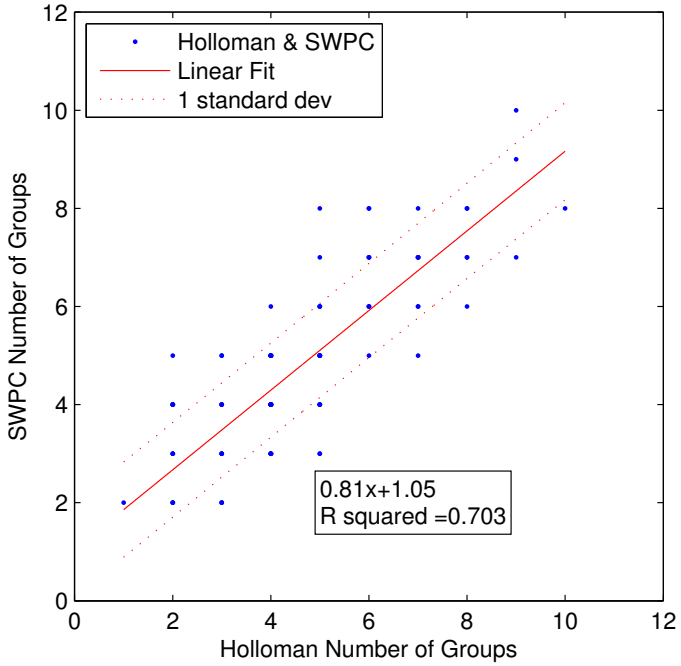

Figure 16. Regression of SWPC and Holloman total number of groups from 6 Jul - 31 Dec 2012.

Sometimes, SWPC will choose to separate out a group into two distinct active regions, even though the two groups are close enough to be considered part of the same group under the McIntosh definition. This is not something that can be influenced in the automated SDO code at the moment, so these particular days will always result in the SDO "missing" a group, meaning that the SDO report did not have a group available to match the location of the other reporting entities. Even so, all the spots comprising the two groups reported by SWPC and Holloman are still contained in the one group defined by the SDO code. Over the course of the 6 months of data tested, only one spot group was missed by the SDO code, and the classification corresponding to this miss showed that the missed group was in the formative stage of its life. In addition, the spot group was very far out towards the

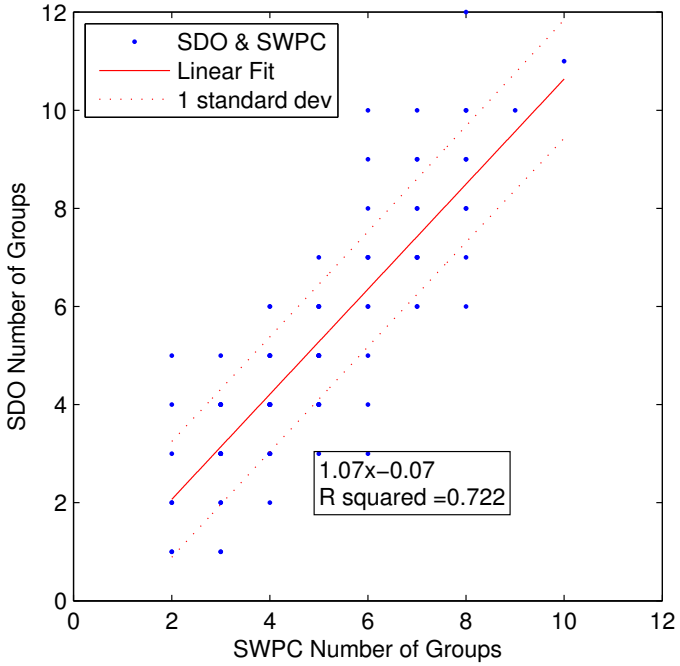

Figure 17. Regression of SWPC and SDO total number of groups from 6 Jul - 31 Dec 2012.

limb of the sun, a region where the SDO code does not perform as well due to the inaccuracy of the limb darkening correction in that region, discussed in Section 2.3.

4.2.3 Number of Spots Comparison.

The final element to compare before moving on to the discussion of classification accuracy is the number of spots reported by SDO compared to SWPC and Holloman. In addition to the difference in resolution, there are some caveats that must be mentioned before a comparison of the number of spots from each entity can be analyzed.

The method by which spots are counted is the same for each reporting entity. Specifically, only umbras are counted as spots in each case. In the situation where one large group enclosed by penumbra contains multiple umbras, the umbras all

contribute to the number of spots. Additionally, if there is a small spot with no mature penumbra surrounding it, that spot is still counted under this system. Applying the system to the SDO code, the process by which sunspots are detected should be quickly reiterated, as outlined in Section 3.4. The threshold is determined iteratively by decreasing step size, resulting in a black and white image representing the penumbra and umbra visible on the solar disk in white pixels. Using this method, the possibility of detecting a sunspot that is comprised of only penumbra results in a complicated determination of spot number.

Understanding that each of these penumbra regions may also contain umbra (due to the fact that if a pixel is darker, it will likely be surrounded by less dark pixels), the black and white labeled image of the penumbra, set equal to the particular sunspot of interest, is multiplied back into the black and white image of the umbra. The result of this matrix multiplication will contain the location of all the umbras within the particular penumbra while all other locations are set to zero. Those umbra are then counted using the black and white labeling technique and, after subtracting one to avoid double counting, these extra spots are added to the total number of penumbra spots from the previous count. Because of the intensity thresholding method used to determine the penumbra and umbra, there is a possibility spots may be separated from one another that perhaps wouldn't separated to an optical observer. It is with this knowledge that the analysis progresses under the assumption that the determination of sunspot numbers through the SDO code is valid.

The evident trend in Figure 18 is that there is clear separation between the SWPC-Holloman and the SWPC-SDO lines. Both the SWPC-SDO and the Holloman-SDO lines sit below the zero line, indicating that the SDO code usually produces a report seeing more sunspots than any of the other two entities. For

example, the solid green line represents the number of spots seen by the SDO code minus the number reported by Holloman. This separation is further confirmed in the subsequent scatter plots displayed in Figures 19-21 where each entity is compared to the others in terms of sunspots counted for any particular day. Figure 19 fully illustrates the skew with a slope of 0.41, significantly less than the one to one relationship seen in either of the area or group number comparisons. With Figure 20, the trend continues. The slope for this figure reduces to a value of 0.46, indicating that the SDO code sees more spots than SWPC as well, concurrent with what was expected. Figure 21 shows a trend similar to the other two figures in that the number of spots reported by Holloman and SWPC are roughly equal with a regression slope of 0.94, slightly skewed towards the Holloman axis. The R squared values all show relatively good fit agreement. This falls in line with the trend seen before where Holloman will generally have more groups than SWPC, further confirming the similarity.

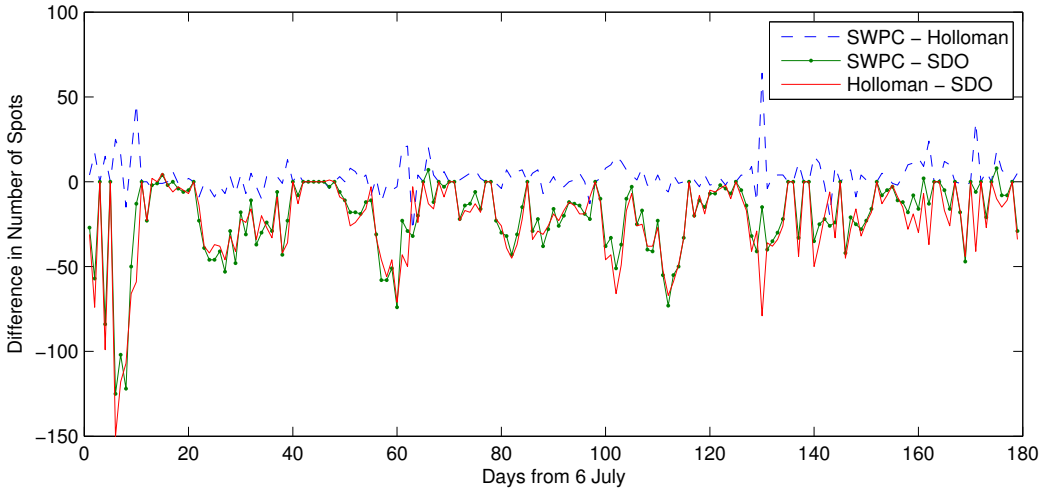

Figure 18. The difference between the daily total number of sunspots detected by each of the three reporting entities is plotted from 6 Jul - 31 Dec 2012.

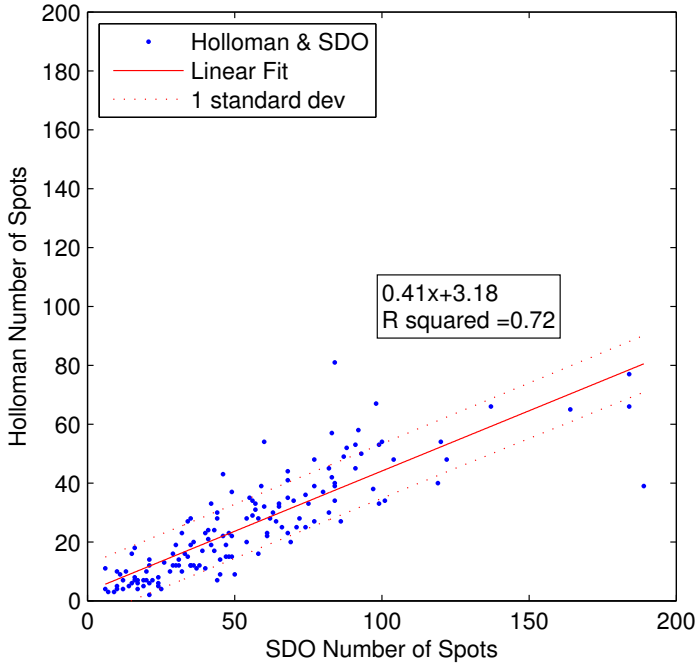

Figure 19. Regression of SDO and Holloman total number of sunspots from 6 Jul - 31 Dec 2012.

4.3 Method of Classification Comparison

After looking at the differences between the SDO classification result, Holloman publications and SWPC reports for total reported area, number of groups, and number of sunspots seen, the next step is to demonstrate the accuracy of the automated classification method compared with the other two reporting entities. In addition, the differences between each product will be quantified and any cause of variation between each entity will be isolated. One of the main difficulties surrounding the task of illustrating the accuracy of the automated classification method is the fact that there are so many specific quantities that go into determining a classification. Numerous variables make it difficult to see the source of variation and they can cause seemingly large differences in classification. Even in specific tests for comparison, it is possible that any differences seen are due

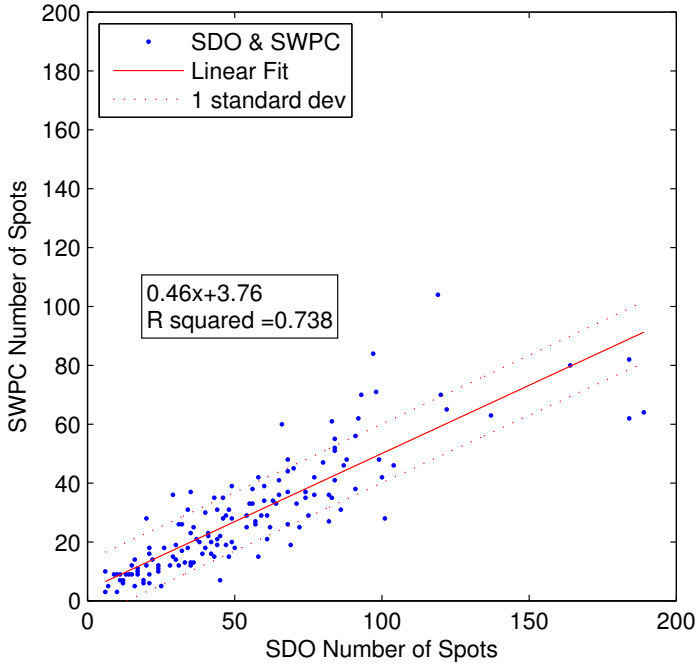

Figure 20. Regression of SWPC and SDO total number of sunspots from 6 Jul - 31 Dec 2012.

to multiple factors altering the classification at the same time. These factors include elements like measuring different lengths of groups and the lengths of spots within a group. After the initial accuracy of the SDO classification method is established, many additional tests are performed while varying a single element of the classification process to demonstrate the effect that particular item holds on the accuracy result.

The first step to determining the validity of the SDO classification method is to ensure that each spot group seen by the SDO was also seen by the other two reporting entities and vice versa. To do this, data from the two sources being compared was taken on a day by day basis and matched based on the longitude and latitude of the group. All reporting entities are matched using the same method to ensure that any error applied through the method would be uniform for every

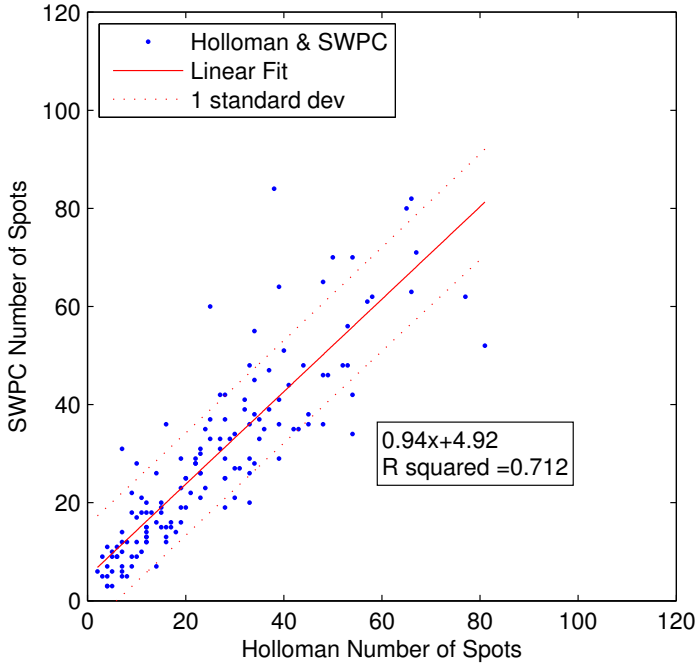

Figure 21. Regression of SWPC and Holloman total number of sunspots from 6 Jul - 31 Dec 2012.

comparison. It should be noted that matching groups in this way results in the percent match between SWPC and Holloman being lower than if spot groups were compared using region numbers.

Displaying the position, area and classification of each spot group compared, Figure 22 demonstrates a typical daily match between Holloman and the SDO code. For this particular section and day, there are equal numbers of detected sunspot groups from both the Holloman observatory and the SDO code. Similar outputs are attainable when comparing SDO to SWPC or SWPC to Holloman. This match in number of groups is not always consistent for any of the comparisons, as was seen in Figure 18, but when there are missing groups in any of the data sets, it is almost exclusively because of a difference in grouping between the SDO and the other two entities.

11/28/2012

SDO	lon	lat	area	class	Holloman	lon	lat	area	class
1	-27.6	15.2	145.2	Hax	1	-27	16	170	Hhx
2	-64.4	8.5	201.5	Dki	2	-67	13	450	Dho
3	54.6	-13.3	221.7	Eai	3	55	-14	540	Ekc
4	-11.4	19.9	3.6	Axx	4	-11	20	10	Axx

Figure 22. Code output illustrating the matching process for each reporting entity. Each day has a certain number of sunspot groups, and those groups will be matched based on their proximity to groups reported by the other reporting entities. From here, the classification of the 'same' group will be compared and the differences in the classification method of each entity will be shown.

To quantify the accuracy of the spot finding mechanism of the SDO code, the comparison output is used to find the number of missed spot groups from each reporting entity when compared to the other reporting entities. Iterating through each spot group that has been reported, the current group is compared to other spot groups that were reported on the same day by another reporting entity. Matches are determined by locating the group with positions that best match the candidate spot group. Ideally, groups reported by Holloman and the SDO will be in the same location on the solar disk because the observation times roughly match. For comparisons to SWPC, longitude coordinates are projected backwards uniformly by 8 hours to the approximate time when the SDO image and Holloman spot drawings were taken. If the closest spot group being compared is within 10 heliographic degrees of the test spot group, it is deemed to be the same spot group. A range of 10 heliographic degrees is chosen because the longitude/latitude layovers used by Holloman to determine the position of the center of a spot group on sunspot drawings have grid marks hatched every 10 degrees. This method therefore assumes that any Holloman observer will not be off on the actual position of the spot group and the reported position by more than one increment on the longitude and latitude layover.

While this safety net does allow for most spots to be correctly related, it has two downsides. The first is that if there are groups that are closely spaced on the solar disk that do not belong in the same group, there is a chance that these groups will be incorrectly linked with another proximate group that should not match. Secondly, the less common occurrence of incorrect reporting of sunspot group position can cause misses when the two groups would have been matched in the case of an accurate report. These mishaps are sometimes corrected when mistakes are discovered by SWPC or Holloman, but the number of missed mistakes in reported position of sunspots is not negligible, totaling 19 miscoded entries over the 6 month test period surveyed for Holloman AFB. This number is out of 707 reported groups in this time period, roughly 2.7% of the total reported groups. This percentage may be considered higher if the post-publishing corrected mistakes are counted. The error percentage is low, but the number of mistakes is equal to over 70% of the miss percentage (2.7/3.8) between the SDO code and Holloman. Said another way, the number of groups that the SDO missed compared to Holloman is comparable to the number of miscoded spot groups reported by Holloman AFB. Extending this realization to SWPC reports, it is reasonable to assume that there are miscoded entries in that data set as well (perhaps to a lesser extent). Unfortunately, this hypothesis is impossible to verify in the same manner; Holloman records their spot drawings for each day making it easy to go back and visually confirm any report. This is not the case for SWPC, so it is impossible to reduce any error in SWPC's publication and the possibility of an incorrect reporting must be considered uncorrectable.

When looking at any particular reporting entity in Table 4, it can be seen that the match percentage of groups found by the SDO code compared to groups that either Holloman or SWPC found is always greater. Displayed in the table in this

case is the number of missed groups by each reporting entity when compared to other entities, and in all comparison tests, the SDO misses the fewest number of groups compared to the other entity. It should be noted that in the case of comparing SDO to both Holloman and SWPC (on the bottom row of Table 4), there are significantly more missed groups. This can be the case because of several different reasons, the main one being that the SDO can detect smaller spots than either Holloman or SWPC. Each spot group detected is required to have more than 0.3 millionths of a solar hemisphere in area in order to be considered an actual spot group. This is more or less an arbitrary requirement, but it was selected based on the achieved match percentage. Because of this limit, additional dark spots that are detected using the SDO code are neglected when comparing to Holloman or SWPC. In the matching process, it is possible to increase the requirements to be considered a spot group so that larger areas must be achieved to be kept in the comparison cycle. The groups that would be cut out in this case are small groups comprised of one or two spots, likely spot groups in the formative stage of evolution. However, the position match percentage drops to lower values after this selective processing. Moreover, the point of this comparison is to show the number of additional spot groups that the SDO code can detect, and the percent increase of additional spot groups matched to either Holloman or SWPC. These positive results demonstrating the limited number of missed sunspot groups between SDO and SWPC/Holloman illustrates the accuracy of this sunspot detection method. While not all groups are detected, a very low miss percentage when comparing SWPC, Holloman, and the SDO code shows the success of this detection method.

Table 4. Location matching between each reporting entity shown in raw count and percentages over the July 2012 - December 2012 time span. Spot groups were limited by requiring that SDO spots seen must have an area of more than 0.3 millionths of a solar hemisphere. When comparing the reporting entity in the left column with any of the other reporting entities listed across the top, the numbers listed illustrate the amount of spot groups the top entity failed to match compared to the left entity.

	Holloman Missed Groups	SWPC Missed Groups	SDO Missed Groups	Total Groups
Holloman	-	61/707 (8.6%)	25/659 (3.8%)	707
SWPC	84/730 (11.5%)	-	44/686 (6.4%)	752
SDO	223/857 (26.0%)	214/857 (25.0%)	-	857

4.4 Classification Accuracy Evaluation

The next stage of analysis involves determining the accuracy of the classification method used on the detected sunspot groups. This comparison is more difficult simply because of the various factors that can affect the determination of as sunspot group's class. In addition to the numerous deciding factors for a sunspot group's classification, the classification process is largely ambiguous meaning that the difference between even the simplest of classifications can be minuscule and subjective. For example, when looking at the first letter of the McIntosh classification, classifications for groups that have developed penumbra on both the leading and trailing spots in the group are determined by the length of the spot group. As an example, groups that are less than 15 heliographic degrees in length are given the classification 'E', while groups of length greater than 15 heliographic degrees are designated 'F' class groups. Because there is a hard cutoff for this distinction, the difference between two separate classifications could simply be that one observer determines the group to be over 15 degrees in length while the other observer determines the group to be under 15 degrees in length. This difference is not major in terms of an accurate representation of the length of the spot group, but it does create a large difference in the classification as a whole and would

therefore be flagged as an incorrect classification in a comparison step. Moreover, the first letter of the McIntosh classification is not the only letter affected by this subjectivity. All three letters of the classification process are subject to unspecific wording and ambiguous thresholds that determine a spot group to be of one classification or another. While separate observers can interpret the data differently, a consistent classification process using the SDO code is of principle importance. It is with this goal in mind that the parameters determining an accurate classification are defined.

In order to establish the accuracy of a classification method, three separate standards for comparison are employed, each level further adapting to the subjectivity of the McIntosh classification. A 60×60 matrix is created where each column and row has been assigned one of the 60 McIntosh classifications. Equal row and column numbers are assigned the same classification so that the diagonal "coordinates" are comprised of matching McIntosh classifications. The order of the 60 classifications across the rows and columns is the same for both columns and rows and objectively follows the best representation of the evolution of a sunspot group (based on length and maturity of the penumbra). The order given to the Zurich classifications is as follows: A, H, B, C, D, E, F. Within each of these classifications, the subsequent letters area also ordered. For example, there are two different types of McIntosh classifications for the 'B' designation. The overall order of the two 'B' classifications in the comparison matrix depends on the letters following 'B'. For the penumbra classification, the order follows the string: x, r, s, h, a, k. The order for the compactness classification is: x, o, i, c. Only the possible McIntosh classifications are listed along each row and column. This matrix will be used to show classifications that are proximate to others as any matched classification will

be proximate to the diagonal. Classifications far off the diagonal are less accurate, in general. The order of classifications in the comparison matrix is listed in Table 5.

Table 5. The order of McIntosh classifications is presented adjacent to both the column and row numbers. Each classification has been assigned both a row and column number in the comparison matrix according to the best representation of sunspot group growth.

Col/Row	Class	Col/Row	Class	Col/Row	Class	Col/Row	Class
1	Axx	16	Chi	31	Dki	46	Ekc
2	Hrx	17	Cko	32	Dkc	47	Fro
3	Hsx	18	Cki	33	Ero	48	Fri
4	Hax	19	Dro	34	Eri	49	Fso
5	Hhx	20	Dri	35	Eso	50	Fsi
6	Hkx	21	Dso	36	Esi	51	Fsc
7	Bxo	22	Dsi	37	Esc	52	Fao
8	Bxi	23	Dsc	38	Eao	53	Fai
9	Cro	24	Dao	39	Eai	54	Fac
10	Cri	25	Dai	40	Eac	55	Fho
11	Cso	26	Dac	41	Eho	56	Fhi
12	Csi	27	Dho	42	Ehi	57	Fhc
13	Cao	28	Dhi	43	Ehc	58	Fko
14	Cai	29	Dhc	44	Eko	59	Fki
15	Cho	30	Dko	45	Eki	60	Fkc

The simplest way to determine the accuracy of the SDO classification method is to do a one to one comparison between the results from two reporting entities. This means that when a group is matched based on proximity to another group reported by a different entity, each letter of the classification must be matched exactly. If any part of the two classifications do not match, or more specifically the match corresponds to a point that does not lie on the diagonal of the comparison matrix, the issued classification is not adequate under this metric. This type of matching method will be referred to as the direct method. Remembering that there is a large amount of subjectivity in the McIntosh classification process, the requirements are loosened to an intermediate category. This metric includes the entirety of the first letter of the McIntosh classification, accepting any classification

that matches the first letter. Finally, for a broad category enclosing most foreseeable subjectivities in the classification process, the relaxed metric is defined. This metric accepts all matches that fit the first letter of the McIntosh classification. The specific regions of acceptable classifications should be outlined. Including all areas accepted in the previous two metrics, this final category accepts neighboring Zurich Classifications with broader acceptance bands in the 'H' category. The order (listed in Table 5) was chosen to most accurately represent the most common evolution of a spot group so that the closest and most similar classifications are neighbors. Typically, the 'H' category is placed after 'F', but that jump in terms of size, shape, number of spots, and complexity of magnetic field is substantial, so instead the 'H' category is placed more towards the formative stage of the sunspot group's life. For this metric therefore, matches accept classifications of the neighboring letter, for example, 'C' accepts both 'B' and 'D'. For the 'H' classification, the 'C' group is also accepted because of the potential loss of small spots surrounding the main spot with developed penumbra in the 'H' classification. If the presence of smaller spots is overlooked, a group's polarity may never be tested and that spot group may be classified incorrectly as a result. This is accounted for in the relaxed metric of comparison. All three metrics are viewable on the matrix representation in Figure 23.

Again, a classification issued from Holloman or SWPC does not necessarily represent the ground truth. Simply coming up with a different classification than was published does not indicate any significant error in a classification process, especially when the issued classification from either of those two reputable sources may have been different if an alternate solar analyst had happened to be on duty that day.

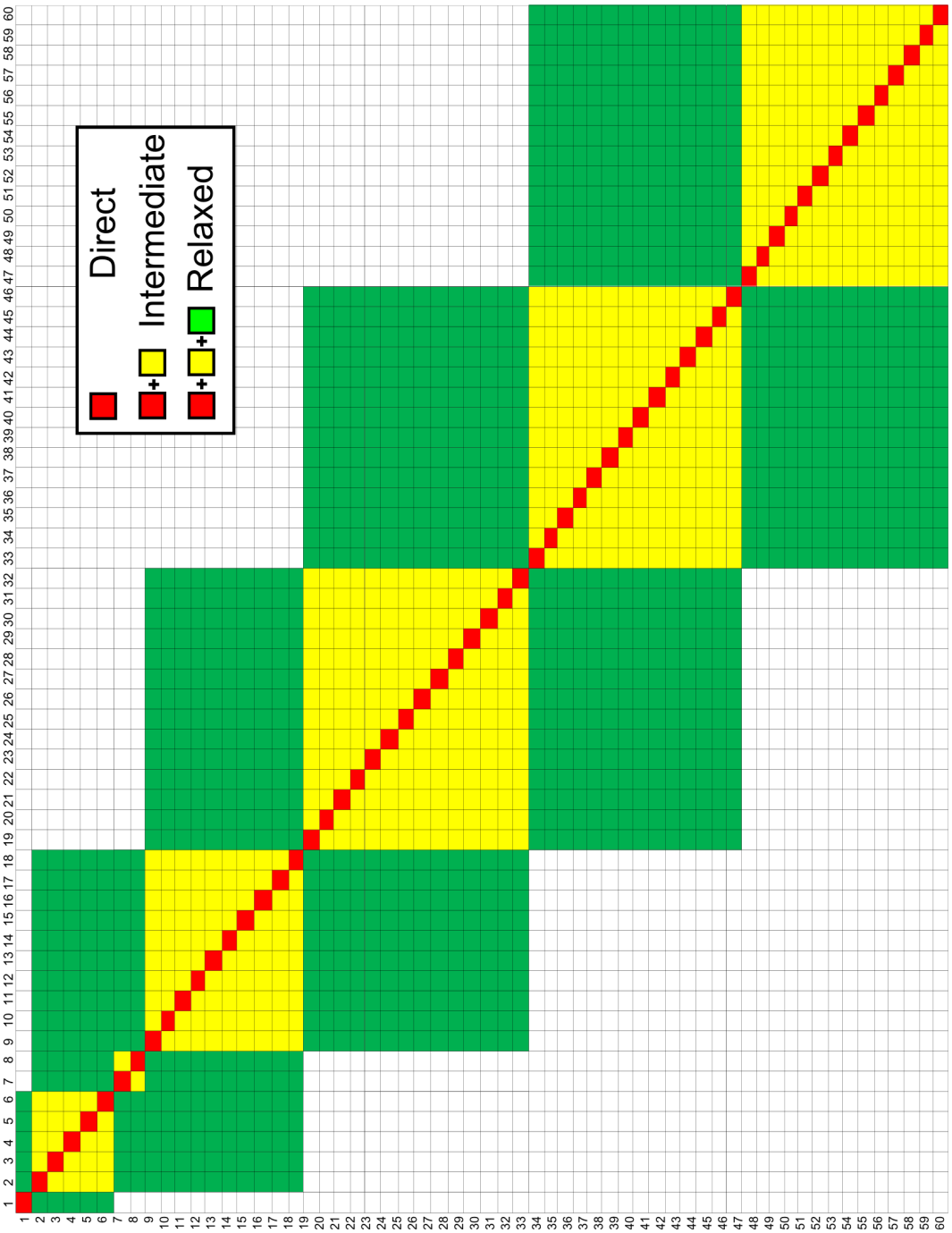

Figure 23. Each metric for classification comparison is summarized on the 60×60 matrix. Every row and column number corresponds to an individual McIntosh classification listed in Table 5. The Direct metric is the most stringent while the Relaxed method is the most open. Each match made between reporting entities will end up somewhere on the matrix, but good matches occur near the diagonal line.

A baseline to compare the classification method of the SDO code is established through a comparison of SWPC reports to Holloman drawings. While still extremely variable, this comparison shows the difference between the classification of Holloman and the reported classifications coming from SWPC. Comparing Holloman to SWPC is not necessarily a good indicator of accuracy as one classification is dependent on, or suffers influence from, the classification of the other. Because SWPC publications are an amalgamation of the classification results of several different observatories, differences in the code may not be as significant as they would be if SWPC was making their own observations. Ideally, the classification process from the SDO should show a difference comparable to the difference between the other two reporting entities. This would illustrate the SDO code result lies within the same amount of difference from the baseline. Therefore, results that are proximate to the difference between SWPC and Holloman are considered good as they demonstrate the ability of the SDO code to replicate the Holloman classification process in an independent, automated manner.

It should be noted that this comparison metric does not capture the consistency of the second and third letter of the McIntosh code. These parts of the classification tend to get lumped into a single percentage, so an additional assumption of this metric is that these later categories are less important to the overall classification scheme, at least at this stage of code development. Additional tests can be run to show specific accuracy for these areas, but these tests have not yet been attempted.

4.4.1 SWPC to Holloman.

The baseline for classification comparisons is set between Holloman and SWPC. The numbers from this section will next be compared to the SDO to SWPC

numbers to establish the proximity of the SDO method to Holloman and SWPC when comparing to the Holloman/SWPC standard.

Table 6. Summary of Holloman and SWPC code match percentages for the three different match metrics.

Metric	Match %
Direct	33.73%
Intermediate	59.28%
Relaxed	87.22%

The relaxed metric contains the vast majority of all the matched sunspot groups. Outliers predominantly lie on the upper side of matching matrix, indicating that SWPC classifications tend to have a higher classification compared to Holloman. For example, when Holloman classifies a group as 'C' and SWPC's classification doesn't match, SWPC will in general give that group a classification of 'D' or higher. The intermediate metric also holds a substantial portion of match points. Many of the sunspots matched fit within the first letter of the McIntosh classification, and this proves to be the highest direct match of any comparison.

4.4.2 SWPC to SDO.

Next, the same type of comparison is applied to the SWPC and SDO match. This will enable a comparison between the SDO code prodct and the baseline SWPC/Holloman match. For the test data set analyzed here, the SDO classification method was programmed to obtain results as close as possible to the McIntosh classification scheme. This means that all values for determining classification were taken directly from [*McIntosh*, 1990]. No attempt was made to alter parameters to best match any of the other reporting entities.

In this SDO to SWPC case, the percent match is dissimilar to the SWPC and Holloman match in almost all categories. Specifically, the direct match is

Table 7. Summary of SWPC and SDO code match percentages for the three different match metrics for the 6 July - 31 December 2012 data set.

Metric	Match %
Direct	13.46%
Intermediate	49.26%
Relaxed	83.74%

significantly lower than the baseline match set in Section 4.4.1, but this fact is not surprising considering the wide variation displayed by the classification process. Paired with the fact that SWPC and Holloman classifications are not unbiased towards each other, it is reasonable to see that the direct match percentage between SWPC and Holloman should be higher than the direct match percentage between SWPC and SDO. Following the same line of reasoning, the intermediate match percentage will be lower as well. As it turns out, the difference has diminished to roughly 10%, cutting the direct match percentage difference by a factor of two. When looking at the relaxed metric, it can be seen that the match between SWPC and SDO is significantly closer to the Relaxed metric from SWPC to Holloman, indicating a good method for classification, within 4% error. A major point to emphasize is the fact that SDO classification code is uninfluenced by any bias from outside sources, and this match percentage is achieved without any user input or influence of past classifications. Additionally, the classification process is not biased by outside observations made prior to the development of the code. This establishes that the SDO classification method is an acceptable tool capable of being effectively compared to other classification methods.

4.4.3 SDO to Holloman.

Next, the method is applied to matches with Holloman AFB. The resulting match percentages are much better than those obtained when comparing SDO to SWPC.

Table 8. Summary of Holloman and SDO code match percentages for the three different match metrics.

Metric	Match %
Direct	20.42%
Intermediate	53.05%
Relaxed	86.04%

With improvement in each of the comparison metrics in contrast with the SDO to SWPC comparison, the SDO to Holloman match is closer to the baseline from Section 4.4.1. The direct metric is the most improved, increasing the match percentage for this category by a little more than 7% from the direct comparison in Section 4.4.2. However, the direct metric match percentage in this comparison is still lower than the Holloman to SWPC match, as expected. The intermediate result improved a little less than 4%, while the relaxed metric sits deficient from the SWPC to Holloman match by a single percent. This comparison demonstrates further the usefulness and accuracy of the SDO method compared to both of the other comparison methods used in this study.

4.5 Classification Consistency

To show the consistency of this classification method, an additional 6 months of data was tested under the same conditions and the resulting percentages were similar, shown in Table 9. This additional 6 months of data represents a blind test executed on a data set that was not used to optimize match percentages. There are

Table 9. Summary of all three metrics for judging accuracy of classification applied to the three comparison scenarios. While the direct and intermediate match percentage is clearly significantly lower in the SWPC to SDO match, the relaxed metric shows that results are still within the general purview of the SWPC to Holloman match. The Testing period data set spans from 6 July 2012 through 31 December 2012 while the Evaluation data set runs from 1 January 2013 to 29 June 2013.

	SWPC to Holloman	SWPC to SDO	SDO to Holloman	
Direct	33.73 %	13.46 %	20.42 %	Testing
Intermediate	59.28 %	49.26 %	53.05 %	
Relaxed	87.22 %	83.74 %	86.04 %	
Direct	33.38 %	20.22 %	24.54 %	Evaluation
Intermediate	57.48 %	51.25 %	50.91 %	
Relaxed	87.67 %	83.80 %	80.65 %	

improvements that can be made to this data set similar to those outlined in Section 4.3 that were not applied to this comparison, indicating that the numbers comparing SWPC to SDO and SDO to Holloman could be better than the ones shown, but the results are similar enough to show consistency between the two different testing periods. Consistency between both data sets shows that the results obtained are statistically significant and will likely not change for additional testing periods.

In addition to establishing the accuracy of the SDO method, this comparison also sheds light on an additional use for the SDO code. Due to the consistency of this method, paired with the fact that this comparison method differs somewhat from the Holloman method, the automated SDO code can be used to evaluate the bias contained in the Holloman drawing and classification method. In theory, there is some amount of bias contained in both methods. However, the SDO code uses the same images to produce the same classification results every run, and the code can be altered to, in turn, alter the resulting data. Therefore, systematically changing elements in the SDO code to produce classification results that better match the results obtained by Holloman will quantify the inherent bias for particular classifications. This research does not endeavor to quantify the bias of the other Air

Force optical observatories, but rather hopes to show the method of comparison for future pursuit of this purpose.

4.6 Holloman AFB Classification Bias Evaluation

The classification process used by the SDO code is based on the same set of defined rules for classification used by Holloman AFB, and an acceptable match percentage has been achieved. If parameters of the SDO code in the classification section are altered (spot eccentricity, spot length and group length), the match percentages change. At some value (different for each of these parameters), the error between matched group classifications will reach a minimum. If parameters are altered one at a time, this minimum point will indicate the exact bias for that parameter with respect to the SDO code. For example, there is a cutoff between 's' and 'a' type sunspot groups at 2.5 degrees. Both the SDO code and Holloman are making classifications according to this metric. If the SDO code is altered to 2.8 degrees, however, and the match percentage increases, this would indicate that the cutoff used by Holloman may actually be closer to 2.8 degrees. Parameters selected to be evaluated are calculated to a much higher precision in the SDO code than their counterpart parameters on the Holloman drawing board (see Appendix 1). The spot symmetry parameter is subjective, but the parameters involving spot length are not. Match percentages improve when these parameters are altered to optimal levels, quantizing the general tendency for Holloman solar analysts to label a spot group one way over another.

This method does not necessarily illustrate any error in the classification process used by Holloman because both methods (SDO and Holloman) are based off the McIntosh method. Rather, this comparison process further illustrates the

differences between the two methods and, most importantly, gives a metric by which to measure the Holloman observer bias.

To determine the correctness of the fit, a new system of analysis based on the 60×60 matrix from Section 4.4 is used. To judge how well the classification fits the spot groups that have been matched with Holloman AFB, a system is created to quantify how the average classification compares to the actual classification given. This comparison can be done with respect to both entities, meaning that both rows and columns can be compared to one another on the matrix. For the explanation of the method, rows will be used, but the same process can be applied to columns as well. To quantify the variation, a single row is isolated in the 60×60 matrix, taking note of the row's number (1 - 60). Next the biased weighted sample variance is determined to show how each parameter change affects the total accuracy.

$$\sigma_{row}^2 = \frac{\sum_{i=1}^{60} (x_i - x_{row})^2 w_i}{\sum_{i=1}^{60} w_i} \tag{16}$$

where x_i represents the current column and w_i is the number of spots in that element. An example calculation is shown in Figure 24. The value of σ_{row} is then solved and added in quadrature to the corresponding σ_{column} value to get a total σ. This parameter is then used to confirm a better fit for matched sunspot classifications. In addition to a σ_{total} value, the summation can be limited to break out each of the various Zurich classifications into separate categories to find more specific weighted sample variances. In this way, it can be seen how altering each parameter affects the individual Zurich classifications alongside the total variation of the matrix.

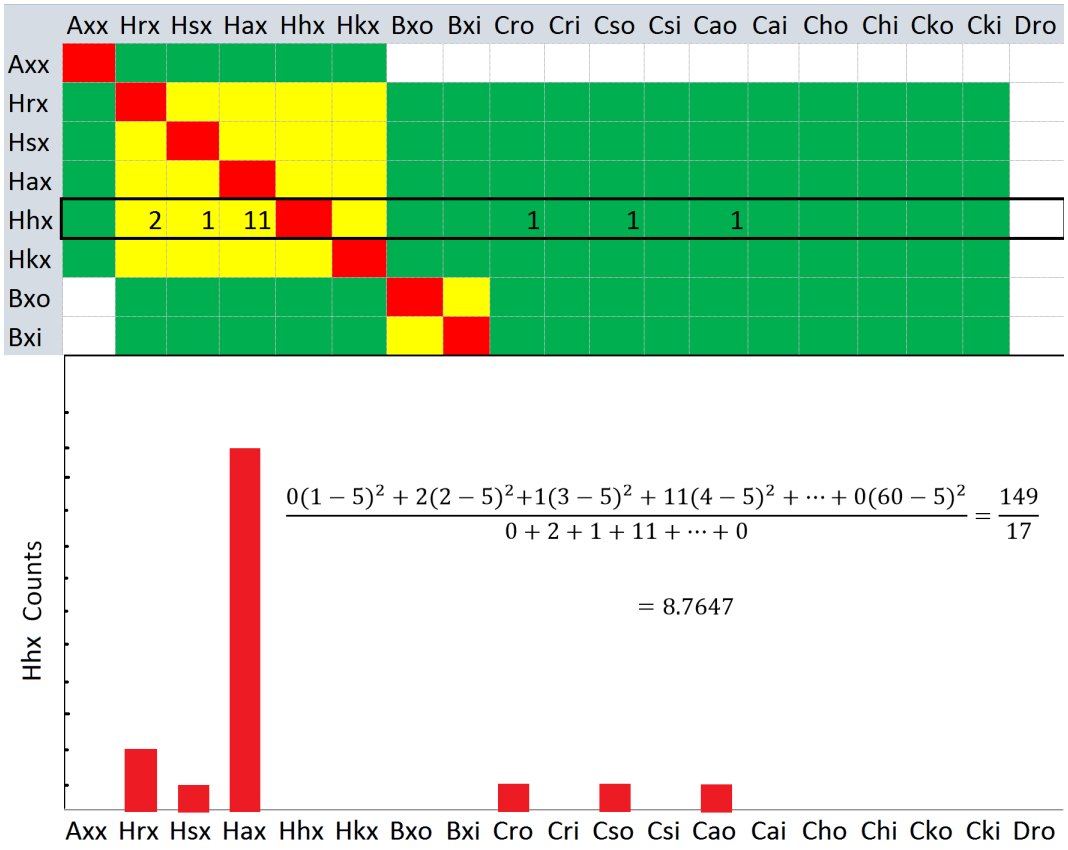

Figure 24. The classification Hhx was selected to highlight the calculation of the biased weighted sample variance for a generic code comparison so all other values outside the single row are set to zero. A classification of Hhx is 5 units from the origin and therefore represents the bias. Summing all the squared weighted distances and dividing by the total weight, the average location for the Hhx comparison is attained. Subtracting the bias yields the final variation from the center point. This comparison is done in the vertical direction as well and added in quadrature to form the variation metric.

4.6.1 Modified Zurich Classification Optimization.

The first bias evaluated was the determination of the first letter of the McIntosh classification, the modified Zurich classification. This letter is determined off the total length of the group for classifications of 'D' and higher. To calculate the classification, it must first established whether or not there is complete penumbra surrounding more than one of the spots in the group. This condition determines whether or not a spot can be considered eligible for a classification above

a ‘C’. Proceeding under the assumption that this classification method is sufficient with respect to both SWPC and Holloman reports, the classification method is also tested while varying the lengths that determine the first letter. To initiate the variation, the length requirements that define classes ‘D’, ‘E’, and ‘F’ were all extended by 0.5° increments. An optimal length combination will provide the best match between Holloman and the SDO code.

From Table 10, it can be seen that there are particular classifications for which the biased weighted sample variance of the match between the SDO code and Holloman classification is minimized. Not all minima for each subdivision lines up with the total minimum. In general, the test that included a bias of 17.5° for the F class, 12.5° bias for the E class, and 7.5° bias for the D class had a lower variance than the other tests. In the break out the variance calculation visible in the subsequent columns, it can be seen that the subsection variance becomes minimum for other tests, potentially providing a more specific bias. However, this evaluation simply focuses on the value of σ_{total}. The main take away from this result is that by altering the length at which each of these classifications is used, the match percentage between the SDO code and Holloman can be increased, indicating that those new length requirements are more appropriate to describe the classification method used for the first letter by Holloman.

It should be noted that the optimization of the modified Zurich classification was established using an older version of code that differed in how sunspot numbers were counted. If each code run was recreated, it is likely that the bias would be similar as the differences between the code is minimal.

Table 10. Biased weighted sample variation for the first letter of the McIntosh classification with respect to group length over the 6 July - 31 December data set. The labeled columns are indicative of the variation in each of the Zurich categories. The final column displays the cutoff values for the F, E, and D classifications in heliographic degrees for the corresponding code run. The variance is minimized in the 8th row (highlighted) for F,E, and D cut off lengths of 17.5°, 12.5°, 7.5° respectively.

Total Weighted Variance	A Variance	H Variance	B Variance	C Variance	D Variance	E Variance	F Variance	F, E, D Cut Off
11.58	2.12	4.21	2.24	7.41	8.64	12.92	15.50	13.5°, 8.5°, 4°
11.48	2.12	4.19	2.18	7.33	7.65	12.72	16.33	14°, 9°, 4°
11.23	3.01	4.00	1.91	6.20	7.23	12.43	16.85	15°, 10°, 5°
11.35	2.12	3.74	2.04	7.50	6.43	11.99	17.14	15.5°, 10.5°, 5.5°
11.10	2.12	3.34	1.99	5.76	5.51	12.47	16.95	16°, 11°, 6°
11.04	2.05	3.25	1.82	5.48	5.14	12.60	16.93	16.5°, 11.5°, 6.5°
11.00	2.05	3.18	1.77	5.43	5.79	12.39	16.74	17°, 12°, 7°
10.87	2.12	3.19	1.75	2.91	6.72	12.46	16.74	17.5°, 12.5°, 7.5°
11.21	2.05	3.13	1.69	4.35	6.74	13.22	16.74	18°, 13°, 8°
12.00	2.05	3.12	1.69	3.30	6.64	13.98	18.89	18.5°, 13.5°, 8.5°
12.50	2.05	3.11	1.65	3.33	7.08	14.28	19.90	19°, 14°, 9°
12.61	2.05	2.89	1.60	3.34	7.10	14.66	19.90	19.5°, 14.5°, 9.5°
12.94	2.05	2.80	1.60	3.43	8.02	15.31	19.90	20°, 15°, 10°

4.6.2 Eccentricity Classification Optimization.

The second bias established was with respect to the penumbra classification's symmetry, the second letter. The value used in the development of the McIntosh classification was the eccentricity of the largest spot. This parameter was used to establish whether or not a spot was symmetric or asymmetric. It was determined that on a scale where a perfect circle has an eccentricity of zero and the most eccentric closed object approaches the limit at unity, that the eccentricity cutoff should be 0.5. Because there is no numerically defined cutoff for a sunspot who is asymmetric vs. symmetric, this particular section of the classification was highly unspecific. The value of eccentricity used to classify each spot group was therefore altered between 0.1 and 0.9 to find the minimum variation point. The variation became minimum at an eccentricity value of 0.8, shown in Table 11. This indicates that in general, Holloman observers require a spot to achieve an eccentricity of 0.8 or higher before labeling that sunspot group to be asymmetric. Interestingly, the variance dips on the other side of 0.5 as well, but to a lesser degree. This indicates that the worst value to choose for eccentricity happened to be 0.5 for the comparison to Holloman.

4.6.3 Largest Penumbra Length Optimization.

The final bias established was with respect to the largest spot length in the penumbra classification, also in the second letter. Typically, the cutoff between large and small penumbra is 2.5 heliographic degrees, but the difficulties surrounding this measurement have already been discussed at length. Given that the smallest increment on the layover is in units of 10 degrees, it comes as no surprise that there would be variance with respect to this classification (the cutoff is $\frac{1}{4}$ the smallest measurable distance). In this case, the test was started at a value of

Table 11. Biased weighted sample variation for the second letter of the McIntosh classification with respect to spot symmetry over the 6 July - 31 December data set. The variance of this letter is broken out into Zurich classifications again, following suit with Table 10. The final column displays the value of eccentricity used in the classification process for each run of the code. The variance is minimized for a spot eccentricity of 0.8 (highlighted). Variance dips for values smaller than 0.5 as well, but to a lesser extent.

Total Weighted Variance	A Variance	H Variance	B Variance	C Variance	D Variance	E Variance	F Variance	Spot Eccentricity
12.48	7.61	7.08	5.40	8.26	9.32	12.81	17.86	0.1
12.47	7.61	7.08	4.87	8.25	9.44	12.81	17.81	0.2
12.48	7.61	7.11	4.87	8.46	9.42	12.81	17.81	0.3
12.77	7.61	7.13	4.87	8.45	9.89	13.68	17.81	0.4
14.09	7.61	7.11	5.40	8.08	9.99	15.13	20.50	0.5
13.21	7.61	7.14	4.78	8.06	10.03	14.72	18.41	0.6
12.64	7.61	7.60	5.05	8.25	9.39	14.24	17.44	0.7
12.44	7.44	7.78	4.67	8.24	9.28	13.88	17.14	0.8
12.48	7.36	8.62	4.57	8.21	9.24	13.75	17.25	0.9

2.0° and the spot length cutoff was increased by increments of 0.1° to find a minimum value. After reaching a length of 3.0°, the trend of minimizing variation was seen, so an additional 1° was tested. At the end of these runs, the variation continues to decrease (Table 12), so it can be concluded that the bias is greater than 3.9°. This is a significant variation from the actual cutoff, but was a likely result of the interpolation performed during the classification step using the latitude/longitude layover.

Table 12. Biased weighted sample variation for the second letter of the McIntosh classification with respect to penumbra length of the largest spot over the 6 July - 31 December data set. The variance of this letter is broken out into Zurich classifications the same as the previous two tables. The final column displays the value of spot length used in the classification process for each run of the code. It can be concluded that the bias is $> 3.9°$ compared to the 2.5° standard (highlighted).

Total Weighted Variance	A Variance	H Variance	B Variance	C Variance	D Variance	E Variance	F Variance	Penumbra Length
13.20	8.00	7.45	4.86	9.28	10.62	15.41	17.10	2.0°
13.28	7.97	7.53	4.87	9.53	10.57	15.60	17.10	2.1°
13.14	8.00	7.48	4.87	8.44	10.51	15.44	17.14	2.2°
13.46	7.63	7.20	4.87	8.39	10.30	15.44	18.27	2.3°
13.45	7.61	7.27	4.87	8.31	10.27	15.45	18.27	2.4°
14.09	7.61	7.11	5.40	8.08	9.99	15.13	20.50	2.5°
14.03	8.00	7.10	4.87	8.06	10.04	14.91	20.50	2.6°
13.22	7.63	7.12	4.87	8.06	9.96	14.89	18.34	2.7°
12.90	7.61	7.21	4.87	8.04	10.00	14.67	17.54	2.8°
12.39	7.63	6.58	4.87	8.04	9.99	14.42	16.29	2.9°
12.22	7.61	6.41	4.87	8.03	9.76	14.05	16.29	3.0°
12.01	7.61	6.41	5.40	7.99	9.72	13.16	16.46	3.1°
11.95	7.61	6.41	4.87	7.99	9.72	13.16	16.29	3.2°
11.69	7.61	6.41	4.87	7.90	9.63	12.31	16.29	3.3°
11.54	7.61	6.41	4.70	7.90	8.79	12.30	16.29	3.4°
11.48	7.61	6.41	5.23	7.90	8.79	12.27	16.12	3.5°
9.14	3.90	6.10	4.68	7.92	7.22	8.28	11.75	3.6°
9.14	3.90	6.10	4.68	7.92	7.22	8.28	11.75	3.7°
9.14	3.90	6.10	4.68	7.92	7.22	8.28	11.75	3.8°
9.06	3.90	6.10	4.68	7.90	6.77	8.27	11.75	3.9°

V. Conclusions

A new fully automatic sunspot detection and McIntosh classification method for SDO HMI imagery implemented in MATLAB has been presented. Processing both HMII and HMIM full disk images, results were obtained that align with the difference between an established standard comparison defined by the juxtaposition of published reports from two standard sources of sunspot data: Holloman AFB and the Space Weather Prediction Center.

5.1 Summary of Results

A fully automated image processing program was created to extract information about detected sunspots on the SDO HMI imagery. This program uses a single time step to calculate the position of sunspot groups detected through an iterative global thresholding method. In conjunction with magnetic field data, sunspots are grouped into their proper regions using an iterative region assignment process. Important sunspot parameters are extracted and processed through a linear logical sequence designed to mimic the classification process outlined by [*McIntosh*, 1990].

Consistent results are shown for the detection of all visible sunspots, as well as calculation of sunspot area, group number and spot number. Missing spot percentages comparing Holloman to SWPC numbered at 11.5% whereas the reverse comparison gave a miss percentage of 8.5%. Comparisons to the SDO code result yielded a miss percentage of 6.4% with respect to SWPC and 3.8% with respect to Holloman indicating a lower miss percentage. Comparison of total calculated sunspot area yielded fit result R squared values between the three data sources of 0.749 (Holloman to SDO), 0.778 (Holloman to SWPC), and 0.780 (SDO to SWPC).

SDO total calculated area was generally less than area reported by SWPC and Holloman. Comparison of total number of groups between the three data sources yielded fit result R squared values of 0.705 (Holloman to SDO), 0.703 (Holloman to SWPC), and 0.722 (SDO to SWPC). SDO reported number of groups was generally more than those reported by Holloman and SWPC. Comparison of total number of sunspots detected yielded fit result R squared values of 0.720 (Holloman to SDO), 0.712 (Holloman to SWPC), and 0.738 (SDO to SWPC). The total number of spots determined by the SDO code was significantly higher than either Holloman or SWPC.

By comparing positions of detected sunspot groups, McIntosh classification results are shown with differences comparable to the difference between Holloman and SWPC, illustrated through a three way analysis of weighted biased variation. The classification accuracy was partitioned into three separate categories: direct, intermediate and relaxed. While the direct comparison yielded low results between all three reporting entities, the relaxed metric of comparison showed uncorrected match percentages of 87.67% for SWPC to Holloman, 83.80% for SWPC to SDO, and 80.65% for SDO to Holloman. Comparing SWPC to Holloman, The algorithm was developed on a test set of images, spanning approximately six months from 6 July 2012 through 31 December 2012, to provide comparable results to our standard sources. Subsequently run on an additional 6 months of data from 1 January 2013 to 29 June 2013 to show consistency, the algorithm yielded similar results to the first 6 months tested.

After establishing the accuracy of the detection and classification method, parameters were perturbed by incremental amounts to show variation in the match percentages compared to our two standard sources. It was shown that match percentages reach maximum values for particular values of classification cutoffs.

Parameters relating to group length, spot length and spot eccentricity were tested to determine the bias associated with each item for Holloman AFB. For group length, it was shown that compared to the regular 5°, 10°, and 15° cutoffs for 'D', 'E', and 'F' class sunspots, Holloman biased their classifications to align with group lengths of 7.5°, 12.5°, and 17.5°. For spot length compared to 2.5°, the bias was found to be greater than 3.9°. For spot eccentricity compared to a standard defined to be 0.5, the bias was found to be closer to an eccentricity of 0.8.

5.2 Future Work

Further work should be done to demonstrate the stability of the SDO code with respect to detection and grouping. This can be addressed by operating the code on a higher cadence of data to produce time dependent values of sunspot area, number of spots, number of groups, spot length, McIntosh classification, etc. This may uncover inaccuracies that could be contributing to classification errors, most likely in the spot finding stage. If found, more work can be done to improve the stability of the drawing process. In addition, more work should be done to look into the predictive capabilities of the code.

Alternate processes for sunspot grouping and classification have been explored as outlined by Aschwanden [*Aschwanden*, 2010]. These processes should be explored for potential expansion of the SDO code as well as a comparison between the different methods. New methods for grouping detected sunspots may significantly improve error. Watershed or neural networking methods may be able to serve this purpose while the original purpose of the SDO code is preserved. Additionally, incorporating region number data into the grouping process may significantly improve classification match percentages by ensuring the propper groups are

matched. Determining a better way to match groupings between the SDO output and SWPC or Holloman may have a large effect.

A more in depth look at the second and third letter accuracy may show that these sections of code need revision. The comparison metric selected for use in this research specifically reflected a direct comparison as well as broader categories that mostly favored an evaluation of the Zurich classification. These specifics should be addressed to ensure complete accuracy for all of the three letters. The type of comparison used in this research can still be applied for other comparison metrics. Other similar metrics may therefore be developed to look at these additional features in the McIntosh classification.

A mechanism for establishing AF observatory bias has been demonstrated, but this concept can be readily applied to all sunspot parameters and Learmonth and San Vito observatories. A more in depth study of the bias should also be applied to Holloman as this can lead to a more precise determination of the bias in addition to a quantification of some additional parameters. There is also a potential to automate this bias evaluation given the code's capacity to operate using several different patterns at once.

Additional tests to improve the statistical significance of the code result should be accomplished. While the SDO satellite has only been in use since 2010, the general nature of the code allows for adaptation to other data sources including SOHO imagery. This may enable easier comparison to other automated classification schemes that may have been designed to function other sources of data.

Appendix 1. Holloman Classification Method

A.1 From Drawing to Classification

The AFMAN15-124 sets standards for the reporting of classified sunspot groups that mirror guidelines for combined McIntosh/Mt. Wilson classification schemes [*USAF*, 2013]. All hand classifications are carried out under the guidelines set by both the Air Force manual and the schoolhouse at Holloman AFB, but interpretation of those guidelines often cause different opinions on the classification of even the simplest spot groups. Therefore, it was decided to contrast the method of automatic classification with the method of hand classification [*USAF*, 2013] over a direct comparison between the two, as there can be large dissent between observers about the classification of a particular spot group (even after published spot reports are referenced). This difference are highlighted when comparing Holloman to SWPC in Section 4.4.1.

A.2 Drawing Procedures

The solar analyst starts the drawing process by initiating the java program scripted to communicate with the SOON telescope used for continual observation of the sun. The SOON telescope is used at every Air Force Optical Solar Observatory. This java program uses the Zulu time, calculated from the computer's internal clock which may need to be adjusted by the observer, to pull important information from the solar ephemeris. Specifically, the solar analyst needs both the P and the B angle to perform the drawing. The P angle is the sun's rotation around the center of the disk with respect to the earth while the B angle is the sun's tilt either towards or away from the earth [*Seidelmann and Urban*, 2010]. These angles are simply a consequence of our orbit around the sun coupled with the tilt in our axis of rotation

and the sun's tilt in axis of rotation. They are necessary to calculate in order to put all observers at the same reference angle with solar north at the top of the drawing. Once recorded on the Air Force Weather Agency (AFWA) Form 21, the solar analyst takes the form to the white light board on the SOON telescope.

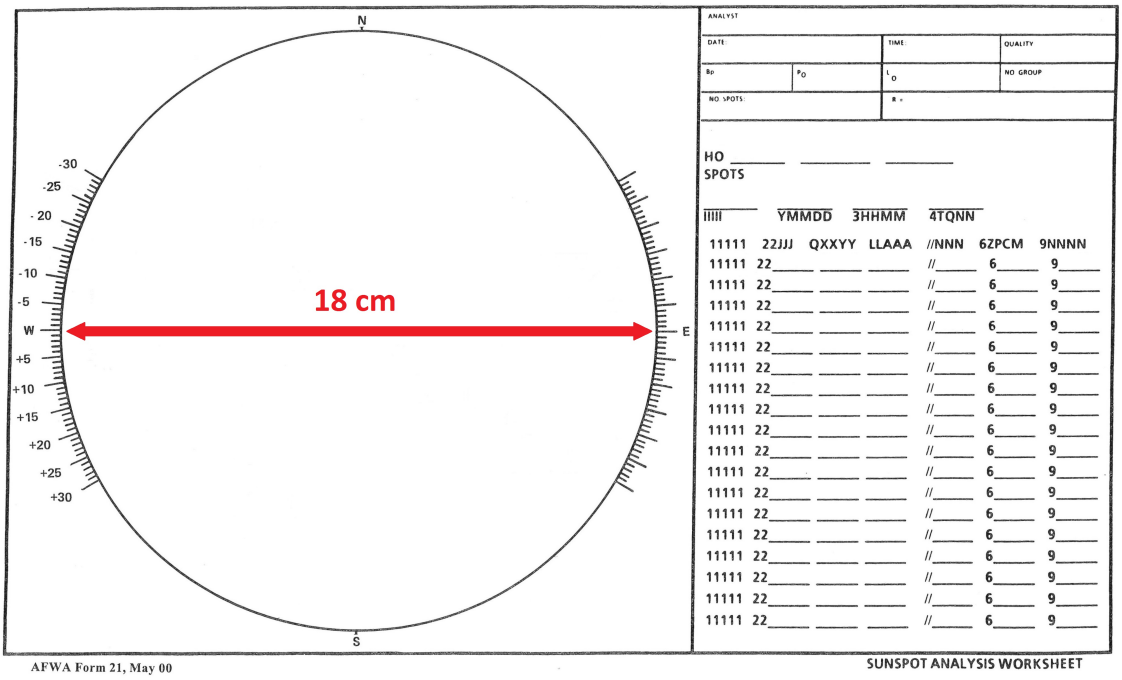

Figure 25. AFWA form used to record the position of sunspots and code in the sunspot report from an AF Solar Observatory. This form is placed on the drawing board of the SOON telescope and all spots are recorded within the 18 cm diameter circle on the left hand side. Then, the classification process is completed and recorded on the right hand side before coding into a sunspot report.

The Form 21 is an elongated sheet of paper incorporating both a section for drawing sunspots projected onto the white light board inside an 18 cm circle, as well as a section for encoding the observation into a spots message after the drawing has been completed. In order to correct for the P angle rotation, the analyst uses the rounded number taken from the observing program and marks the hatch mark on the side of the drawing disk corresponding to the proper P angle. On the Western limb of the disk on the Form 21, there are positive and negative rotation angles to

which the analyst must attempt to match the P angle to the best of his or her ability, and the angles along the side of the drawing go to positive and negative 30 as the P angle can range between $\pm 26.4^{\circ}$ visible in figure 25. From this point, the analyst places the paper onto the white light board, orienting the paper with the line through the appropriate P angle, perpendicular to the base of the drawing board. By rotating the paper on the drawing board in this way, the P angle rotation is corrected, and no rotation about the center of the disk is present in the drawing, at least to the accuracy that the Analyst can orient the drawing on the board.

The image is subsequently focused on the drawing board. Because of seeing conditions varying throughout the day, as well as variation between days, it may be necessary to re-focus the drawing board to get the most accurate representation of the spot region being drawn. Often times, the seeing conditions will prevent a sharp image from being formed, but it is the analyst's job to get the best picture possible to most accurately represent the sun at the observation time. This focusing endeavor is performed by sliding the board along a rail that runs the length of the telescope optics.

Because the seeing conditions and the heat index of the day will alter the focal length of the mirror, the analyst adjusts the board to sit at the approximate location of the focal length. Depending on the change in conditions from the previous drawing, it may be unnecessary to re-focus the image. The next step for the analyst to take is to record the start time of the drawing on the bottom of the form (there is no line on the form for this recording). Both the start and stop time of the drawing will be averaged in order to determine the approximate time the drawing was done. This information isn't necessarily important for SWPC, but is important in order to compare the Observatory method to any other spot

Figure 26. A technician stands in front of the drawing board on the Holloman SOON telescope. White light is reflected down the length of the telescope to the 45° mirror. This image is then reflected down on the drawing board where solar analysts record all the sunspots visible on the AFWA form 21 from Figure 25. The guide instrument is visible above the 45° mirror while the rail along which the drawing board can slide can be seen with a measuring tape running its length.

classification method as the observation time needs to be synchronized to minimize error that may be associated with timing.

After the time is recorded, the analyst begins the drawing. Before actually putting pencil to paper, a high gloss sheet of paper is held by the analyst and moved in swift, tight circles over the top of the Form 21. The analyst uses this technique in order to visibly distinguish between spots visible on the sun and any paper defects on the form. If a defect is seen, a small "x" is placed over the mark in

order to prevent confusion later on when determining the classification of each spot group. Next, using dabbing strokes in order to represent each spot, the analyst outlines each spot region containing penumbra, and fills in each umbra using a pencil. This dabbing motion is adopted because the object being outlined is reflected off the mirror directly above the paper. When drawing, the analyst's pencil generally will cast a shadow over the region he or she is currently addressing, and this prevents the outline of the spot group from being seen while actually drawing on the paper. In addition to this projective hindrance, the atmospheric conditions of the day may also cause turbulence that shakes the projection of the spots on the white light board. Therefore, the analyst must do their best to accurately represent a moving target on the stationary paper. This vibration effect is considerable near the edge of the drawing as small variation on the paper in that region corresponds to larger variation in longitude or latitude. A quick calculation shows that variations of a single millimeter in the East/West direction on the drawing board correspond to a minimum longitude error of 0.3° in the center of the disk out to 5.5° error on the limb, illustrating that this may be a significant source of error in the drawing process. Because of these atmospheric and vibrational effects, a dabbing motion tends to work the best in order to correctly draw all the spots on the sun. After each spot is drawn, the high gloss paper is used again to check how well each spot has been represented on the form. Any errors are erased and re-drawn on the form before moving the next step.

A.3 Magnetic Maps

In general, an analyst can visually group spots they have drawn on the form solely based on their proximity to other spots. However, it may sometimes become necessary to choose the groupings of spot regions based off the magnetic polarity of

those regions. In this case, the analyst must run a polarity diagnostics program, generally referred to as the "magnetic map" of the region in question, in order to determine the magnetic polarity of that region and the surrounding spots [*USAF*, 2013]. This is usually done anyway because the magnetic field lines are often needed to perform the Mt. Wilson classification (unused in this research). The diagnostic tool takes advantage of the fact that light coming from regions of opposite magnetic polarity will be polarized in reverse directions. The analyst therefore uses a polarized lens placed on the front of the SOON telescope to determine the polarity of light coming from each region. Regions usually take about 5 minutes to process, so the magnetic map is generally run while performing the drawing in order to best capture the magnetic field configuration of the spot groups when the drawing was completed. This process can be lengthy, however, sometimes spanning over an hour depending on how many active regions need to be processed. In addition, the diagnostic tool can only accommodate up to 6 regions at a time. If more than 6 active regions are visible on the sun, obtaining a magnetic map for each becomes very time consuming. Because each map is accomplished separately, these magnetic field representations obtained by the program are not synchronized in time, nor do they line up with the observation time at which the drawing was performed. This fact is important to remember when actually performing the classification as the magnetic field lines may not actually line up with the outline of a spot group, potentially introducing a source of error in the determination of the polarity of a spot. It should also be mentioned that small groups are generally not analyzed using a magnetic map. This means that the magnetic polarity of these regions is sometimes assumed and not actually determined using the telescope. When matching group classifications later on therefore, it is possible that some groups

were assumed to be unipolar or bipolar because they were small, but the true polarity may be different.

A.4 Positions and Grouping

After the completion of the magnetic map, the analyst can move into grouping each spot. Groupings of this nature are determined based on the McIntosh paper, outlined again in the AFMAN15-124 [*USAF*, 2013], although the solar analyst generally uses these same guidelines when grouping by simple observation even though the groups may be obvious to a seasoned observer. This grouping technique is performed by first collecting all the spots within 3 heliographic degrees from a leader spot and subsequently accepting spots generally no more than 20 heliographic degrees from the leader spot, depending on the polarity of any of the trailing spots. Visually, the analyst makes these determinations and can separate groups that are close in proximity with dashed lines on the drawing, making it easier to look back later and understand the decisions made in the classification step. In addition, SWPC will sometimes direct observation of specific boxes on the Sun where there are active regions. This direction provided to the analyst on duty may also influence the sunspot groupings.

Once the groups have been determined, the analyst moves into determining the position, length and area of each spot group. Generally, the position of each spot is determined first using a transparency with a printed grid on the front, shown in Figure 27. This grid must be angled with the center of the grid at a higher and higher latitude for decreasing B angle. If the B angle is increasing, the layover can be flipped upside down for the same effect, doubling the usefulness of each layover. This angling is because as the spherical sun tilts either towards or away from our satellite, the zero mark for latitude will no longer be in the center of the disk.

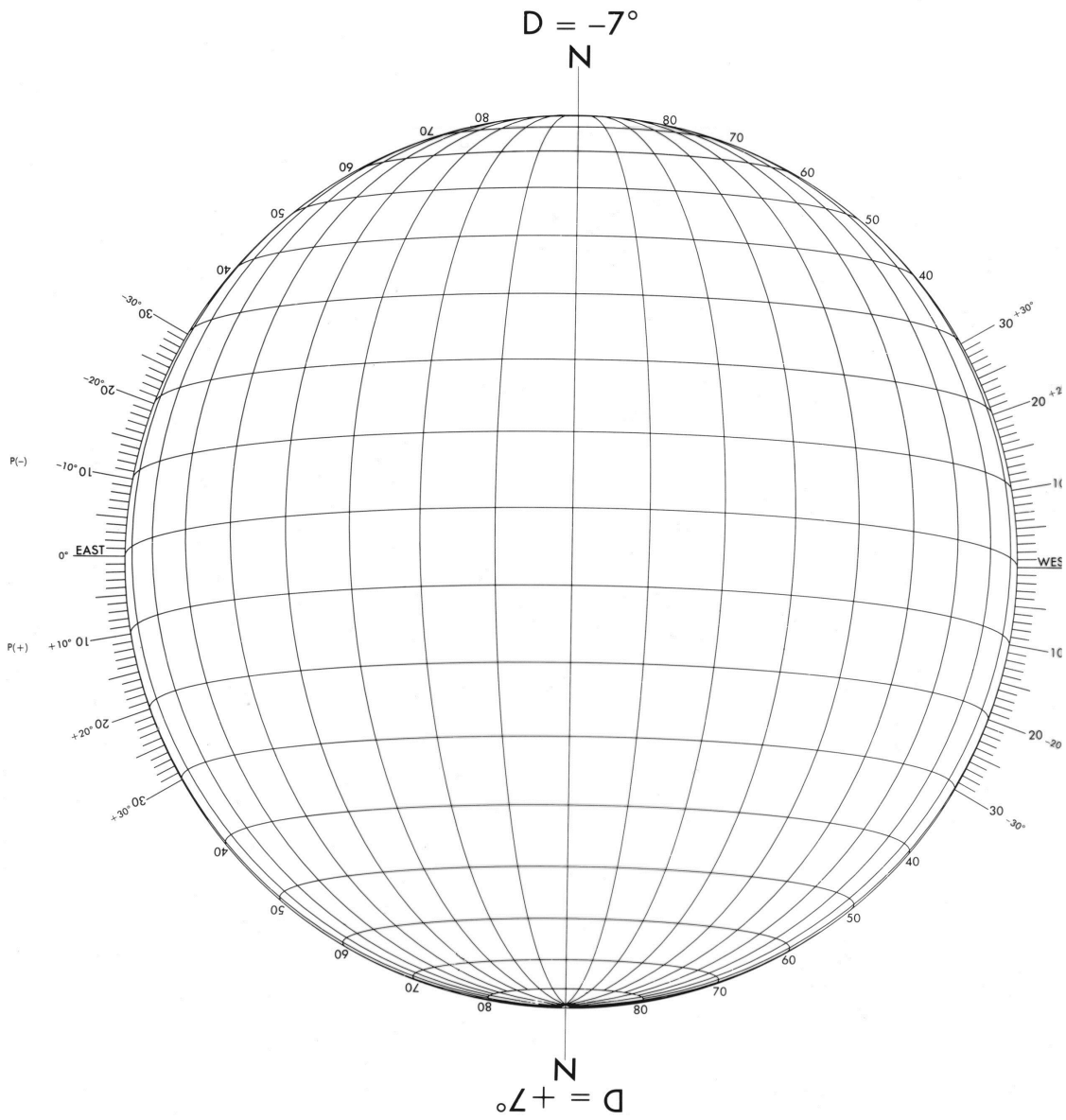

Figure 27. Latitude and longitude overlay used by Holloman Air Force Base to determine the approximate position of sunspots drawn on the 18 cm disk represented on the AFWA form 21 in Figure 25. This particular layover is only applicable for drawings performed when the B angle, or the angle describing the tilt of the sun towards or away from the observer, is rounded to $\pm 7°$. For other cases, separate latitude and longitude layovers are available in one degree increments, noting that each one works for both positive and negative tilt.

Shifting the grid either up or down will correct for this fact. The grid used by analysts has a spacing between lines of 10 heliographic degrees, meaning that

greater accuracy requires mental interpolation performed by the analyst. In addition to this interpolation requirement, it may sometimes be difficult to determine where the center of the group is on the disk. Since the longitude and latitude of the spot group is reported for the centroid of the group only, this determination, coupled with the 10 degree separation of grid lines on the 18 centimeter wide drawing can lead to some significant error in the determination of the position of the group. The length of each group is determined off the same layover by simply picking the end of the East-West extent of the group and comparing it to the other end. Again, if the end of the group does not line up with a grid line, the Analyst will interpolate the value of both the longitude and latitude to get the approximate location of the end of the group. Interpolations for both length and position must be done to the nearest whole degree. Positions of each group are written in adjacent to each spot group with lines pointing to the location on the drawing that the analyst has determined to be the center of the group.

A.5 Area Determination

After the length and position of each group has been determined, the analyst's next step is to determine the approximate area of each group using a layover similar to the longitude/latitude situation. In this case, the transparent layover has representations of different shapes of spots as drawn on an 18 cm diameter disk matching the one printed on the Form 21, seen in Figure 28. These spots are representations of best fit ellipses encompassing the proper amount of area in units of millionths of a solar hemisphere. At this point, the analyst's job is to determine which spot outline on the layover best fits the spot they have drawn on the page, annotating on the form the corresponding area of that fitted spot outline in millionths of a solar hemisphere. For smaller spot groups, the size of outlined spots

on the layover increases slightly by 10 millionths of a solar hemisphere. However, for larger groups, the difference between one size and the next step up can be as great as 200 millionths of a solar hemisphere. If a spot does not fit completely within the layover, analysts often use a series of smaller ellipses and add them up to arrive at a final area value for the group.

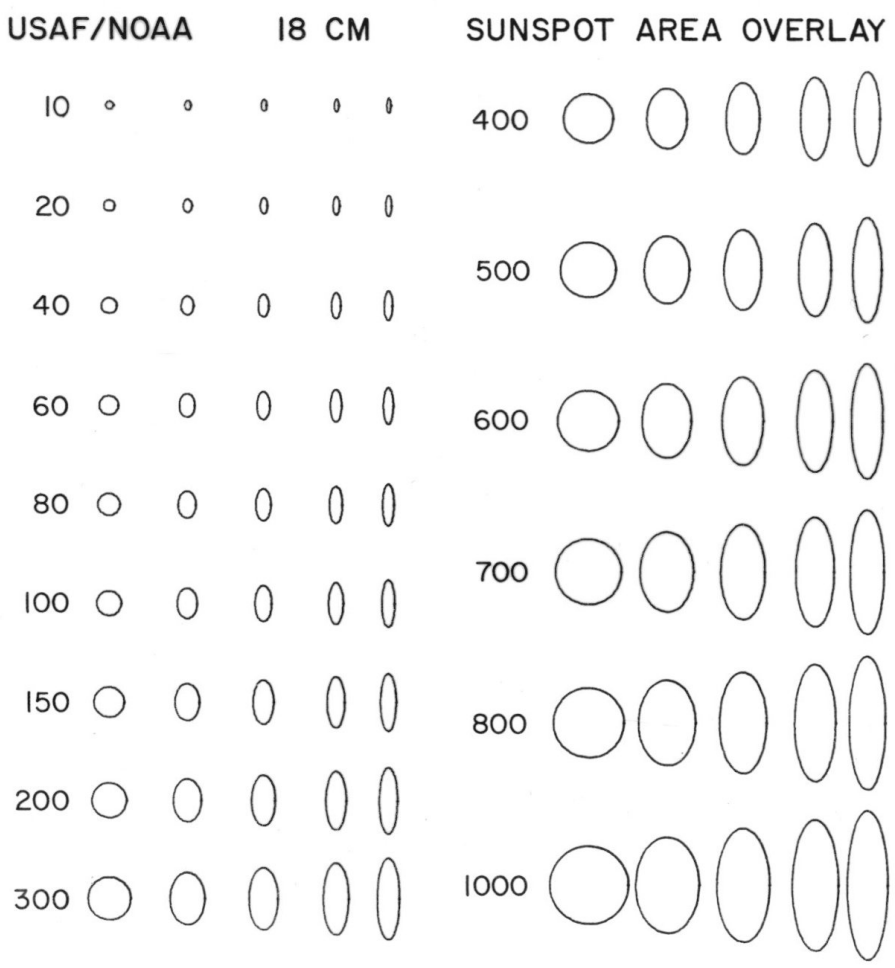

Figure 28. Area overlay used by Holloman Air Force Base to determine the approximate area of the sunspots drawn on the 18 cm disk represented on the AFWA form 21 in Figure 25. Transparency is placed over the form and the best fit circle is determined visually. The corresponding area is recorded before being multiplied by the geometric foreshortening correction factor from Figure 29.

After the approximate area is determined using the area overlay, the solar analyst uses another overlay to finalize the reported area. This overlay displays a geometric foreshortening factor based on position away from the center of the disk. While not certain, it is believed that the layover was created by using a $\frac{1}{cos(\theta)}$ relationship. This factor is multiplied by the area result obtained from the area overlay. The solar analyst determines the approximate position of the center of the sunspot group and finds the corresponding mark for foreshortening correction on the layover, seen in Figure 29. If the approximate position lies between two markers on the foreshortening overlay, the observer rounds in towards the center of the overlay to get the number to multiply with the area from the previous step.

In this way, the group area is approximated based on the visual observations of each analyst. Once these preliminary steps are completed, the solar analyst can begin classifying each spot group. These classifications are completed using the guidelines developed by McIntosh and restated in the AFMAN15-124 [*USAF*, 2013].

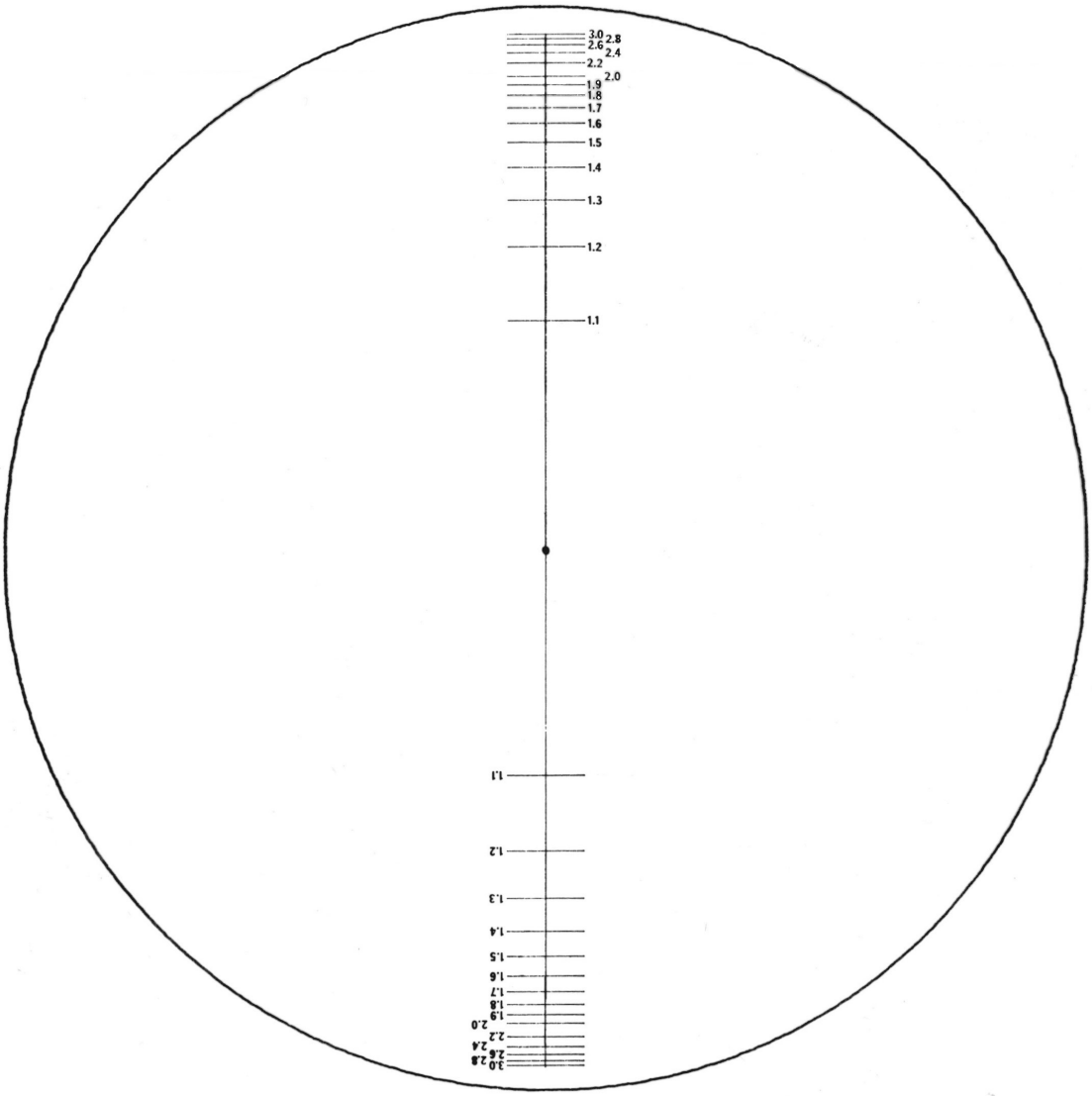

Figure 29. Foreshortening overlay used by Holloman Air Force Base to determine the approximate position of sunspots drawn on the 18 cm disk represented on the AFWA form 21. After determining the area of the sunspot group using the layover in Figure 28, the resulting number is multiplied by the foreshortening factor obtained on this layover. If a spot group lies in the center of two markers, the number closer to the center of the layover is used without interpolating. Additionally, it is important to note that the foreshortening factor does not increase over a value of 3 for high longitudes.

Appendix 2. Derivation of Longitude and Latitude Coordinates

To derive the relationship between pixels in an image and points on the solar sphere, a two dimensional picture is addressed first. The derivation of this result was directed by the National Solar Observatory (NSO) and can be seen in Smart's Text on Spherical Astronomy [*Smart*, 1947].

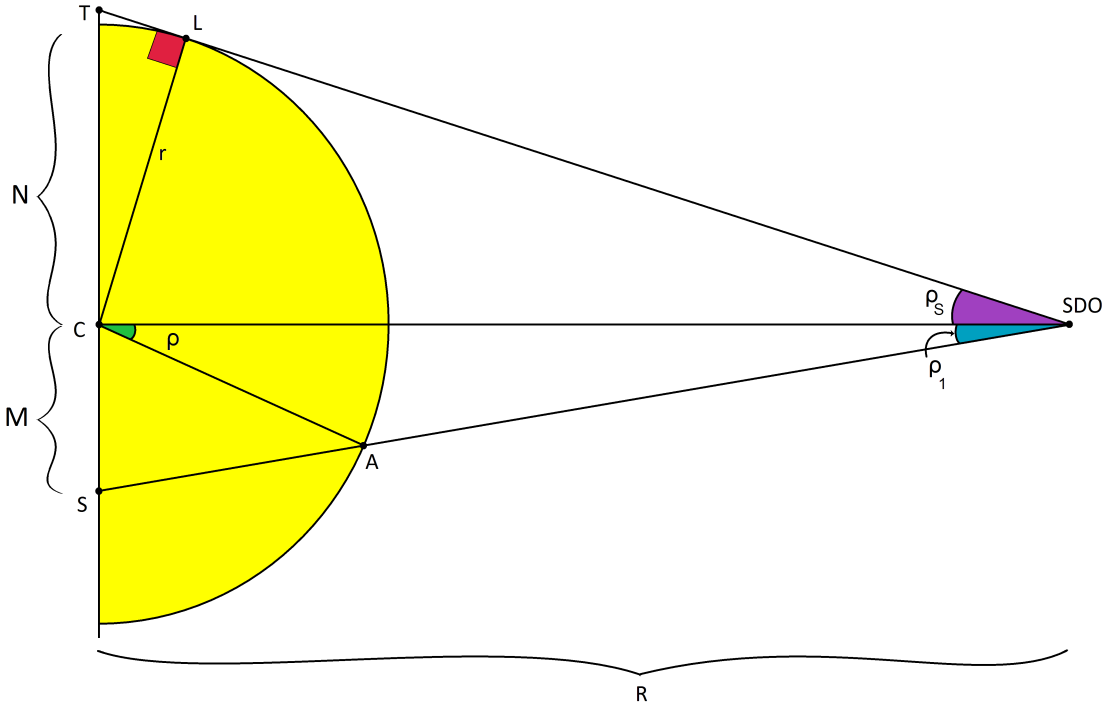

Figure 30. Projecting the line of sight between the SDO, at a distance R from C, and point L onto some point T on the two dimensional plane where $\overline{TSDO}$ is tangent to the edge of the sun, and point A at some point interior to the edge of the sun onto some point S, two triangles are formed. Using similar triangles described by angles ρ_s and ρ_1, a relationship is drawn to find the angle between the center of the sun with respect to the observation point of the SDO and the point A at which any given spot on the surface of the sun exists. This angle ρ is later used to determine both the longitude and latitude of the spot at point A on the sun.

First, an angle $\rho_s = \tan^{-1}\frac{r_0}{R}$ is defined where $r_0 = k[\frac{meters}{pixel}]N$ illustrated in Figure 30. N is defined to be the radius of the sun in pixels. Likewise, $\rho_1 = \tan^{-1}(\frac{r_a}{R})$

where $r_a = k[\frac{meters}{pixel}]M$ and M is defined to be the pixels from the center point C to S. In this case, k is simply a constant with the appropriate units. By dividing the two expressions into each other, an expression between ρ_1 and ρ_s is obtained where R, the distance between C and the SDO in Figure 30, cancels:

$$\frac{\tan(\rho_s)}{\tan(\rho_1)} = \frac{N}{M} \tag{17}$$

Using the law of sines, an expression relating ρ_1 and ρ_s to ρ is determined:

$$\frac{\sin(180 - \rho_1 - \rho)}{R} = \frac{\sin(\rho_1 + \rho)}{R} = \frac{\sin(\rho_1)}{r}. \tag{18}$$

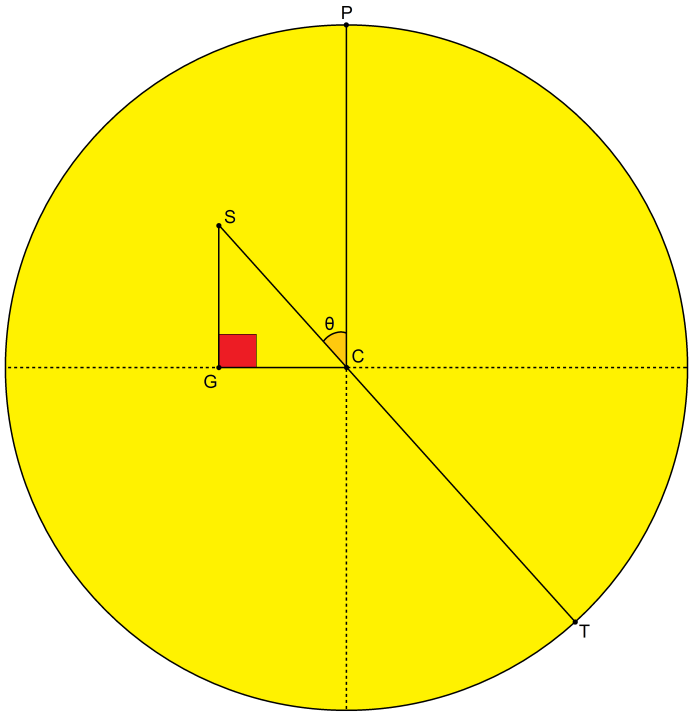

Figure 31. In looking at the sun from the SDO perspective, the base legs of the two like triangles are seen from Figure 30 in lengths $\overline{SC}$ and $\overline{TC}$. Angle $\angle SCP$ describes θ, and in this figure, the P angle has been taken out as all SDO images are without P angle.

Next, using the first relation obtained in Equation 17, an expression relating ρ_1 and ρ_s to the distance to S from C in both x and y coordinates is solved. This is done through simple trigonometric relations and the Pythagorean Theorem:

$$\tan(\rho_1) = \frac{\tan(\rho_s)}{N}\sqrt{M_x^2 + M_y^2}. \tag{19}$$

$$\frac{\tan(\rho_x)}{\tan(\rho_y)} = \frac{M_x}{M_y} = \tan(\theta) \tag{20}$$

where θ is represented in Figure 31. Next, noticing triangle AOP on the sphere, shown in Figure 32, with side lengths ρ, $90 - B$, $90 - B_0$, the spherical law of sines is used to arrive at the following relationship:

$$\frac{\sin(\rho)}{\sin(L - L_0)} = \frac{\sin(90 - B)}{\sin(\theta - P_0)} \Rightarrow \sin(\rho)\sin(\theta - P_0) = \sin(L - L_0)\cos(B) \tag{21}$$

Next, variables in terms of known values (includeing ρ, θ, and the B angle) are isolated for substitution. Therefore, two separate cases are considered to which the spherical law of cosines can apply. The first is for any point visible on the disk when the distance between O and P is less than 90 degrees, shown in Figure 32. From the law of cosines

$$\cos(\rho) = \cos(90 - B)\cos(90 - B_0) + \sin(90 - B)\sin(90 - B_0)\cos(L - L_0) \tag{22}$$

so that substituting in for $\theta - P_0$ gives an expression for both longitude and latitude with no other unknown variables. This process is similar for the second case where the distance between O and P is greater than 90 degrees, resulting in the final expression for relating all three known components and the longitude and latitude.

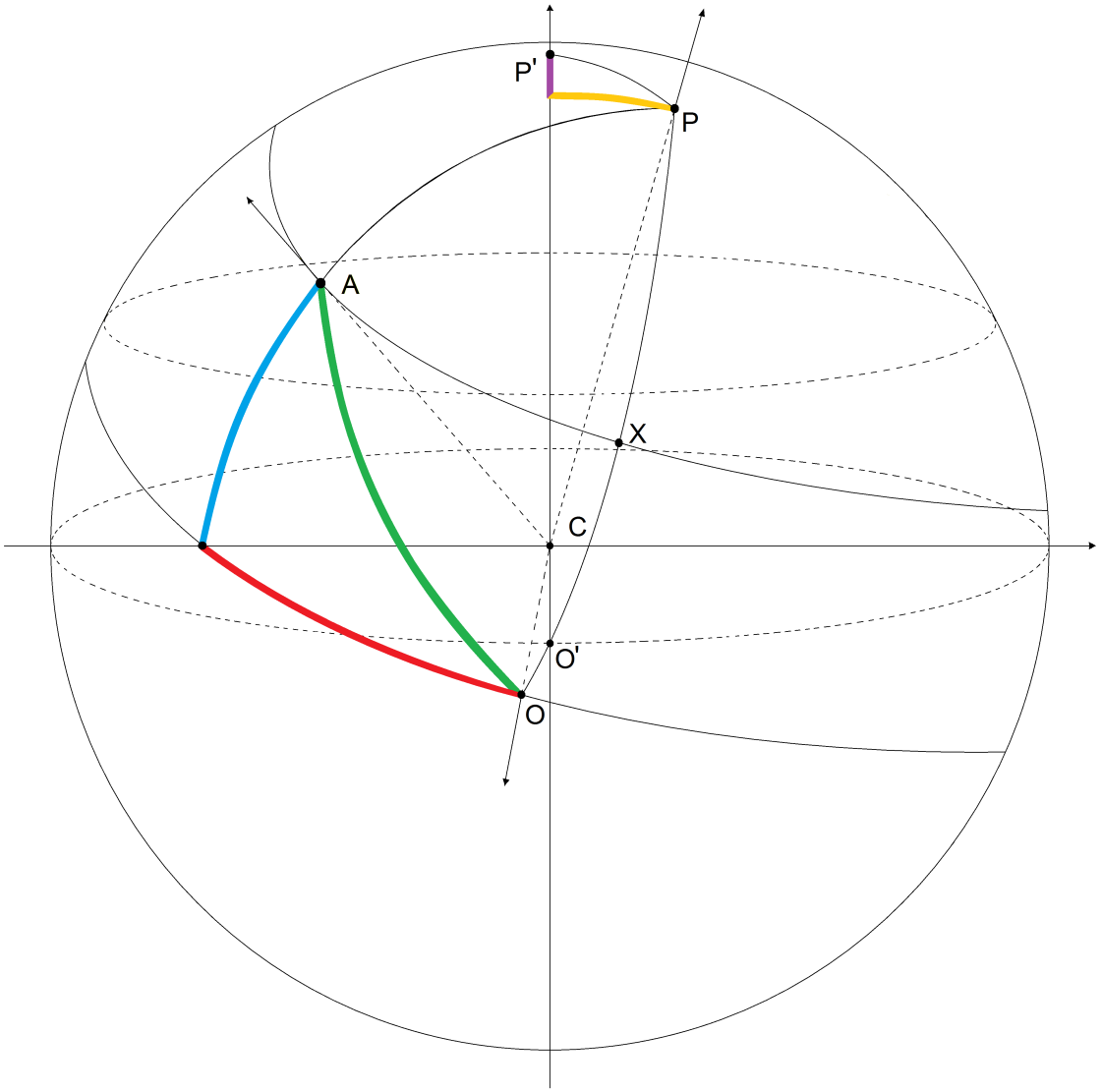

Figure 32. The three dimensional projection of the two dimensional sun is represented in terms of longitude (seen in red) and latitude (seen in blue). For some sunspot at point A on the two dimensional sun, both longitude and latitude can be found by determining their relationship to ρ (described as the angle between O and A from an observer off the sphere on a ray from C through O) and θ (described as $\angle ACO$) through the spherical law of sines. Next, the spherical law of cosines is applied to retrieve each variable in terms of the center, radius, and angle off center, all found through the edge finding routine applied in the beginning stages of the code.

$$\cos(B)\cos(L - L_0) = [\cos(B_0)\cos(\rho) \pm \sin(B_0)\sin(\rho)\cos(\theta - P_0)] \qquad (23)$$

After defining each of these relationships, it is now possible to take points in the Cartesian plane of the image and place them onto the three dimensional sphere of the sun. Some additional logic is required to ensure that the proper expression is being used in any given situation because of the cosine ambiguities involved in the final solution, but this is simply incorporated into the mapping function. In this way, given a point on the image and the time at which the image was taken, both the solar ephemeris calculations and the point mapping function are combined to get a position in longitude (shown in red) and latitude (shown in blue), visible in Figure 32. It should be noted that the illustration of the point mapping scheme shown in Figure 32 are left in the most general form. Published SDO images [*Pesnell et al.*, 2012; *Schou et al.*, 2012; *Scherrer et al.*, 2012] are already corrected for the P angle (shown in orange) making this value zero in these calculations. However, the B angle must still be corrected for, illustrated in purple in Figure 32.

Appendix 3. Code Test on an Additional 6 Months

In order to generate additional confidence that the accuracy of the SDO code could be applied to all potential sunspot configurations, the algorithm was run on an additional 6 months of data, spanning from 1 January 2013 to 29 June 2013. This additional test was run to show accuracy in reported area, number of groups, number of sunspots, and classification.

The same analysis seen in Chapter IV can be applied to these additional plots and they are included for completeness.

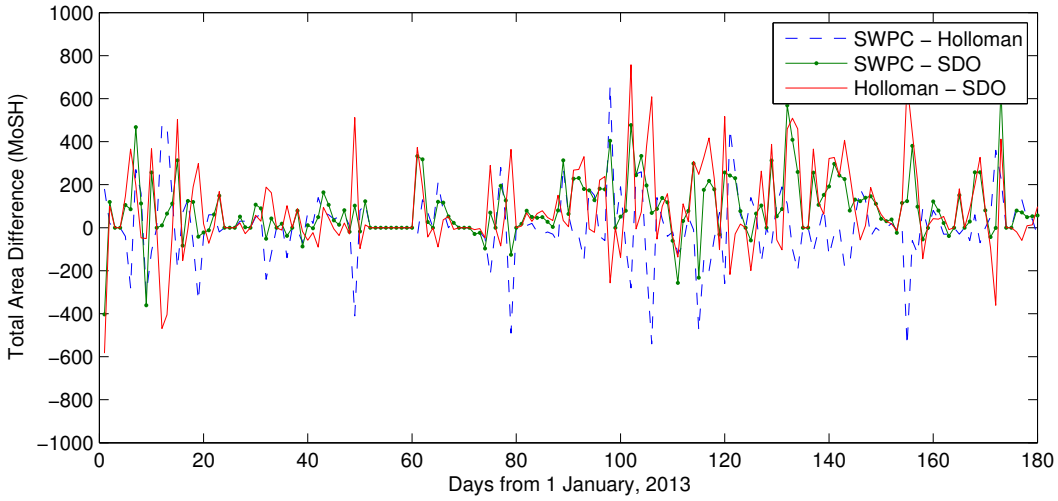

Figure 33. The difference between the daily total area calculated by each of the three reporting entities is plotted from 1 Jan - 29 Jun 2013.

The difference between reported area calculations follows suit with the discussion in Chapter IV. There are no reported areas of significant difference and some of the same trends are visible. Specifically, Holloman tends to have an area lower than that of either SWPC or the SDO, although this is not always the case as is seen in Figure 33. The regression lines seen in the subsequent scatter plots further demonstrate the area accuracy achieved by the SDO code. Figure 34 shows a regression line slope of 0.84 tilted towards the Holloman axis and an R squared

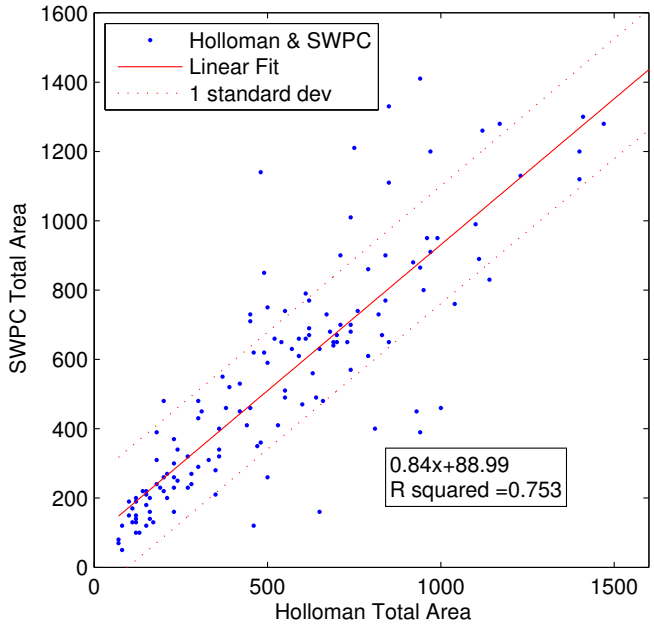

Figure 34. Regression of SWPC and Holloman total area from 1 Jan - 29 Jun 2013.

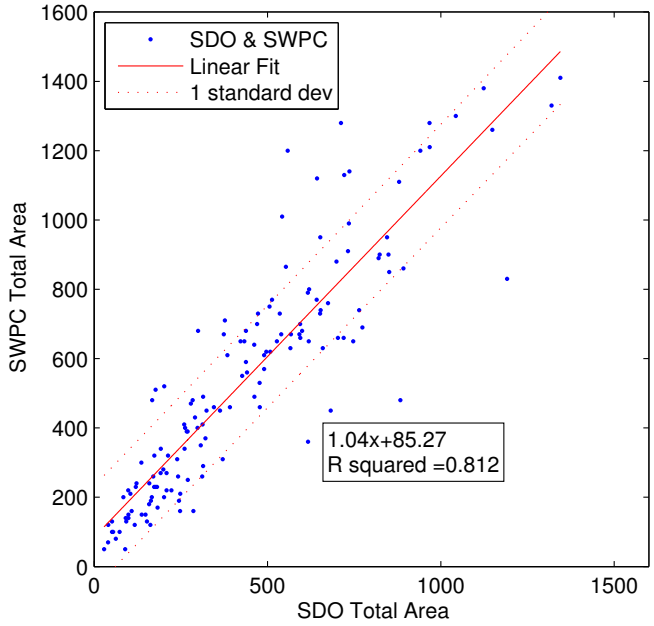

Figure 35. Regression of SWPC and SDO total area from 1 Jan - 29 Jun 2013.

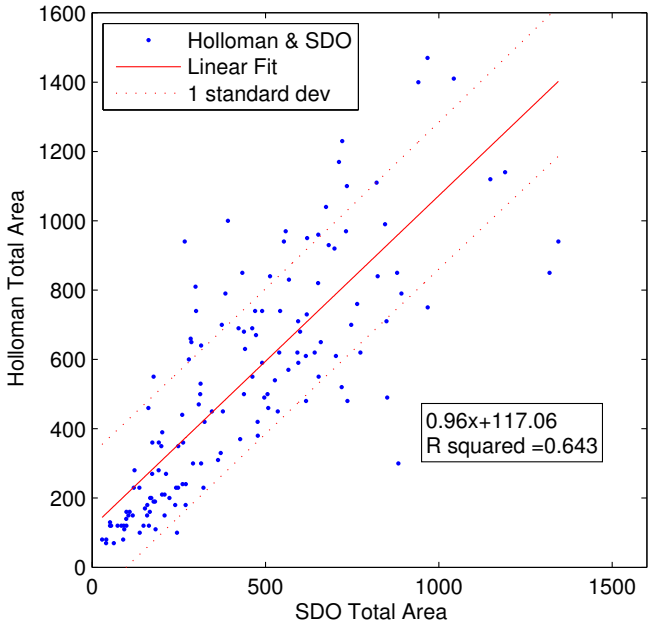

Figure 36. Regression of SDO and Holloman total area from 1 Jan - 29 Jun 2013.

value of 0.753. Figure 35 demonstrates that the SDO code reports consistent areas coming in with a slope value of 1.04 and a high R square value of 0.8116. The final area plot in Figure 36 shows that Holloman areas are generally higher than SDO areas for this set of test data with a regression slope of 0.96 and a comparatively low R squared value of 0.643.

Differences between reported group numbers are also consistent with the test data shown previously. Separation between the difference lines in Figure 37 is not anomalous compared to the group separations seen previously. Figure 38 shows a regression slope of 0.88 and good agreement on the R squared value between SWPC and Holloman. Number of groups for the SDO SWPC comparison is skewed to 0.67 with a low R squared value in Figure 39, indicating less agreement than has been previously seen. The final item in this section, Figure 40, shows slightly better R squared agreement at 0.627 but a more promising regression slope of 0.88.

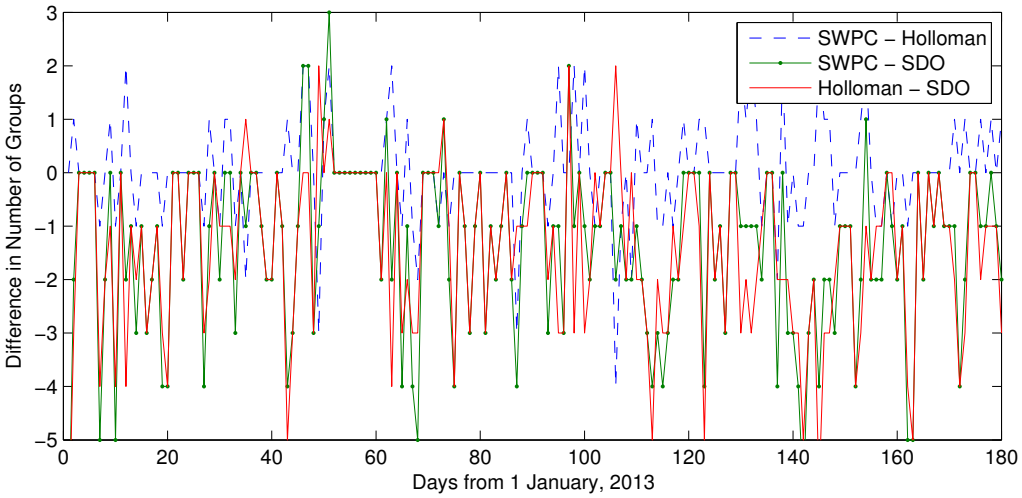

Figure 37. The difference between the daily total number of groups determined by each of the three reporting entities is plotted from 1 Jan - 29 Jun 2013.

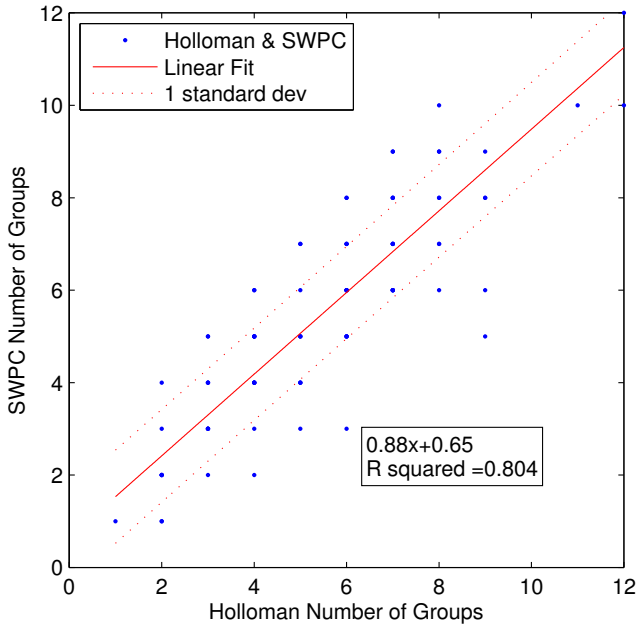

Figure 38. Regression of SWPC and Holloman total number of groups from 1 Jan - 29 Jun 2013.

Comparing the number of spots calculated by the SDO code again reveals the great advantage of spatial resolution in Figure 41. Significant separation exists for days where large numbers of spots are seen on the disk. Figure 42 shows the slope

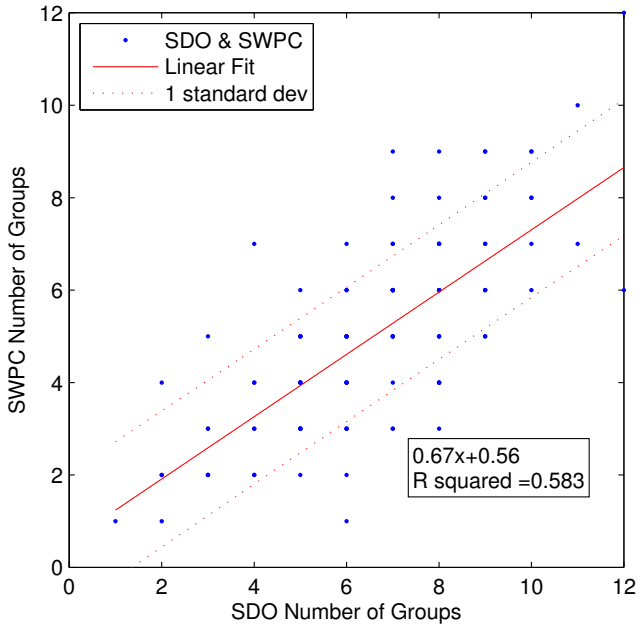

Figure 39. Regression of SWPC and SDO total number of groups from 1 Jan - 29 Jun 2013.

of regression fit tilted in no particular direction with a good slope agreement of 0.99 and an R squared value of 0.739. Figure 43 on the other hand shows significant tilt towards the SDO axis as expected with a good R squared fit value of 0.747. Finally, the regression in Figure 44 demonstrates the same feature with tilt of 0.38 towards the SDO axis again. The R squared value for this regression is fair at 0.704.

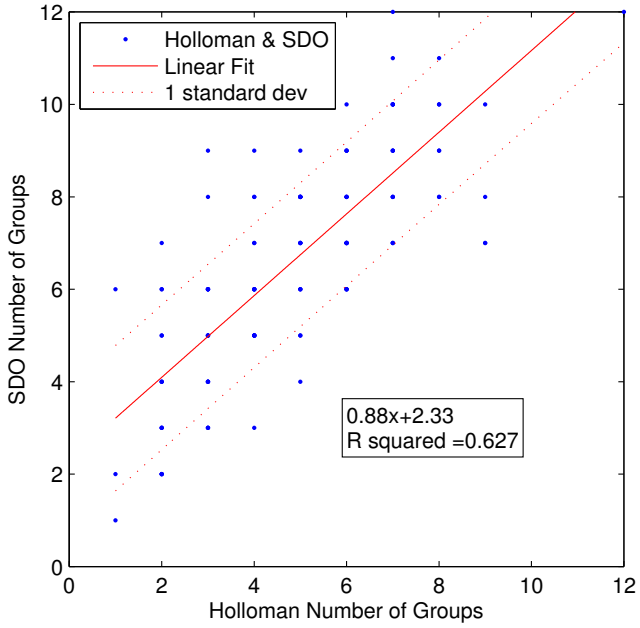

Figure 40. Regression of SDO and Holloman total number of groups from 1 Jan - 29 Jun 2013.

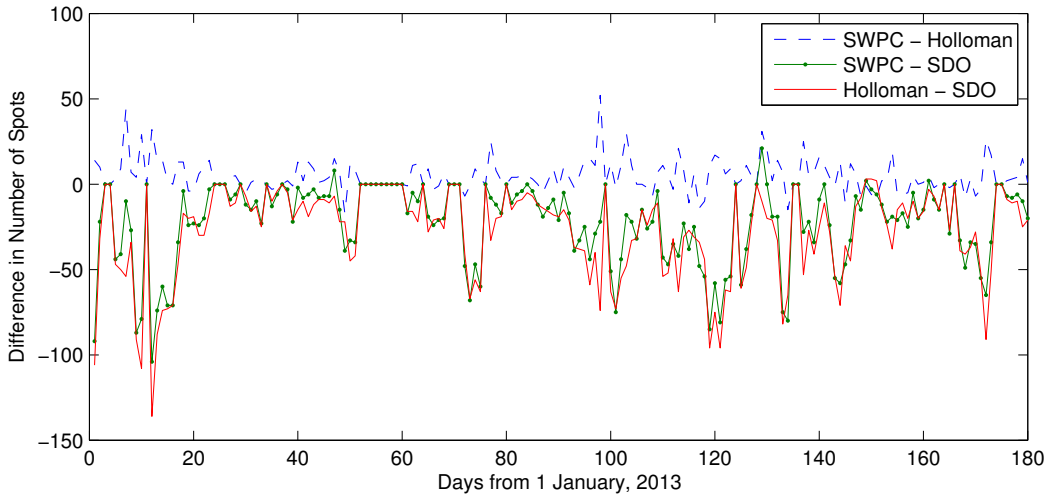

Figure 41. The difference between the daily total number of sunspots detected by each of the three reporting entities is plotted from 1 Jan - 29 Jun 2013.

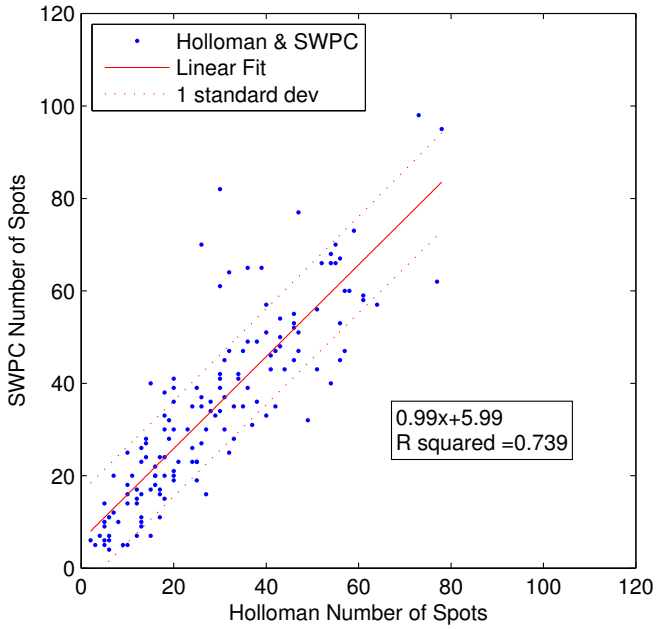

Figure 42. Regression of SWPC and Holloman total number of sunspots from 1 Jan - 29 Jun 2013.

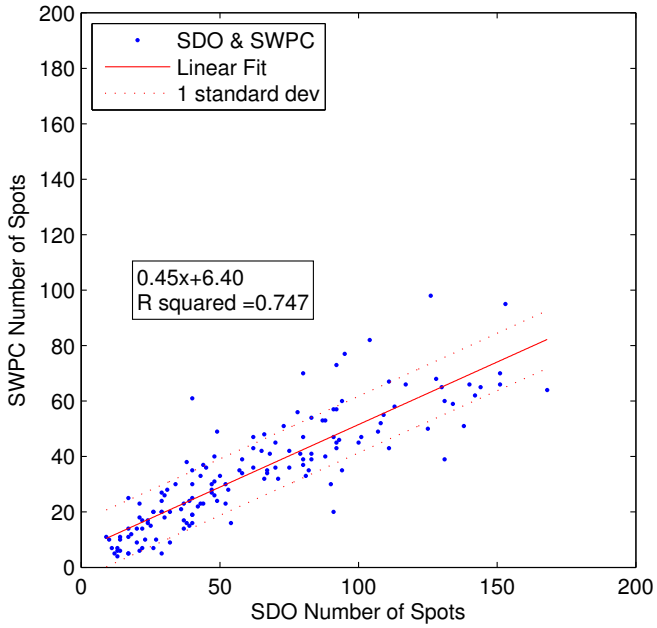

Figure 43. Regression of SWPC and SDO total number of sunspots from 1 Jan - 29 Jun 2013.

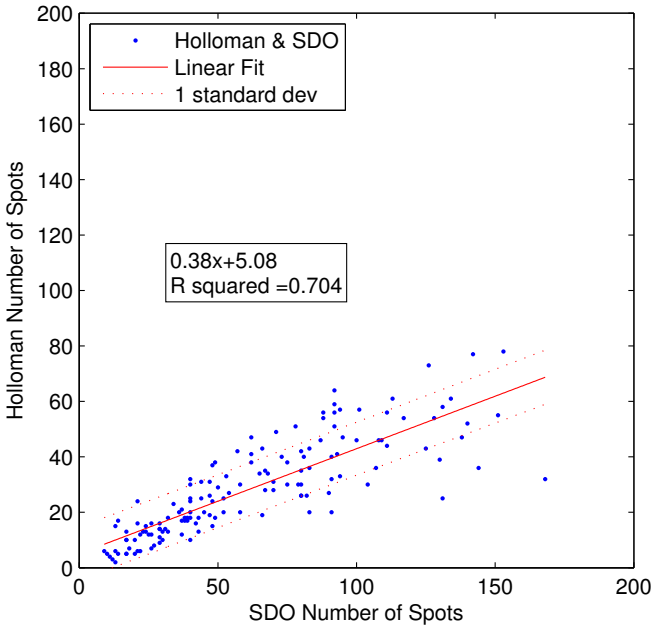

Figure 44. Regression of SDO and Holloman total number of sunspots from 1 Jan - 29 Jun 2013.

Appendix 4. Alternate Image Processing Techniques

There are many other image processing techniques that can be employed within the SDO coding framework. Any process that accomplishes a coding step yielding the same or a similar result can be considered, especially if that new step is faster or more accurate. Many different types of techniques were considered throughout the development of the code, but often times, a functional method was selected for simplicity and not necessarily optimization.

To illustrate, an example alteration is executed addressing the limb darkening correction step. The current code steps involve the addition of an inverted correction image (derrived from the Eddington appriximation) to the grayscale sun in order to flatten out the intensity levels of the sun. This process is described in depth in Section 3.3.3.

An alternative way to complete this step would be to multiply a correction function into the grayscale image to achieve the flattening. The theory behind this relates to the concept of optical depth. The derivation of the Eddington relation (to the first order approximation) gives the intensity profile of the sun for varying angles of θ off from the center of the sun. This function is an approximation of the intensity drop visible on the photosphere, but if it is inverted and multiplied into the grayscale sun, all intensity drop off with angle should be corrected to the first order. This would be equivalent to having a uniform intensity and multiplying first by some intensity profile a to obtain the limb darkened sun (the starting image) and then multiplying by the $\frac{1}{a}$ in order to re-scale the whole multiplicative factor to 1.

In practice, this method is simple enough to construct because the limb darkening function is already known to first order. Figure 45 shows the results of the multiplication of the inverse Eddington approximation with the gray sun image before any correction has been applied. Figure 46 shows the limb darkening

correction obtained through the addition method used currently in the code, and there is some clear difference on the limb of the sun.

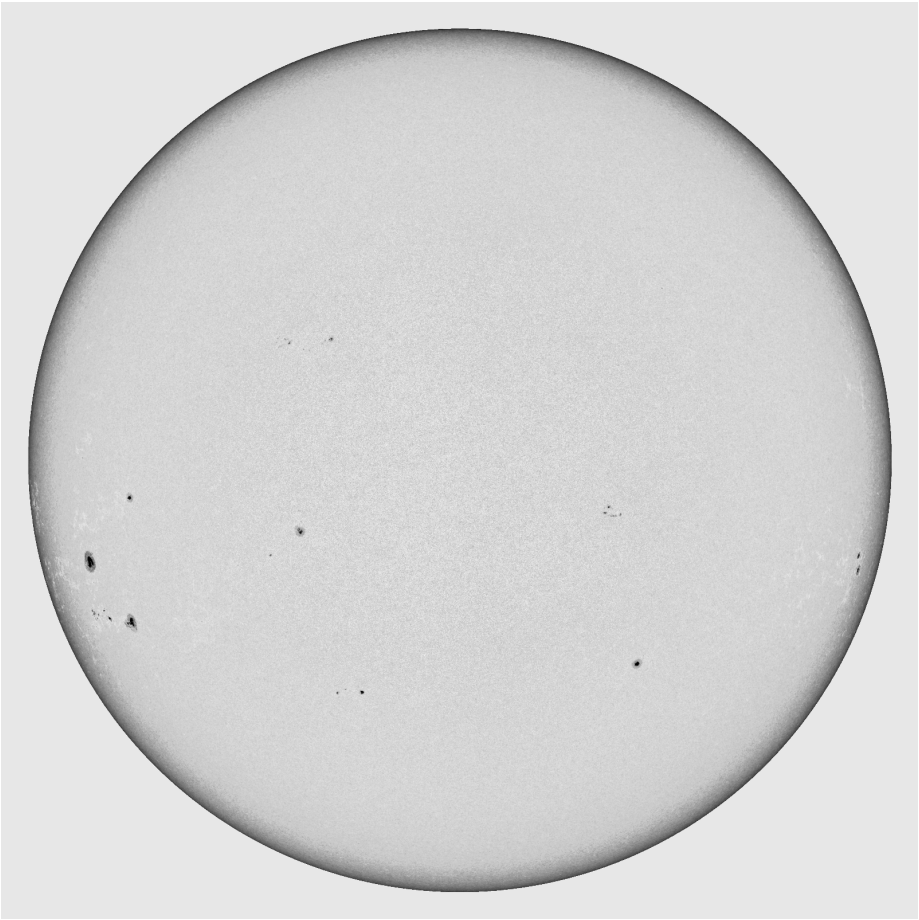

Figure 45. The inverse of the Eddington approximation function is multiplied into the grayscale sun to correct for limb darkening.

Some differences are clear, including a faster drop off on the multiplied image near the very edge of the sun. In order to highlight these differences, the multiplied image is subtracted from the added image, shown in Figure 47.

The difference image shows some higher intensity near the edge of the sun, indicating that the added image yields higher pixel intensity in those regions. The

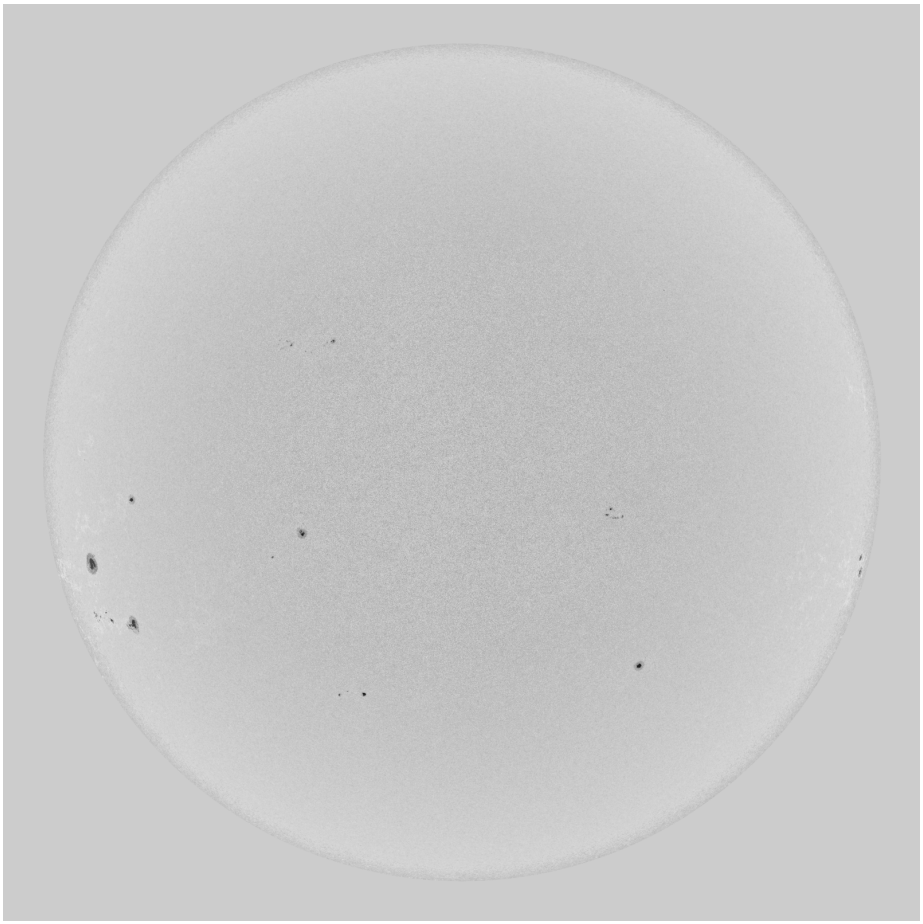

Figure 46. The inverse of the Eddington approximation function has been added to the grayscale sun in this case to correct for limb darkening. This is the method currently used by the SDO code.

intensity of spots in those regions looks to be visible as well, indicating that there will be a difference in the spot finding if the multiplication method is used. The correction may improve if the intensity correction function is found to a higher order. This may be a path for additional research, in addition to other image processing techniques that may be used to speed up the execution of the code.

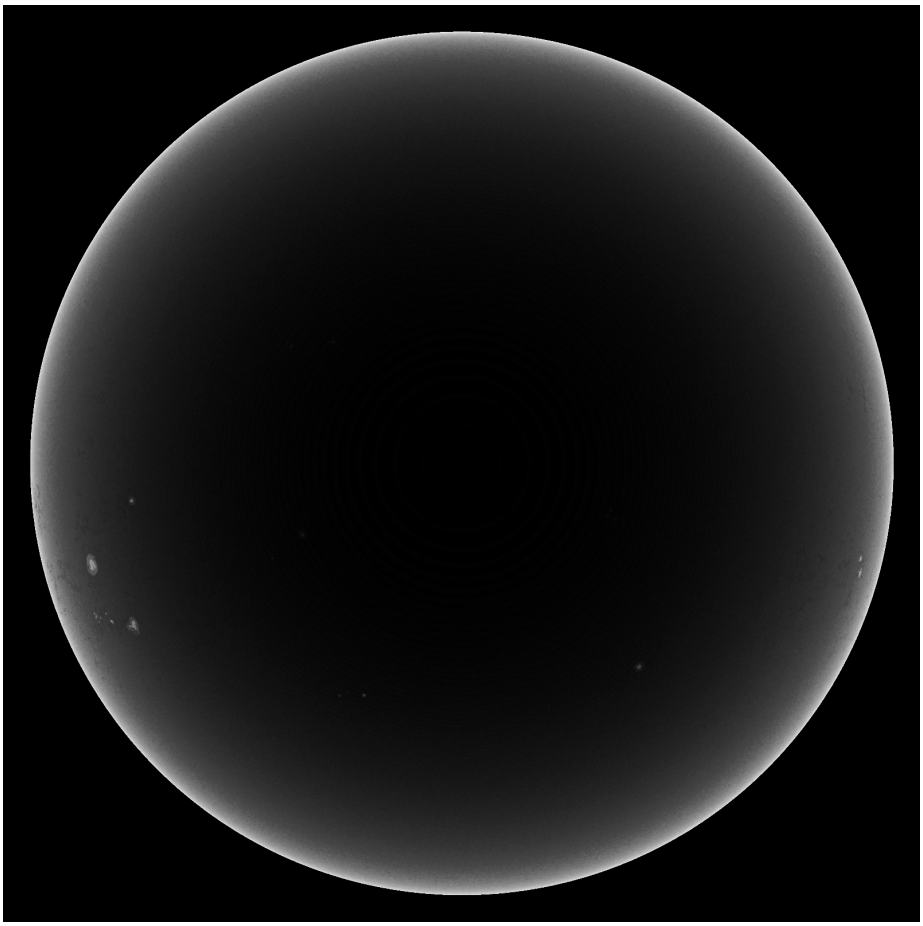

Figure 47. The multiplication method for limb darkening correction is subtracted from the addition method used by the SDO code. The result proves to have higher pixel intensity near the edge of the sun.

References

Al-Omari, M., R. Qahwaji, T. Colak, S. Ipson, and C. Balch, Next-day prediction of sunspots area and mcintosh classifications using hidden markov models, in *CyberWorlds, 2009. CW'09. International Conference on*, pp. 253–256, IEEE, 2009.

Aschwanden, M. J., Image processing techniques and feature recognition in solar physics, *Solar Physics*, *262*(2), 235–275, 2010.

Benkhalil, A., V. Zharkova, S. Ipson, and S. Zharkov, Automatic identification of active regions (plages) in the full-disk solar images using local thresholding and region growing techniques, in *Proceedings of the AISB*, vol. 3, pp. 66–73, 2003.

Benkhalil, A., V. Zharkova, S. Ipson, and S. Zharkov, Automatic detection of active regions on solar images, in *Knowledge-Based Intelligent Information and Engineering Systems*, pp. 460–466, Springer, 2004.

Bornmann, P., and D. Shaw, Flare rates and the mcintosh active-region classifications, *Solar physics*, *150*(1-2), 127–146, 1994.

Canny, J., A computational approach to edge detection, *Pattern Analysis and Machine Intelligence, IEEE Transactions on*, (6), 679–698, 1986.

Colak, T., and R. Qahwaji, Automated mcintosh-based classification of sunspot groups using mdi images, *Solar Physics*, *248*(2), 277–296, 2008.

Curto, J., M. Blanca, and E. Martínez, Automatic sunspots detection on full-disk solar images using mathematical morphology, *Solar Physics*, *250*(2), 411–429, 2008.

De Wit, T. D., Fast segmentation of solar extreme ultraviolet images, *Solar Physics*, *239*(1-2), 519–530, 2006.

Delouille, V., B. Mampaey, C. Verbeeck, and R. de Visscher, The spoca-suite: a software for extraction and tracking of active regions and coronal holes on euv images, *arXiv preprint arXiv:1208.1483*, 2012.

Foukal, P. V., *Solar astrophysics*, Wiley-VCH, 2008.

Gonzalez, R., R.C.and Woods, and S. Eddins, *Digital Image Processing Using MATLAB*, Gatesmark Publishing, United States of America, 2009.

Jewalikar, V., and S. Singh, Automated sunspot extraction, analysis and classification.

Kiepenheuer, K., Solar activity, *The Sun*, *1*, 322, 1953.

Lemen, J. R., The atmospheric imaging assembly (aia) on the solar dynamics observatory (sdo), *Solar Physics*, *275*(1-2), 17–40, doi:10.1007/s11207-011-9776-8, 2012.

McIntosh, P. S., The classification of sunspot groups, *Solar Physics*, *125*(2), 251–267, 1990.

Meeus, J., Astronomical formulae for calculators, *Richmond, Va., USA: Willmann-Bell, c1982. 2nd ed., enl. and rev.*, *1*, 1982.

Nguyen, S. H., T. T. Nguyen, and H. S. Nguyen, Rough set approach to sunspot classification problem, in *Rough Sets, Fuzzy Sets, Data Mining, and Granular Computing*, pp. 263–272, Springer, 2005.

Nguyen, T. T., C. P. Willis, D. J. Paddon, and H. S. Nguyen, A hybrid system for learning sunspot recognition and classification, in *Hybrid Information Technology, 2006. ICHIT'06. International Conference on*, vol. 2, pp. 257–264, IEEE, 2006.

Park, D.-C., Sunspot series prediction using adaptively trained multiscale-bilinear recurrent neural network, in *Computer Systems and Applications (AICCSA), 2011 9th IEEE/ACS International Conference on*, pp. 135–139, IEEE, 2011.

Pesnell, W. D., B. Thompson, and P. Chamberlin, The solar dynamics observatory (sdo), *Solar Physics*, *275*(1-2), 3–15, 2012.

Qahwaji, R., and T. Colak, Automatic detection and verification of solar features, *International Journal of Imaging Systems and Technology*, *15*(4), 199–210, 2005.

Qahwaji, R., and T. Colak, Neural network-based prediction of solar activities, *CITSA2006: Orlando*, 2006.

Qahwaji, R., and T. Colak, Automatic short-term solar flare prediction using machine learning and sunspot associations, *Solar Physics*, *241*(1), 195–211, 2007.

Scherrer, P., et al., The helioseismic and magnetic imager (hmi) investigation for the solar dynamics observatory (sdo), in *The Solar Dynamics Observatory*, pp. 207–227, Springer, 2012.

Schou, J., et al., Design and ground calibration of the helioseismic and magnetic imager (hmi) instrument on the solar dynamics observatory (sdo), in *The Solar Dynamics Observatory*, pp. 229–259, Springer, 2012.

Seidelmann, P. K., and S. Urban, Explanatory supplement to the astronomical almanac, in *Bulletin of the American Astronomical Society*, vol. 42, p. 522, 2010.

Smart, W. M., *Text-book on spherical astronomy*, CUP Archive, 1947.

Socas-Navarro, H., Strategies for spectral profile inversion using artificial neural networks, *The Astrophysical Journal*, *621*(1), 545, 2005.

Thompson, W., Coordinate systems for solar image data, *Astronomy and Astrophysics*, *449*(2), 791–803, 2006.

Turmon, M., J. Pap, and S. Mukhtar, Automatically finding solar active regions using soho/mdi photograms and magnetograms, in *Structure and Dynamics of the Interior of the Sun and Sun-like Stars*, vol. 418, p. 979, 1998.

Turmon, M., J. Pap, and S. Mukhtar, Statistical pattern recognition for labeling solar active regions: application to soho/mdi imagery, *The Astrophysical Journal*, *568*(1), 396, 2002.

USAF, Meteorological codes, *AFMAN 15-124*, *HQ USAF/A3O-W*, 2013.

Verbeeck, C., P. A. Higgins, T. Colak, F. T. Watson, V. Delouille, B. Mampaey, and R. Qahwaji, A multi-wavelength analysis of active regions and sunspots by comparison of automatic detection algorithms, *Solar Physics*, *283*(1), 67–95, 2013.

Watson, F., and L. Fletcher, Automated sunspot detection and the evolution of sunspot magnetic fields during solar cycle 23, *Proceedings of the International Astronomical Union*, *6*(S273), 51–55, 2010.

Watson, F. T., Investigating sunspot and photospheric magnetic field properties using automated solar feature detection, Ph.D. thesis, University of Glasgow, 2012.

Wilson, W. H., Solar ephemeris algorithm, *SIO Ref*, *80*, 13, 1980.

Zharkov, S., V. Zharkova, S. Ipson, and A. Benkhalil, Technique for automated recognition of sunspots on full-disk solar images, *EURASIP journal on applied signal processing*, *2005*, 2573–2584, 2005.

Vita

Second Lieutenant Gordon Spahr was born in Oakland, CA. After graduating from Acalanes High School in 2008, he was accepted to the United States Air Force Academy as part of the Class of 2012. Graduating with a Bachelor of Science Degree in Physics, he was commissioned into the United States Air Force from Cadet Squadron 34.

Lieutenant Spahr's initial assignment upon commissioning was to the Air Force Institute of Technology at Wright Patterson AFB, OH. In fall of 2012, he entered the Applied Physics program to obtain a Master's Degree, concentrating in Solar Physics and Space Weather. Upon graduation, Lieutenant Spahr will be assigned to the 47th Flying Training Wing for Specialized Undergraduate Pilot Training.

REPORT DOCUMENTATION PAGE

Form Approved
OMB No. 0704–0188

1. REPORT DATE *(DD–MM–YYYY)*	2. REPORT TYPE	3. DATES COVERED *(From — To)*
27–03–2014	Master's Thesis	Aug 2012 — Mar 2014

4. TITLE AND SUBTITLE

Fully Automated Sunspot Detection and Classification Using SDO HMI Imagery in MATLAB

5a. CONTRACT NUMBER

5b. GRANT NUMBER

5c. PROGRAM ELEMENT NUMBER

6. AUTHOR(S)

Spahr, Gordon M., Second Lieutenant, USAF

5d. PROJECT NUMBER

5e. TASK NUMBER

5f. WORK UNIT NUMBER

7. PERFORMING ORGANIZATION NAME(S) AND ADDRESS(ES)

Air Force Institute of Technology
Graduate School of Engineering and Management (AFIT/EN)
2950 Hobson Way
WPAFB OH 45433-7765

8. PERFORMING ORGANIZATION REPORT NUMBER

AFIT-ENP-14-M-34

9. SPONSORING / MONITORING AGENCY NAME(S) AND ADDRESS(ES)

Capt. Thomas M. Wittman
Air Force Weather Agency
101 Nelson Drive
Offutt AFB, NE 68113
DSN 271-0690, COMM 402-294-0690
Email: 2syosdor@offutt.af.mil

10. SPONSOR/MONITOR'S ACRONYM(S)

AFWA

11. SPONSOR/MONITOR'S REPORT NUMBER(S)

12. DISTRIBUTION / AVAILABILITY STATEMENT

DISTRIBUTION STATEMENT A: APPROVED FOR PUBLIC RELEASE; DISTRIBUTION UNLIMITED.

13. SUPPLEMENTARY NOTES

This material is declared a work of the U.S. Government and is not subject to copyright protection in the United States

14. ABSTRACT

An automatic sunspot detection and classification method is developed combining HMII and HMIM imagery procured from the Solar Dynamics Observatory. Iterative global thresholding methods are employed for detecting sunspots. Groups are selected based on heliographic distance between sunspots via area-based grouping lengths. Classifications are applied through logical operators adhering to the standard McIntosh classification system. Calculated sunspot parameters and classifications are validated in three way comparisons between code output, Holloman AFB and the Space Weather Prediction Center. Accuracy is achieved within the margin of difference between Holloman and SWPC reports for sunspot area, number of groups, number of spots, and McIntosh classification using data spanning 6 July 2012 to 29 June 2013: SWPC/Holloman (33.38%,57.48%,87.67%), SWPC/SDO (20.22%,51.25%,83.80%), and SDO/Holloman (24.54%,50.91%,80.65%). The automatic classification system is used to evaluate bias inherent in Holloman classification methods. Parameters are altered to reach optimal match percentages with Holloman, indicating differences between computed parameter values and hand-calculated counterparts. Group length cutoffs are shown to differ by 2.5°, eccentricity is quantified at 0.8, and penumbra length cutoffs are shown to exceed differences of 1.4° from McIntosh values.

15. SUBJECT TERMS

Sunspots, Automatic, Detection, McIntosh Classification, Space Weather, Bias Evaluation, Solar Dynamics Observatory, Iterative Thresholding, Image Processing

16. SECURITY CLASSIFICATION OF:			17. LIMITATION OF ABSTRACT	18. NUMBER OF PAGES	19a. NAME OF RESPONSIBLE PERSON
a. REPORT	b. ABSTRACT	c. THIS PAGE			Dr. Ariel O. Acebal, AFIT/ENP
U	U	U	UU	146	19b. TELEPHONE NUMBER *(include area code)* (937) 255-3636, x4518; ariel.acebal@afit.edu